Influence of processing conditions on the structural properties of electrodeposited CdS films

by

Jacqueline Margot Nel

Submitted in fulfillment of the requirements for the degree

Philosophiae Doctor

in the Faculty of Natural and Agricultural Sciences

University of Pretoria
Pretoria

January 2001

To my husband Kobus, and
my daughters Elaine and Andrea

SUMMARY

Influence of processing conditions on the structural properties of electrodeposited CdS films

by

Jacqueline Margot Nel

Supervisor: Prof. H. L. Gaigher

Co-supervisor: Prof. F. D. Auret

Department: Physics

Degree: Philosophiae Doctor

Cadmium sulphide (CdS) films were electrodeposited from an aqueous electrolytic solution onto indium tin oxide and fluorine doped tin oxide substrates, commonly used in photovoltaic applications.

The CdS films were deposited for between 1 minute and 4 hours at temperatures ranging from 30°C to 90°C and a deposition potential of 600 mV with respect to a Ag/AgCl reference electrode. Some films were annealed in an argon atmosphere at temperatures of 300°C, 400°C and 460°C for 15 minutes and 30 minutes with and without $CdCl_2$ treatment.

The cleaning efficiency of the substrates by several solvents was determined using atomic force microscopy (AFM), surface roughness and scanning electron microscopy (SEM). It was found that the cleaning of the substrates could be monitored by the RMS roughness of the surfaces, and that the efficiency of the cleaning methods was substrate dependent.

The microstructure, composition and optical properties of the films were determined using SEM, transmission electron microscopy, transmission electron diffraction, AFM, x-ray photoelectron spectroscopy (XPS), transmittance and Raman spectroscopy.

All films, including those formed at the lowest deposition temperature of 30°C, were crystalline with the hexagonal (wurtzite) structure. At deposition temperatures ≤50°C the crystallites were extremely small as evidenced by broad diffraction rings and Raman peaks. At higher deposition temperatures (≥60°C) the deposition rate increased and the crystalline quality improved significantly.

At the very early stages of deposition the deposits consisted of isolated, three-dimensional particles. Rapid lateral growth of these particles dominated the initial stages of deposition. Field emission SEM and AFM showed that ostensibly single particles consisted of agglomerates of elongated and plate-like grains with no preferred orientation. The final films had a columnar structure with good contact between the substrate and the film.

XPS results showed that there was no significant compositional change in the deposition temperature range used and the films were all slightly cadmium rich. Carbon, oxygen and chlorine were detected mainly on the surface of the films.

After annealing, the composition of the CdS films were close to stoichiometric once the surface layer had been removed. There was an improvement in the crystallinity of the films after annealing.

Table of Contents

1 Introduction

Cadmium sulphide (CdS) has been the topic of research and development projects for photovoltaic applications for more than 50 years, but it was only in the 1980's that the transfer of technology to the industrial applications started with the production of Cu_2S-CdS thin film solar cells (Bloss *et al.* (1983)). Due to the wide band gap of 2.42 eV, much of the solar spectrum cannot be absorbed effectively by the CdS, resulting in a low theoretical conversion efficiency (Figure 1.1). Cadmium sulphide has, however, been used successfully in photovoltaic applications in conjunction with other semiconducting materials such as Cu_2S (Bloss *et al.* (1983)), CdTe (Bonnet *et al.* (1972), Ferekides *et al.* (1996), Aramoto *et al.* (1997)) and copper indium diselenide ($CuInSe_2$) (Sebastian *et al.* (1999)) to produce photovoltaic cells. CdS has also recently been used in conjunction with organic thin films to produce hybrid organic-inorganic photovoltaic cells with among the highest efficiencies for this type of cell (Nguyen Cong *et al.* (2000)).

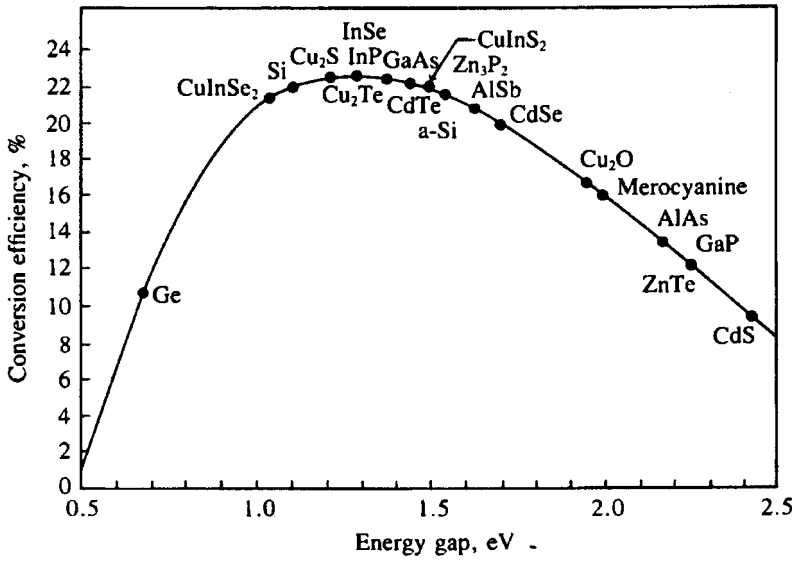

Figure 1.1: The maximum theoretical conversion efficiency vs. energy gap for solar cells in AM1 sunlight (Hu and White (1983)).

In the CdTe based photovoltaics, CdS is an efficient window layer that allows much of the solar radiation to pass through to the CdTe absorber layer. The CdS has also

been utilised in the copper indium diselenide ($CuInSe_2$) photovoltaics as a buffer layer between the CIS and the n-ZnO window layer, preventing the diffusion of Cu, In and Se into the ZnO layer.

n-CdS makes an effective partner with CdTe in the solar cell applications, since p-CdTe has the nearly ideal band gap for a solar absorber material (Figure 1.1), coupled with the high absorption coefficient. This means that a 1μm layer absorbs more than 99% of the incident visible light. The CdS window layer is deposited on the front contact, which is usually a transparent conducting oxide (TCO) layer (commonly SnO_2 or indium tin oxide (ITO)) on a glass substrate. The CdTe is then deposited on the CdS layer. The cell is then heat treated to affect the type conversion of CdTe to p-CdTe after which the necessary etching produces a p^+-CdTe layer on which the back contact is fixed.

Most previous studies concentrated on the processing of the CdTe and little attention was paid to the influence of the CdS processing on the properties of the final cell (Das *et al.* (1993(a), (b)), Das (1993(a)), Britt *et al.* (1993)). The structure of the CdS will certainly influence the photovoltaic behaviour of the device. Structural properties which will affect behaviour include: surface morphology (including the surface roughness), pinholes, grain size, grain boundaries, preferred orientation of grains, composition, impurities and crystallographic structure (cubic or hexagonal). Cadmium sulphide exists in two crystallographic structures, namely cubic and hexagonal (wurtzite). The cubic phase is a meta-stable phase which is sometimes formed during lower temperature processing (Kohle *et al.* (1984), Stoev *et al.* (1996), Johnson (2000)). The hexagonal phase is the naturally occurring form of CdS and is thermally more stable than the cubic phase (Rossetti *et al.* (1983), Zahn *et al.* (1991)).

The structure is influenced by the substrate (Das (1993(a)), Ferekides *et al.* (1994), Johnson (2000)), the deposition technique (Ferekides *et al.* (1994)), the deposition temperature (Froment *et al.* (1995), Sasikala *et al.* (2000)), the annealing temperature and time (Shirai *et al.* (1996), Johnson (2000)), the treatment of the film

prior or during annealing with $CdCl_2$ and the annealing atmosphere (Al-Jassim *et al.* (1993), Ebothe (1996), Johnson (2000)).

Several processing techniques have been successfully used to deposit the CdS onto the TCO layer used as the front contact of the cell in the superstrate configuration. These include electrodeposition (Basol (1984), Das (1993(a))), close space sublimation (Ferekides *et al.* (1993)), spray pyrolosis (Kohle *et al.* (1987)), screen printing (Lee *et al.* (1987), Aramoto *et al.* (1994)) and chemical bath deposition (Danaher *et al.* (1985), Al-Jassim *et al.* (1993), Jayakrishnan *et al.* (1996)).

Das (1983(a)) and Ferekides *et al.* (1994) have shown that the substrate used influenced the properties of the final CdS/CdTe solar cell. In both of these cases, just the final electrical properties of the cell were determined; the effect of the substrate on the CdS films was not investigated.

A better understanding and optimisation of the structure of the CdS films will facilitate better control of the device characteristics. Very few systematic studies of the microstructural development of CdS, *per se*, exist (Rami *et al.* (1999)). In most previous studies, CdS was studied as part of a complete cell.

In this study electrodeposited CdS was chosen as the processing route, since it is a relatively inexpensive, controllable, low temperature process, which produces high purity stoichiometric CdS films of uniform thickness, which are ideal for photovoltaic applications.

Before electrodeposition of the CdS onto the transparent conducting oxide, the substrates need to be cleaned in order to produce a homogeneously deposited film with good adhesion and substrate-CdS interface. In order to do this, a study of some solvent cleaning methods was undertaken to determine the most efficient cleaning method for the substrates used. Atomic force microscopy (AFM) was used to analyse the surface before and after cleaning and the RMS roughness values of the surfaces were also determined.

This study aims to correlate the effect of processing conditions on the properties of the CdS film, which in turn influences the properties of the photovoltaic cell.

The first priority was to determine whether effective cleaning of substrates was occurring prior to deposition. Two substrates, which are typically used in solar cell technology, namely indium tin oxide (ITO) and flourine doped tin oxide (FTO), were used in this study. The substrates were studied before and after cleaning with various solvents in an atomic force microscope to identify the optimum cleaning conditions.

The study then concentrated on the microstructural and structural properties of the electrodeposited CdS films deposited at -600 mV with respect to a Ag/AgCl reference electrode, at temperatures between 30°C and 90°C (at 10°C intervals) and for times of typically 90 minutes (but up to 4 hours on both substrates). Some films were then annealed in an argon atmosphere at temperatures of 300°C, 400°C and 460°C for 15 to 30 minutes. The as deposited and annealed films were then analysed using the following techniques:

- X-ray photoelectron spectroscopy (XPS)
- Optical transmittance
- Raman spectroscopy
- High resolution field emission scanning electron microscopy
- Transmission electron microscopy
- Transmission electron diffraction
- Atomic force microscopy

A detailed microstructural development study was also carried out at 60°C and 90°C by depositing the CdS for times ranging from 1 minute to 90 minutes on both substrates using the field emission scanning electron microscope and atomic force microscope.

The effect of the processing conditions (different substrates, deposition temperature, deposition time, annealing temperature, annealing time and $CdCl_2$ treatment prior to annealing) on the resulting CdS films is reported.

2 Electrodeposition Theory

Electrodeposition of metals was a well-established technique, both in theoretical understanding and industrial application, prior to the development of the semiconductor industry. However, it is only recently that it has been identified as a cost-efficient means of depositing a wide range of materials, including semiconductors. There are three categories into which electrodeposition can be divided, namely aqueous electrolytes, non-aqueous electrolytes and molten electrolytes (Pandey *et al.* (1996)).

Electrodeposition of cadmium sulphide (CdS) was first reported in 1976 by Miller and Heller. The deposition techniques and understanding of the mechanism have since been investigated by a number of researchers and will be discussed later in this section.

Other cost effective deposition techniques, such as chemical bath deposition (Lundin and Kitaev (1965), Danaher *et al.* (1985)) and screen printing (Matsumoto *et al.* (1984)) have been successfully used to produce polycrystalline CdS films.

Apart from the cost efficiency of electrodeposition, some of the other key advantages of the technique are listed below: (Pandey *et al.* (1996), DeMattei & Feigelson (1992)):

- It is possible to produce uniform films on large areas, including irregularly shaped surfaces.
- Compositionally modulated structures and non-equilibrium alloys can be deposited.
- Growth temperatures are well below the melting points when using aqueous or organic electrolytes.
- Minimum oxide impurities are incorporated due to the fluxing effect of the solvents.

- The purity and stoichiometry of the film can be controlled due to differences in the deposition potentials between major and minor components in solution and by changes in the concentration of the species.
- A wide range of elements and compounds can be deposited.
- Thin films can be deposited uniformly.
- A vast range of industrial experience can be tapped.
- It is specifically attractive in terms of cost, high throughput and scalability.

2.1 Basics of Electrodeposition of Semiconductors

Electrodeposition is a chemical process governed by thermodynamics. The thermodynamic conditions of the electrodeposition process are unfavourable and will not occur spontaneously. The driving force of the electrodeposition process is externally applied electrical energy.

The simplest form of electrodeposition consists of an electrolyte (containing the cations and/or anions required for deposition) and two electrodes. When a high enough voltage is applied, the current flows. The anions migrate towards the anode and the cations towards the cathode. The ions may deposit on the respective electrodes after undergoing a charge transfer reaction. During cathodic deposition, the metal cations deposit on the cathode, which is called the working electrode, while the anode is generally called the counter electrode. For anodic deposition, the anions are deposited on the anode (working electrode) and the cathode will be the counter electrode. The potential across the working electrode interface cannot be directly measured, but the potential of the working electrode relative to a third electrode, the reference electrode, can be measured (Figure 2.1 (Atkins (1995))).

A number of reference electrodes exist, three of the most common being the Standard Hydrogen Electrode (SHE) (against which most of the reference tables of electrochemical reaction potentials are measured), the saturated calomel electrode (SCE) and the Ag/AgCl electrode (Atkins (1995)).

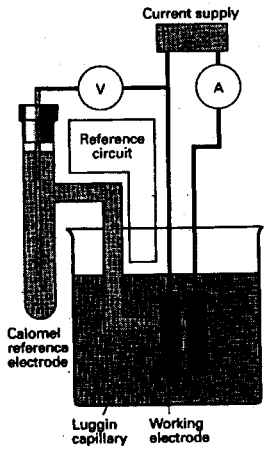

Figure 2.1: Conventional three electrode configuration for electrodeposition (Atkins (1995)).

When sufficient electrical energy is supplied to the electrodes in an electrolyte containing cations, M^{z+}, in solution, these cations will move towards the cathode and deposit as the elemental form of the ion according to the following reaction:

$$M^{z+} + ze^- \rightarrow M \qquad \Delta G < 0 \qquad \text{Equation 1}$$

For the reaction to occur spontaneously, $\Delta G < 0$, where ΔG is the change in the Gibbs free energy of formation. ΔG can be related to the activity of the species present or the concentration of the ions in solution or the electrical potential as follows (Atkins (1995), DeMattei & Feigelson (1992)):

$$\Delta G = \Delta G^\circ + RT \ln\left(\frac{a_M}{a_{M^{z+}}}\right) \qquad \text{Equation 2}$$

where ΔG° is the standard Gibbs free energy for the reaction in Equation 1, R the universal gas constant, T the absolute temperature and a_i (i = M or M^{z+}) the activity of the species (ion or element), which is given by $a_i = \gamma c_i$. γ is the activity coefficient and c_i is the concentration of species in the solution usually represented by $[M^{z+}]$. The activity, a_i, of an element in the electrolyte is usually 1 and in dilute solutions with no complexation, $\gamma \approx 1$, therefore $a_i \approx c_i$ (Atkins (1995)).

This results in Equation 2 becoming:

$$\Delta G = \Delta G^{\circ} + RT \ln\left(\frac{1}{[M^{z+}]}\right) \qquad \text{Equation 3}$$

But ΔG can also be related to the electric potential:

$$\Delta G = -nFE \qquad \text{Equation 4}$$

where n is the number of moles of electrons involved, F is Faraday's constant and E is the electric potential. On substituting this into Equation 3, we get the Nernst Equation relating the applied electrical potential, E, to the concentration of the species, $[M^{z+}]$:

$$E = E^{\circ} - \frac{RT}{nF} \ln\left(\frac{1}{[M^{z+}]}\right) \qquad \text{Equation 5}$$

where E° is the standard electrode potential for the reaction in Equation 1 referenced to the standard reference electrode with $[M^{z+}]$ = 1 mole/litre (Atkins (1995), DeMattei and Feigelson (1992)).

From the Nernst Equation (Equation 5), the deposition potential of a species can be regulated at a specific temperature by adjusting the concentration of the species, e.g. $[M^{z+}]$, in the solution. When the electrolyte contains the necessary ionic species at the appropriate concentrations, more than one species can be simultaneously deposited to form a binary (e.g. CdS) or even ternary compound, if deposition conditions are favourable. For cathodic deposition the reaction process is usually written as:

$$M^{z+} + ze^{-} \rightarrow M$$
$$N^{y+} + ye^{-} \rightarrow N \qquad \text{Equation 6}$$

with the over all reaction being

$$M^{z+} + N^{y+} + (z+y)e^{-} \rightarrow MN$$

Factors governing co-deposition of binary and ternary compounds have been summarized by Lokhande and Pawar (1989) and are:

- The electrode potentials of individual ions in the electrolyte.
- Cathodic polarization due to differences in deposition potentials.
- Relative concentration of the ions in the electrolyte.
- The solution potential, i.e. the dissolving tendency of the deposited compound.
- The hydrogen overpotential on the deposited cathode surface.

These parameters are highly sensitive to changes in the electrolyte temperature and the current density during electrodeposition.

Although the deposition of semiconductors and metals is very similar, there are a number of problems which are unique to the electrodepostion of both elemental and compound semiconductors (Pandey *et al.* (1996)):

- The relatively high resistivity of semiconductors compared to metals may drastically change the interfacial potential and the charge distribution once a few layers of semiconductor have been deposited. This may even lead to changes in the morphology of thicker films.
- Defects and orientation are just two of the factors which influence the resistivity of the semiconductor and, during deposition, the introduction of these may cause the resistivity to change significantly.
- In the semiconductor-electrolyte contact, the space charge layer within the electrode is dominant.
- The resistivity, density of defects and/or surface states and the space charge layer can also result in controlling effects in the transfer of charge in the reaction. The Tafel plot (interfacial potential vs. logarithmic current density) may not be the same as for metallic deposits.

Apart from the problems mentioned above, there are three typical problems which arise when depositing compound semiconductors. These compound materials form a large proportion of semiconductor interest.

- Most compound semiconductors have at least one metallic component (e.g. Cd, Ga) and one non-metallic component (e.g. S, As) as in CdS and

GaAs. There is generally a wide difference between the reduction potentials of the non-metals and the metal ions. A general pre-requisite for co-deposition from different components is that these reduction potentials be equal.

- The Gibbs free energy of formation of most compound semiconductors is very negative, which may shift the deposition of the less noble component to a more positive value, assisting the co-deposition.
- Multiple phases of the compound semiconductor often exist and may be co-deposited leading to complexities in the activity term, $a_{M^{z+}}$, which controls the current density across the interface between the electrode and the electrolyte.

These problems have been successfully overcome by varying the concentration of the species in solution by using complexing agents to form complex ions or by using the role of favourable Gibbs free energy of formation and its relation to the deposition potential.

The process described above is cathodic deposition, where the deposition occurs on the cathode. Most electrochemical deposition is cathodic since most metal ions are cations. Anodic deposition is also possible, but has been found to generally give poor stoichiometry and adhesion (Pandey *et al.* (1996)). Anodic deposition uses the negative anions, which oxidize at the anode, liberating electrons according to the following equation:

$$B^{x-} \rightarrow B + xe^{-} \qquad \Delta G < 0 \qquad \text{Equation 7}$$

2.2 Electrodeposition of CdS

CdS films were first reported to be electrochemically produced by Miller and Heller (1976) by anodizing a cadmium electrode in a solution of Na_2S. This technique requires the sulfide ions to be initially absorbed on the surface of the electrode and then react to form a monolayer of CdS. This is followed by the growth of a CdS layer with a thickness of up to 50Å. Films thicker than this, grown at higher potentials, were found to be porous and it was presumed that the layer then grew by a different mechanism, probably a diffusion-controlled mechanism (Peter (1978 (a), (b))). The properties of the anodic CdS films are poor, with high density of donor states, low absorption coefficient and poor quantum efficiency (Pandey *et al.* (1996)).

For cathodic deposition of CdS, from Equation 6, we could have:

$$Cd^{2+} + 2e^- \rightarrow Cd$$
$$S^{4+} + 4e^- \rightarrow S$$

with the over all reaction being

$$Cd^{2+} + S^{4+} + (2+4)e^- \rightarrow CdS$$

From the Nernst Equation the quasi-rest potentials (deposition potential minus polarization (Kröger (1978))) of Cd and S are:

$$E_{Cd} = E^{o}_{Cd} + \frac{RT}{2F} \ln\left(\frac{a_{Cd^{2+}}}{a_{Cd}}\right) \qquad \text{Equation 8}$$

$$E_{S} = E^{o}_{S} + \frac{RT}{4F} \ln\left(\frac{a_{S^{4+}}}{a_{S}}\right) \qquad \text{Equation 9}$$

where $a_{Cd^{2+}}$ and $a_{S^{4+}}$ are the activities of the two ion species in the electrolyte at the interface during deposition and a_{Cd} and a_S are the activities of Cd and S in the deposit. Cd is less noble than S since $E°_S > E°_{Cd}$. The activities of Cd and S in the

deposit are not ≈1 as in the case for bulk electrolyte solutions, but are related through:

$$Cd(s) + S(s) \rightarrow CdS \qquad \Delta G° < 0$$

where $\Delta G°$ is the standard Gibbs free energy change for the reaction. In equilibrium:

$$\frac{a_{CdS}}{a_{Cd}a_S} = \exp\left(-\frac{\Delta G°}{RT}\right)$$

and since $a_{CdS} \approx 1$:

$$a_{Cd}a_S = \exp\left(\frac{\Delta G°}{RT}\right). \qquad \text{Equation 10}$$

Since $\Delta G°$, R and T are constant for a specific deposition temperature, it can be seen that a small a_{Cd} gives rise to a large a_S, and vice versa. The activities of coexisting phases in the phase diagram will determine the limiting values of a_{Cd} and a_S. If we assume that CdS is the only compound present, then Cd co-exists with CdS as pure Cd, and S co-exists with CdS as pure S at the two phase boundaries. This will lead to the limiting values of the activities at these boundaries being:

$$a_{Cd} = 1 \qquad a_S = \exp\left(\frac{\Delta G°}{RT}\right) \qquad \text{Equation 11}$$

and

$$a_S = 1 \qquad a_{Cd} = \exp\left(\frac{\Delta G°}{RT}\right) \qquad \text{Equation 12}$$

The quasi-rest potentials of Cd and S vary by :

$$\Delta E_{Cd} = -\frac{\Delta G^{\circ}}{2F} \qquad \Delta E_{S} = -\frac{\Delta G^{\circ}}{4F}$$

due to the variation in the activities of Cd and S between the phase boundaries. Since $\Delta G^{\circ} < 0$, the change in the potentials of both components becomes more positive when the activities increase (Kröger (1978)).

The potential at which the two components form a homogeneous deposit of certain composition (with corresponding specific activities a_{Cd} and a_S) is a result of the exchange processes between the electrode and the electrolyte, which are determined by the rate constants of the exchange currents for the two components. Two possibilities exist, i.e. when these rate constants are of the same order of magnitude and when they differ considerably (Kröger (1978)).

When the rate constants are of the same order of magnitude, each species has an equal weight in determining the potential. A change in the individual contributions of the species can only occur as a result of a change of the activities of the species in the electrolyte and the corresponding change in the deposit. This is the case when the source of sulphur in the electrochemical reaction is S(IV) complexed (Kröger (1978)).

In this case, since there is only one quasi-rest potential for the deposition of a specific composition

$$E_{CdS} = E_{Cd} = E_S \qquad \text{Equation 13}$$

From Equations 8, 9 and 13, E_{Cd} and E_S can be eliminated and gives:

$$\frac{RT}{F}\ln\frac{(a_{Cd^{2+}})^{1/2}}{(a_{S(IV)})^{1/4}} = (E_S^{o} - E_{Cd}^{o}) + \frac{RT}{F}\ln\frac{(a_{Cd})^{1/2}}{(a_S)^{1/4}} \qquad \text{Equation 14}$$

At the limits on the phase diagram as depicted by Equations 11 and 12, Equation 14 above becomes:

$$\frac{RT}{F}\ln\frac{(a_{Cd^{2+}})^{1/2}}{(a_{S(IV)})^{1/4}} = (E_S^o - E_{Cd}^o) - \frac{\Delta G^\circ}{4F} \qquad \text{Equation 15}$$

for the CdS-Cd phase boundary, and:

$$\frac{RT}{F}\ln\frac{(a_{Cd^{2+}})^{1/2}}{(a_{S(IV)})^{1/4}} = (E_S^o - E_{Cd}^o) + \frac{\Delta G^\circ}{2F} \qquad \text{Equation 16}$$

for the CdS-S phase boundary.

Since $(E^\circ_S - E^\circ_{Cd}) > 0$ and $\Delta G^\circ < 0$, Equation 15 indicates that, at the Cd-CdS boundary, $a_{Cd^{2+}} >> a_{S(IV)}$ and, therefore, the less noble species, Cd, is the potential determining species.

At the S-CdS boundary there are two cases, which depend on whether $(E_S^o - E_{Cd}^o) > \left|\frac{\Delta G}{2F}\right|$ or $(E_S^o - E_{Cd}^o) < \left|\frac{\Delta G}{2F}\right|$.

In class 1, we have $(E_S^o - E_{Cd}^o) > \left|\frac{\Delta G}{2F}\right|$; this implies that $a_{Cd^{2+}} >> a_{S(IV)}$ for the S-CdS boundary and the Cd-CdS boundary. This means that, for the whole deposition range, the cadmium is the potential determining species.

In class 2, we have $(E_S^o - E_{Cd}^o) < \left|\frac{\Delta G^\circ}{2F}\right|$; this implies that $a_{S(IV)} >> a_{Cd^{2+}}$, i.e. at the S-CdS boundary, the S is the potential determining species. This means that there is a change in the potential determining species between the Cd-CdS boundary and the S-CdS boundary. This cross-over occurs near the point where the contributions of the exchange currents of Cd and S are of the same order. Near this point, both Cd and S contribute towards determining the potential.

From the standard electrode potentials and formation energy tables for the deposition of CdS we have:

$E°_{Cd}$ = -0.403 V vs. NHE

$E°_{S}$ = 0.449 V vs. NHE (H_2SO_3)

$\Delta G°_{CdS/298}$ = -140.4 kJ/mol

From this data:

$(E°_S - E°_{Cd}) = 0.852$ V

$$-\frac{\Delta G°}{2F} = -\frac{-140.4\,\text{kJ/mol}}{2(9.65\times10^4\,\text{C/mol})} = 0.726\,\text{V} < E°_S - E°_{Cd}$$

Therefore CdS formation from S(IV) is a class 1 reaction and Cd is the potential determining species for the whole range (Kröger (1978)).

An example of when the rate constants of exchange currents of the individual components are vastly different is where the oppositely charged ions react as in the case of

$$Cd^{2+} + S^{2-} \rightarrow CdS$$

There are no electrons involved in the net reaction and the deposition potentials of the two ionic species (Cd^{2+} and S^{2-}) are equal, thus, either species can be used to determine the deposition potential (Kröger (1978)).

2.2.1 Cathodic deposition of CdS

The first cathodic deposited CdS films were reported in 1981 by two separate research groups almost simultaneously (McCann & Kazacos (1981), Power *et al.* (1981)). McCann and Kazacos (1981) used a bath composition of:

0.1 M $CdCl_2 \cdot H_2O$ + 0.1 EDTA + 0.010 M $Na_2S_2O_3$ +0.2 M NH_3 + 0.2 M NH_4Cl

(EDTA: ethylene diamine tetra-acetic acid). The cathodic deposition was performed at –1.15 V (SCE) on a Ti electrode. The Cd-EDTA-NH_3 complex was formed in the bath and made the co-deposition of CdS possible. NH_3 had to be continually added to maintain the correct concentration essential for good quality films. A NH_3 deficiency resulted in Cd-rich film, while an excess inhibited the film growth.

Power *et al.* (1981) used a different bath composition with very different concentration ratios and, hence, the activities of the species differed from those above:

$$0.002\ M\ CdSO_4 + 0.1\ M\ S_2O_3^{2-}$$

The CdS was co-deposited on a platinum rotating disc electrode at 25°C. They found that it was essential to reduce the pH to 2.8, which then resulted in the decomposition of the thiosulphate. No appreciable deposition occurred when the natural pH of 6.7 was used. The deep yellow, uniform, translucent CdS film, which was deposited, was photoactive in sulphide, thiosulphate, sulphite and sulphate solutions.

A number of aqueous bath compositions have been used since the first reports. These have consisted mainly of a cadmium salt and thiosulphate in an acidic medium (Fatas *et al.* (1984), Basol (1988) Dennison (1993)).

The concentrations of the two species differ by a factor 10 to 100 (McCann *et al.* (1981), Power *et al.* (1981), Basol (1988)). This difference in concentration is necessary to bring the reduction potentials closer to each other so that co-deposition can take place. Figure 2.2 shows typical voltammograms of the deposition of the individual species, namely sulphur (from 0.01 M $Na_2S_2O_3$) and cadmium (from 0.2 M $CdCl_2.H_20$), and the co-deposition of CdS (from 0.2 M $CdCl_2.H_2O$ + 0.01 M $Na_2S_2O_3$) (Sasikala *et al.* (1997)). The difference in the concentrations of the species is a factor 20. The pH of the electrolyte solutions also influences the availability of species for electrodeposition as found by Power *et al.* (1981), where lowering the pH to 2 caused the $S_2O_3^{2-}$ to decompose. The concentration of NH_4^+ in solution influences the complexing

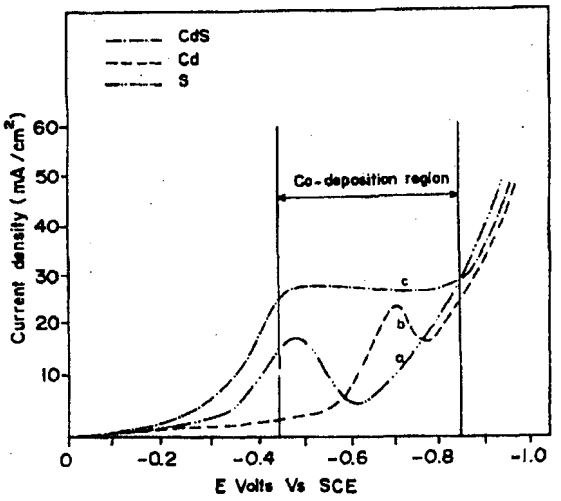

Figure 2.2: Voltammograms of the deposition of (a) sulphur from 0.01 M $Na_2S_2O_3$, (b) cadmium from 0.2 M $CdCl_2.H_2O$ and (c) the codeposition of CdS from a combination of the previous two electrolytes (Sasikala *et al.* (1997)).

of Cd^{2+} species, which in turn inhibits the Cd deposition at certain potentials (McCann and Kazacos (1981)).

2.2.2 *Reaction Mechanisms*

Dennison (1993) proposed that two possible overall reactions could describe the aqueous electrodeposition process under the conditions employed (0.2 M Cd^{2+} and 0.009 M $S_2O_3^{2-}$ at 90°C):

$$Cd^{2+} + S_2O_3^{2-} + 2e^- \rightarrow CdS + SO_3^{2-} \quad (1)$$

or

$$2Cd^{2+} + S_2O_3^{2-} + 8e^- + 6H^+ \rightarrow 2CdS + 3H_2O \quad (2)$$

The first reaction (1) involves $2e^-$ which are used to reduce $Cd^{2+} \rightarrow Cd$. The CdS is then formed by reaction with sulphur which is removed from the $S_2O_3^{2-}$ in the reaction:

$$S_2O_3^{2-} + 2H^+ \rightarrow S + H_2SO_3 \quad (3)$$

This reaction was also previously suggested by Power *et al.* (1981) and Jackowska *et al.* (1986).

The second reaction (2) involves both the reduction of Cd^{2+} and $S_2O_3^{2-}$ before CdS can be formed. This reaction requires additional H^+ to be present and would become more favourable at lower pH values. Dennison (1993) was not able to specify which reaction was dominant since both were electrochemically viable under the conditions used.

Recently, an alternative, three step mechanism for the deposition of CdS from $CdSO_4$ and $Na_2S_2O_3$ was proposed (Nishino *et al.* (1999)). It was proposed that the thiosulphate dissociates to form elemental sulphur, as in reaction (3) above, and then elemental sulphur undergoes a further reaction before the CdS is formed, namely:

$$S + 2H^+ + 2e^- \rightarrow H_2S$$

The overall reaction is then:

$$H_2S + Cd^{2+} \rightarrow CdS + 2H^+$$

This reaction involves two oppositely charged ions which react to form the electrodeposited CdS. From these reaction equations, it can be seen that this mechanism would require an acidic environment for the formation of the H_2S, which is in agreement with previous reports (Power *et al.* (1981)).

All three of these reaction mechanisms are viable and are influenced by the pH of the electrolyte. It is, as yet, not clear which mechanism actually occurs during the electrodeposition process and it could be that it is dependent on the concentration, pH and/or temperature of the electrolyte.

2.2.3 *Rate limiting step*

Until recently, it was generally accepted that the rate limiting step in the electrodeposition of CdS films was the dissociation of the thiosulphate to elemental sulphur (Power *et al.* (1981), Morris and Vanderveen (1992), Dennison (1993)). The reaction mechanism proposed by Power *et al.* (1981), involving the dissociation of the thiosulphate to colloidal sulphur was promoted by the lowering of the pH, and was supported experimentally when lowering the pH resulted in an increase in the deposition (cathodic) current during cyclic voltammetery (Figure 2.3). A similar cyclic voltammogram was obtained by Morris and Vanderveen (1992) using $CdCl_2$ and thiosulphate in an electrolyte solution at 90°C and pH of 2. The anodic peak in Figure 2.3 (b) is attributed to the stripping of elemental Cd from a Cd-rich deposit.

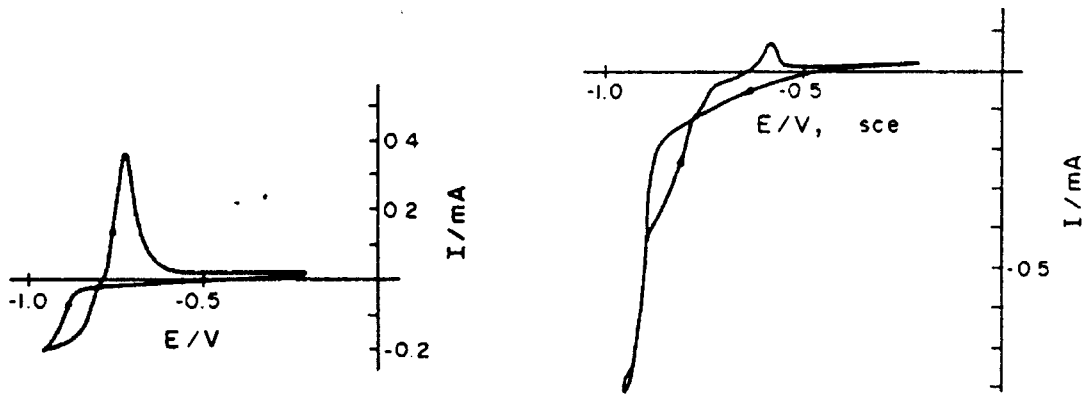

(a) (b)

Figure 2.3: Cyclic voltammograms using (a) the natural pH of 6.7 and (b) the lower pH of 2.8. The solution consisted of 0.002 M $CdSO_4$ + 0.1 M $Na_2S_2O_3$ at 25°C (Power *et al.* (1981)).

Morris and Vanderveen (1992) also reported that increasing the concentration of the thiosulphate increased the rate of deposition at 90° (resulting in the thicker films), which suggested that the deposition rate was dependent on the availability of the sulphur which reacted with the cadmium. These observations are consistent with the mechanism proposed by Power *et al.* (1981), that the thiosulphate dissociation is the rate limiting step.

Using a different electrolytic solution (cadmium source (A in Figure 2.4) – $CdSO_4$ + $(NH_4)_2SO_4$ + glycerol and sulphur source (B in Figure 2.4) – $Na_2S_2O_3$ + NaCl) and room temperature (20°C) conditions with a pH of 3.1, Nishino *et al.* (1999) found that increasing the concentration of the sulphur source with respect to the cadmium source did not change the deposition rate of the CdS (Figure 2.4). This implies that the thiosulphate dissociation is not the deposition rate determining step under the conditions used because the increase in the thiosulphate concentration would have increased the availability of sulphur for the deposition of CdS.

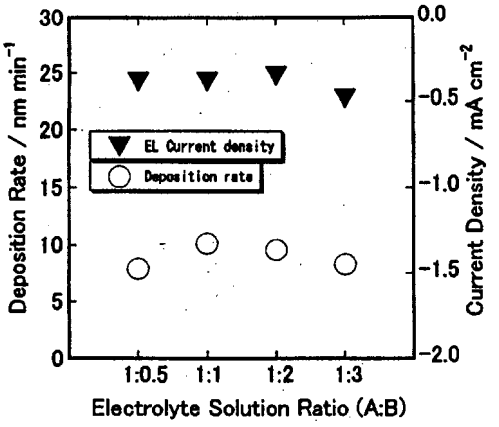

Figure 2.4: Current density and deposition rate as a function of ratio between cadmium source (A) and sulphur source (B) at 20°C (Nishino *et al.* (1999)).

This finding by Nishino (1999) is contrary to previous findings where an increase in the concentration of the thiosulphate was accompanied by an increase in the film thickness and deposition rate at deposition temperatures of 85 - 90°C (Basol (1988), Morris and Vanderveen (1992)). It can therefore be concluded that the decomposition of the thiosulphate is highly temperature sensitive. It is probable, that at much lower temperatures (such as 20°C), a further step that is also temperature dependent could become the rate limiting step in the electrodeposition of CdS, such as the mass transfer of Cd^{2+} to the surface of the substrate, as suggested by Nishino *et al.* (1999). This is most likely when we consider the results obtained by Morris and Vanderveen (1992)

when they increased the concentrations (and therefore the activities) of both the Cd^{2+} and the $S_2O_3^{2-}$ five-fold in relation to their ideal solution. The resulting CdS films were found to be rich in cadmium.

2.2.4 *Influence of deposition conditions on composition*

CdS usually deposits in a near stoichiometric ratio (Das & Morris (1993(b)), Ileperuma *et al.* (1998), Rami *et al.* (1999)). Dennison (1993) concluded that the CdS electrodeposition process is self-regulatory. Unlike CdTe where the composition and electrical properties of the film can be manipulated by adjusting the deposition potential, the CdS deposition was found to self-adjust, making the process independent of the deposition potential. This, however, is contrary to the theory proposed by Kröger (1988) who treated CdS and CdTe electrodeposition in the same way. Nishino *et al.* (1999) found that the incorporation of sulphur in the film decreased as the applied potential was increased from -1.6 V to -1.0 V while depositing at 20°C from the solution mentioned previously. The deposition mechanism reaction proposed by Nishino *et al.* (1999) includes the reduction of the sulphur prior to reacting with Cd^{2+} to deposit as CdS and this involves electron transfer near the substrate surface which would be sensitive to changes in the applied potential.

2.2.5 *Temperature Dependence*

The effectiveness of the initial aqueous electrodeposition of CdS was improved by increasing the bath temperature to 85 – 90°C in a bath composition of:

$$0.1 - 0.5\ M\ CdCl_2 + 0.01\ M\ Na_2S_2O_3$$

when depositing on metallic or ITO coated glass substrates (Basol (1988)). This increase in temperature results in an increase in the rate of disproportionation of $S_2O_3^{2-}$, which was determined to be the rate limiting step (Morris *et al.* (1992)).

This bath composition and temperature range has also been used for depositing CdS films on ITO coated glass substrates using periodic pulsed electrodeposition (Morris and Vanderveen (1992), Das and Morris (1993(a), (b)). A deposition bath combination of:

$$0.2\ M\ CdCl_2 + 0.01\ M\ Na_2S_2O_3$$

used at a pH of 2 (adding HCl) at 90°C produced 100 – 110 nm thick yellow CdS films in 2 hours. The preferred pulsed electric potential condition was a square wave of anodic potential of +0.6 V for 2 s and cathodic potential of 0.95 V for 1 s.

2.2.6 *Non-aqueous electrodeposition*

A number of non-aqueous solvents have also been used for electrodeposition of CdS, such as dimethyl sulphoxide (DMSO), ethylene glycol (EG), diethylene glycol (DEG) and dimethyl glycol (DMG) (Lokhande and Pawar (1989)). These solutions contained cadmium salts (e.g. $CdCl_2$) and elemental sulfur (Baranski & Fawcett (1980)). Since this study concentrates on the aqueous deposition of CdS, no further detail will be given regarding the non-aqueous electrodeposition. A summary of the development and conditions of non-aqueous electrodeposition can be found in Lokhande and Pawar (1989), DeMattei and Feigelson (1992) and Pandey *et al.* (1996).

2.3 Mechanism of electrodeposition nucleation and growth

Most literature on the mechanisms of nucleation and growth of electrodeposits deals with metals. It is expected that the electrodeposition of semiconductors exhibits the same basic mechanisms as the metals.

The overall growth of the electrodeposited thin films is affected by the substrate morphology. Using ideal single crystals as electrodes would provide a perfectly smooth surface, but most electrodes are non-ideal and when a single crystal is used, it will generally contain surface defects such as kinks, steps, dislocations and adsorbed layers, which are sites for growth. Polycrystalline substrates have the added complication of different grain orientations and grain boundaries between the grains (Pandey *et al.* (1996)).

The four basic steps of the electrodeposition process have been summarised graphically in Figure 2.5 and are: (i) transport of the ion toward the interface (ii) discharge of ions at the electrode surface to form the adatoms (iii) nucleation and growth via surface diffusion or formation of clusters of critical nuclei, and (iv) formation of the film (Pandey *et al.* (1996)).

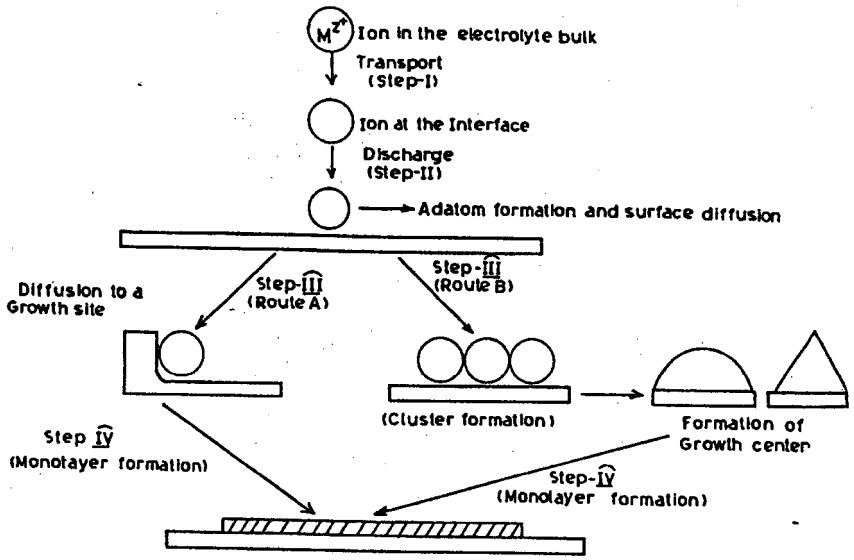

Figure 2.5: Electrodeposition process summary (Pandey *et al.* (1996)).

For nucleation and growth via surface diffusion there are two views on how the monolayer grows once the ions have reached the proximity of the electrode. Pandey *et al.* (1996) are of the view that once the ion reaches the electrode surface, it will usually discharge and desolvate before attaching to the surface to form an adatom. The coulombic forces involved when discharge does not occur make the diffusion of the adions less favourable than the diffusion of adatoms. The adatoms reach the energetically more favourable kinks either by first attaching to the planar surface (and then through planar diffusion reaching the kink) or by directly attaching to the kink site. Further adatoms will attach and diffuse across the surface to the growth sites until the monolayer is complete.

Bunshah (1986) views the nucleation and growth via surface diffusion taking place with the stepwise desolvation of the ion. The adion is first deposited on the electrode in a partly bound state at the surface sites. Diffusion of the adion then occurs until a growth edge or step is encountered, where further desolvation occurs. Further deposition, diffusion and desolvation occurs until the adion is co-ordinated with other ions (and electrons) to become incorporated into the lattice and a monolayer is formed.

The nucleation and growth can also occur by the formation of clusters of critical nuclei; polycrystalline substrates lend themselves particularly to this mechanism. The first stage of growth is the adsorption of individual adatoms on the surface. During the next stage, the adatoms form clusters, which become stable once a critical size has been reached. These clusters provide steps and kinks and act as nucleation sites where further adatoms are accommodated. Nucleation can proceed to form two or three dimensional clusters. Nucleation can be divided into two categories depending on the relationship between nucleation and growth: progressive nucleation and instantaneous nucleation (Fleischmann and Thirsk (1963)).

In progressive nucleation, the nucleation rate is much faster than the propagation rate of new lattice sites. The nucleation and growth are expected to occur side by side. Instantaneous nucleation has the nucleation rate slower than the rate of propagation of new lattice sites. In this case the nuclei form and grow rapidly and the

monolayer is completed (Pandey *et al.* (1996)). According to Despic and Djarovic (1984), both these nucleation processes can occur at any overpotential.

2.4 Influence of substrate on electrodeposited CdS film

In ideal substrates, which are perfectly flat, the diffusion layer thickness and the limiting current are constant over the substrate surface and the uniform film is deposited. Slight variations may occur due to convection effects (Pandey *et al.* (1996)).

For real substrates, the situation is a complex one, since the surface consists of elevations and recesses. Due to a shorter diffusion path which the ion travels from the outer plane of the diffusion layer to the surface of the elevation, these variations on the surface can result in a higher deposition rate at the tip of the elevation compared to the bottom of a recess. The growth at the tips may also be faster since the diffusion in this area may approach spherical diffusion, which is faster than linear diffusion (Kirtchmar (1965)). Despic *et al.* (1968) developed a theory of surface roughness amplification for dc electrodeposition, whereby the surface roughness will increase with time according to the relation between the original height of the protrusion $h(y,0)$ and the height of the protrusion at time t, $h(y,t)$:

$$h(y,t) = h(y,0)\exp\left(\frac{t}{\tau}\right) \qquad \text{Equation 17}$$

where the time constant, τ, is given by:

$$\tau = \frac{\rho}{MD}\left[\frac{\left(\delta_o + zFDc_r^o / j_o f_c\right)^2}{\left(1 - f_a / f_c\right)c_r^o}\right] \qquad \text{Equation 18}$$

M is the molecular weight of the deposit, ρ the density of the deposit, δ_o the diffusion layer thickness, j_o the exchange current density, z the ionic charge involved, F Faraday's constant, D the diffusion coefficient, c^o_r the reactant concentration.

$f_c = e^{-\alpha_c zF\eta/RT}$ and $f_a = e^{+\alpha_a zF\eta/RT}$, where η is the overpotential, α_a and α_c are the transfer coefficients and T the temperture. (Despic *et. al.* (1968), Pandey *et al* (1996)).

The sketch below, Figure 2.6, shows the morphology evolution of the electrodeposit on a smooth ideal substrate (Figure 2.6.(a) left) and on a real rough substrate (Figure 2.6(a) right) (Despic *et al.* (1968), Pandey *et al.* (1996)). The surface roughness amplification can clearly be seen in the sketch as the heights of the protrusions increase exponentially with time (Figure 2.6.(b)).

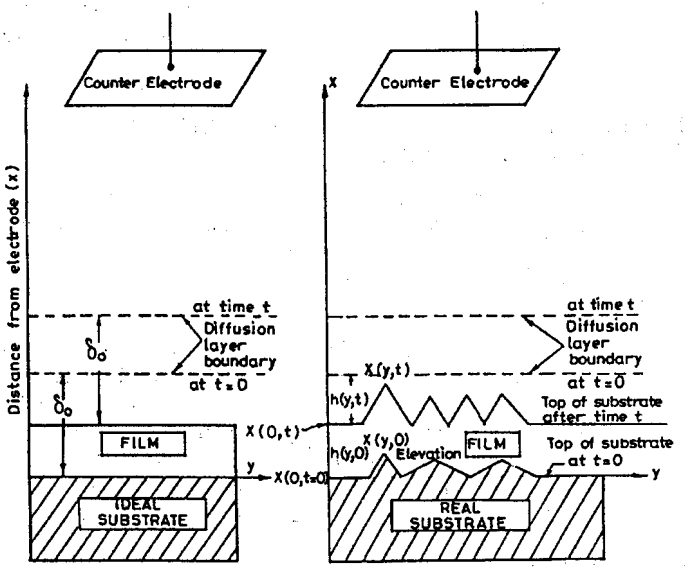

(a)

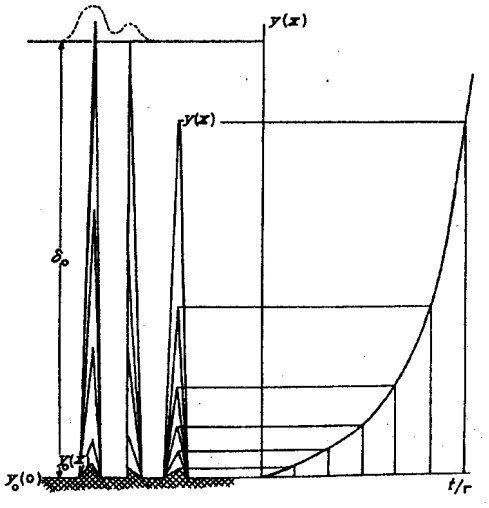

(b)

Figure 2.6: (a) Comparison of the morphology of films on an ideal (left) and real (right) substrate (Pandey *et al.* (1996)). (b) the exponential growth of the protrusion is shown as a function of time.(Despic *et al.* (1968)).

3. Review of Pertinent Literature

3.1. Cleaning of substrates

Preparing the substrate surface prior to deposition of semiconductor thin films is an extremely important part of the processing procedure. The surface preparation is a substrate-specific process and can, in general, consist of grinding and polishing, cleaning and testing the surface cleanliness (Pandey *et al.* (1996)).

For reproducible properties, the cleaning process needs to remove as much of the surface contamination as possible, before the initial thin film is deposited. The cost effectiveness of the deposition and cleaning methods employed need to be considered, as well as the contamination that has to be removed. Elaborate cleaning methods used in single crystal production are expensive and would defeat the purpose of using a cost effective deposition method such as electrodeposition or chemical bath deposition.

Residual contaminants on the surface due to inefficient cleaning methods can affect the nucleation, adhesion, electrical properties of the film and the film-substrate interface, and the morphology of the deposited film, such as the introduction of pinholes due to shadowing effects during deposition or contamination pullout (Pandey *et al.* (1996), Mattox (1996)). The cleaning efficiency of a specific cleaning process depends on, amongst others, the properties of the surface to be cleaned, such as porosity and roughness, and the type of contamination present on the surface. Some common contaminants are fingertip grease, dust, glue and left-over abrasives. A number of cleaning methods can be used to prepare the surface for electrodeposition. Cleaning by solvents, heating and etching are a few techniques that are used extensively. Pandey *et al.* (1996) discuss the cleaning of substrates at some length. The important factors to bear in mind are the type of surface and the type of contamination expected. In the case of deposition onto coated glass substrates, the solvent cleaning method is the most commonly used.

Trichloroethylene (TCE) is commonly used as a degreasing agent. It is, however, toxic and carcinogenic and leaves a residue on the surface which needs to be removed using additional cleaning solvents such as isopropanol (Mattox (1996)). Acetone and hexane are also widely used as degreasing agents. They too, require further washing in solvents such as isopropanol to remove residues from the surface, but the health hazards are not as serious as those of TCE (Pandey *et al.* (1996), Mattox (1996)).

Two of the most commonly used cleaning methods previously used to prepare transparent conducting oxide substrates for electrodeposition or chemical bath deposition of thin film photovoltaic cells, such as CdS/CdTe, are:

- acetone, methanol and isopropanol washes of 15 minutes followed by isopropanol vapour degreasing of 3 hours (Das (1993(a)))
- ultrasonic isopropanol wash, ethanol wash, ethanol wipe, ethanol wash, deionised water wash, isopropanol wash and isopropanol degreasing (Danaher (1985))

The effectiveness of these cleaning methods was not reported.

A number of tests are available to determine the cleanliness of the surface after cleaning. These vary from a simple breath figure test to the use of low energy electron diffraction (LEED). Some of the other methods include atomizer test, coefficient of friction test, edge lighting test, water drop contact angle and Auger electron spectroscopy (Brown (1970), das Neves *et al.* (1994), Pandey *et al.* (1996)). Atomic Force Microscopy was used to characterise Si-SiO_2 surfaces after H-plasma cleaning to determine whether a reaction between the surface and the plasma had occurred (Carter *et al.* (1994)).

3.2. Influence of Temperature and pH on the Deposition Process

The first cathodic electrodeposition of CdS from aqueous solutions were carried out at room temperature (25°C) (Power *et al.* (1981), McCann & Kazacos (1981), Fatas *et al.* (1984)).

Using a bath composition of:

$$0.1\ M\ CdCl_2 \cdot H_2O + 0.1\ EDTA + 0.010\ M\ Na_2S_2O_3 + 0.2\ M\ NH_4 + 0.2\ M\ NH_4Cl$$

it was essential to maintain the correct NH_4 concentration, since an excess inhibited the electrodeposition of the CdS. In this case the Cd^{2+} formed a complex with the EDTA, and the NH_4 concentration influenced the potential at which CdS deposited exclusively. A lower concentration of NH_4 resulted in the co-deposition of Cd, forming a Cd-rich film (McCann et el (1981)).

When depositing from the aqueous solution of $CdSO_4$ + $Na_2S_2O_3$ at 25°C, no appreciable deposition occurred at the natural pH of 6.7. The deposition rate increased significantly when the pH was lowered to 2.8 and this resulted in the increase in the rate at which the thiosulphate dissociated to sulphur (Power *et al.* 1981)). Dennison (1993) also reported an increase in the thickness of films electrodeposited for 60 minutes as the pH decreased from 4.35 to 3.48, which implies an increase in the deposition rate.

Lowering the pH of the aqueous solution of Cd^{2+} + $S_2O_3^{2-}$ to below 2, yellow CdS precipitates developed rapidly in the electrolyte at temperatures above 40°C, while pH values of higher than 3 resulted in white precipitates, $Cd(OH)_2$ (Sasikala *et al.* (1997), Rami *et al.* (1999)). These precipitates could attach themselves to the substrate, and therefore need to be avoided in order to produce a homogeneous thin film. CdS precipitates did form in the electrolytes with pH values between 2 and 3, at temperatures of 90°C, as the solution aged, but not as rapidly as with the lower pH values (Rami *et al.* (1999)). The pH of an electrolyte (0.2 M $CdCl_2$ + 0.009 M $Na_2S_2O_3$) at 90°C was found to decrease significantly from an initial value of 4.8 to

below 3.5 with time. When the temperature of the electrolyte was lowered to room temperature, the pH was stable (Dennison (1993)). No decrease in pH has been reported when using electrolytes with initial pH values of 2 – 3. This would suggest that the ideal pH for aqueous electrodeposition therefore lies between 2 and 3, since the deposition rate is increased to an acceptable level, the rate of precipitate development is not as rapid and, therefore, incorporation of the CdS precipitates into the film is minimal, resulting in a uniform and adherent deposit.

Using similar electrolytic solutions to Power *et al.* (1981), an increase in the deposition temperature (from 25°C to approximately 90°C) resulted in an increased deposition rate and thickness of the films (Basol (1988), Morris & Vanderveen (1992), Dennison (1993), Sasikala *et al.* (1997)). This was attributed to the increase in the rate of disproportionation of the $S_2O_3^{2-}$, making more sulphur available for deposition at the higher temperatures. The microstructural quality of the films examined by scanning electron microscopy improved with an increase in temperature (Morris and Vanderveen (1992)).

3.3. Deposition of CdS thin film on different substrates

The substrate used for the deposition of CdS influences the structure and morphology of the final thin film for all types of deposition. This, in turn, influences the properties of these films. A few examples of the influence of the substrate will be discussed further below.

Evaporated CdS films have been grown on single crystal NaCl and germanium substrates of different orientations (Wilcox *et al.* (1969), Abdalla *et al.* (1973)). It was found that the (100) and (110) surfaces resulted in CdS with a cubic structure, while, on the (111) surface, the hexagonal CdS with a preferred orientation of (0001) was deposited. This is due to the symmetry matching between the substrate surface and the deposit. MOCVD of CdS onto glass and InP (100) and (111), on the other hand, have all resulted in hexagonal CdS. The CdS on the glass substrate had a slight (0001) orientation, while the CdS deposited on the single crystal substrates had strong (0001) orientation when depositing at 450°C. At 500°C , the InP (111)

substrate resulted in (0001) orientation while on InP(100) substrate CdS films consisted of macro-scale domains with (0001) and ($10\bar{1}1$) orientations (O'Brien *et al.* (1996(b))).

Using chemical bath deposition onto glass substrates and indium tin oxide (ITO) /glass substrates has produced CdS films with a mixed cubic and hexagonal phase (Uda *et al.* (1990), Bhattacharyya *et al.* (1996)). Bhattacharyya *et al.* (1996) reported peak shifts towards lower 2θ values for films deposited on the ITO/glass substrates relative to the glass substrates in the as-deposited films. This shift was attributed to tensile stresses in the films due to differences in the lattice constants of the CdS and ITO. Cubic CdS has also been reported when depositing on ITO/glass substrates using various CBD solutions (Toušková *et al.* (1998)). As with vapour deposition, CBD onto single crystal surfaces resulted in preferential growth of one of the phases either as polycrystalline films or monocrystalline film. The (111) InP and (111) Si resulted in the formation of cubic phase CdS from chemical bath deposition in contrast to the hexagonal phase when evaporating CdS films. Amorphous carbon and ($\bar{1}\bar{1}\bar{1}$) InP favoured the formation of hexagonal CdS (Froment *et al.* (1995)).

For the cathodic electrodeposition of CdS films from non-aqueous based electrolytes, various metal substrates influenced the final quality of the films such as the roughness, preferred orientation of the cubic-CdS and the thickness of the films (Baranski *et al.* (1981), (1983)).

Cathodic electrodeposition from aqueous electrolytes onto various metal substrates (platinum, molybdenum and aluminium) at 25°C resulted in significant differences in the cyclic voltammograms, final film quality and composition (Fatas *et al.* (1984)). The CdS films deposited on the platinum substrates had a maximum thickness of 1000Å with stoichiometric CdS (Power *et al.* (1981), Fatas *et al.* (1984)), however, the molybdenum substrate produced poor deposits which were very thin and had a very high sulphur content (~98%). This is contrary to the successful electrodeposition onto molybdenum substrates from diethylene glycol (DEG) based electrolytes by Baranski *et al.* (1983) at 120°C. Based on impedance measurements, the poor film quality on the molybdenum was attributed to a blocking

effect of the adsorbed sulphur on the molybdenum which prevented further deposition under the conditions used by Fatas *et al.* (1984). When replacing the molybdenum with aluminium, the resulting deposit was a thick, yellow, translucent film which was found to be near stoichiometric, hexagonal CdS with no preferred orientation after long deposition times (Fatas *et al.* (1986)). This different deposition behaviour has been attributed to a different electrode mechanism compared to the molybdenum substrate, in that for the aluminium, a chemical reaction, coupled to the charge transfer, was proposed to have taken place. This was also supported by impedance studies (Fatas *et al.* (1984)).

Cathodic electrodeposition onto non-metallic substrates such as indium tin oxide (ITO) / glass and SnO_2 / glass have been the focus of more recent studies due to the application of CdS as window layer in the CdS/CdTe solar cell. The ITO substrates generally resulted in hexagonal electrodeposited CdS films (Morris and Vanderveen (1992), Dennison (1993), Shirai *et al.* (1996), Sasikala *et al.* (1997), Yoshida *et al.* (1999), Nishino *et al.* (1999), Rami *et al.* (1999)). Using potentials of –1.4V and –1.6V (vs. Ag/AgCl) (Nishino *et al.* (1999)) and low temperatures (Rami *et al.* (1999)), CdS films with amorphous structure, as determined by XRD, have been identified. Cubic CdS has also been electrodeposited on SnO_2/glass substrates (Fatas *et al.* (1987), Chu *et al.* (1992)).

Hexagonal, fine grained CdS films have been successfully electrodeposited onto copper indium diselenide (CIS) substrates to form good quality rectifying diodes for photovoltaic applications (Raffaelle *et al.* (1999)).

In summary, it has been shown that the orientation of the substrate influences the structure and quality of the CdS due to resulting stresses, lattice mismatch, differences in thermal expansion and deposition mechanisms. The type of deposition technique used also influences the structure of the CdS film (Wilcox *et al.* (1969), Abdalla *et al.* (1973), O'Brien *et al.* (1996(b)). Although deposition onto metallic substrates is no longer frequently used, the earlier reports indicate that, even when depositing on different good conducting metallic substrates, the deposition mechanism is significantly influenced by the type of metal and its properties (Fatas *et al.* (1984), (1986)). Deposition onto conducting oxide

substrates, such as indium tin oxide, using chemical bath deposition, produces films with mixed cubic and hexagonal phase CdS present (Toušková *et al.* (1998)). The electrodeposited CdS films have the tendency to deposit from aqueous solutions, at temperatures in the range of 80 – 90°C, in the hexagonal phase, onto conducting oxide substrates such as ITO / glass substrates (Morris and Vanderveen (1992), Shirai *et al.* (1996), Sasikala *et al.* (1997)). Amorphous CdS films have been reported when lowering the deposition temperature (Rami *et al.* (1999)) or the deposition potential (Nishino *et al.* (1999)).

The substrate does not only influence the morphology and structure of the film, but has been found to influence the electrical properties of the CdS film and CdS/CdTe solar cell as a whole.

Das (1993(a)) electrodeposited the CdS on three different transparent conducting oxide (TCO) substrates, having the same sheet resistivities (10 Ω/□), under the same conditions. The growth rates were observed to be the same on all three substrates. The properties of the individual CdS layers were not reported. Having deposited a CdTe film onto the CdS, the solar cells were analysed after annealing, etching and contact deposition. It was found that the cells differed in their current-voltage curves, spectral response and efficiencies – Table 3.1 below. The current transport in the cells was found to be substrate specific, in that the tin oxide

Table 3.1: Summary of results by researchers using different substrates.

Reference	Deposition method of CdS	Substrate	Efficiency
Das (1993(a))	Electrodeposited	Flourine doped tin oxide (FTO)	8.1%
		(ITO/SnO_2)	8.9%
		Indium tin oxide (ITO)	11.5%
Ramanathan *et al.* (1993)	CBD	SnO_2/Soda-lime glass	10.6%
		SnO_2/Borosilicate glass	11.3%
Ferekides *et al.* (2000)	Close space sublimation	SnO_2/Soda-lime glass SnO_2/Borosillicate glass	14.3% 15.0%
Britt *et al.* (1993)	CBD	SnO_2/Borosilicate glass	>15.8%
Ferekides *et al.* (1994)	RF Sputtered	SnO_2/Soda-lime glass	11.6%

substrate cells were controlled by recombination/generation in the depletion layer and by interface recombination and tunnelling, while in the ITO substrate cells were solely controlled by interface recombination and tunnelling (Das (1993(a)).

The cell properties where CdS was chemical bath deposited onto tin oxide substrates with different glass substrates (soda-lime and borosilicate) were found to differ significantly (Ramanathan *et al.* (1993)). CdTe deposited on CdS/SnO_2 / soda-lime reacted more vigorously with $CdCl_2$ compared to those deposited on CdS/SnO_2/ borosilicate glass and areas of discoloration and lifting of the CdTe were sometimes evident. The differences in the reactivity were attributed to thermal stresses in the films and diffusion of impurities from the soda-lime glass into the cell. These differences also influenced the electrical properties of the cells, resulting in differences in efficiencies of nearly 1% in the solar cells produced on these substrates (Table 3.1). Ferekides and co-workers (Britt *et al.* (1993), Ferekides *et al.* (1994), Ferekides *et al.* (2000)) used various deposition techniques such as CBD, RF sputtering and close space sublimation (CSS), for the deposition of CdS onto soda-lime and borosilicate glass substrates. As with Ramanathan *et al.* (1993), the soda lime substrate exhibited poorer cell properties and lower efficiencies than the borosilicate glass substrates. The difference in the efficiencies could be due to the lower substrate temperature during deposition of the CdTe by CSS, which was necessitated by the lower softening point of the soda-lime glass (Ferekides *et al.* (1994)) (Table 3.1). None of these studies reported the band gaps of the CdS films.

It can be concluded that the substrate usually forms part of the cell, in that the transparent conducting oxide is also used as a front contact for the cell in most cases and the interface properties between the substrate and the CdS film are pertinent to the efficiency of the cell. Niles *et al.* (1993) have studied the photoemmission properties of the front contact consisting of CdS and SnO_2 in an attempt to determine whether the contact is thermally stable. They found that there was no diffusion of Cd, Sn or S across the interface, even after annealing.

3.4. Microstructure and Composition

CdS can be deposited in two crystalline structures, namely the cubic and hexagonal (wurtzite) structures. The type of CdS structure depends on the substrate used and the deposition technique, as discussed in section 3.3. This discussion of the microstructure and composition of CdS films will concentrate on electrodeposited CdS films, but pertinent results from other studies will be discussed where they are relevant. The influence of the substrate on the crystal structure has been discussed in detail in Section 3.3, and will not be dealt with again.

3.4.1. Electrodeposited CdS

In one of the first studies of aqueous cathodically electrodeposited CdS on platinum substrates, it was reported that the film consisted of a closely packed polycrystalline deposit (Power *et al.* (1981)). The composition of the film was determined with a microprobe and reported to have approximately equal amounts of cadmium and sulphur and no contaminants were detected, but a precise determination of the stoichiometry was not possible. The x-ray analysis of the films was not conclusive due to the thinness (<1μm) or the poor crystallinity of the films.

Using the same conditions as above, Fatas *et al.* (1984) deposited CdS onto different substrates at 25°C. The CdS deposits were not homogeneous in composition or structure and depended on the substrate used. The molybdenum substrates produced sulphur rich films consisting of up to 98% sulphur according to EDX studies. The CdS deposited on the aluminium substrates had two types of deposit, namely large deposited particles containing >90% sulphur and smaller particles with a porous structure which contained 68% Cd and 32% S. For longer deposition times, the cadmium content decreased from 68% to 58% (Fatas *et al.* (1984), (1986)). Using both XRD and TEM the thin film CdS deposit was identified as hexagonal CdS particles with no preferred orientation. These differences in deposition have been attributed to deposition mechanism onto the substrate (Section 3.3).

Electrodeposition of CdS from aqueous solutions resulted in predominantly hexagonal CdS films with a yellow, yellow-orange to greenish-yellow colour for deposition temperatures ranging from 90°C to 25°C (Morris *et al.* (1992), Das *et al.* (1992), Shirai *et al.* (1996), Sasikala (1997), Ileperuma *et al.* (1998), Rami *et al.* (1999), Nishino *et al.* (1999)). Amorphous (Rami *et al.* (1999), Nishino *et al.* (1999)) and cubic (Fatas *et al.* (1987), Chu *et al.* (1992)) CdS films have also been electrodeposited under certain conditions.

The influence of the deposition potential on the morphology, microstructure and composition of the electrodeposited CdS is varied. Dennison (1993) reported that a change in the deposition potential did not change the rate of deposition and concluded that the electrodeposition mechanism was self-regulating and therefore the composition of the CdS could not be adjusted by potential variation. No phase or compositional analysis was reported and the conclusions were based on voltammogram studies.

A more detailed investigation of the dependence of the structure and composition of the CdS films on deposition potential was undertaken by Sasikala *et al.* (1997). When altering the deposition potential between –0.5 V to –0.8 V vs SCE, with a pH of 2-3 and temperature of 90°C, there was no shift in the peak positions of the hexagonal CdS phase, although there were significant differences in the physical appearance of the thin films. It was reported that depositing between –0.5 V and –0.6 V resulted in stoichiometric CdS films which had a yellow colour. Decreasing the deposition potential to between –0.6 V and –0.7 V resulted in a greenish-yellow coloured cadmium-rich film and for deposition potentials of –0.7 V to –0.8 V the film was metallic grey coloured with Cd dendrites observed on the surface. No quantitative compositional analyses were reported for these films, but Raeffaelle *et al.* (1999) also reported an increase in the elemental cadmium concentration with more negative potentials. These results are not in agreement with the findings of Dennison (1993) which were based on voltammograms, using similar electrolyte solutions at higher pH values of 3 – 4.8.

Using a similar electrolyte solution at room temperature, Nishino *et al.* (1999) reported an orientation difference in the hexagonal CdS films when the negative deposition potential in rectangular voltage cycles was changed from a low of –1.0 V and a high of 0 V to –1.2 V and 0 V vs Ag/AgCl with a pH of 3.1. The –1.0 V deposition potential produced hexagonal CdS with a preferred orientation along the a-axis, while the –1.2 V deposition potential had a preferred orientation along the c-axis. This change in preferred orientation was attributed to the higher deposition rate when using the –1.2 V potential, which then favours growth along the c-axis due to the lower surface energy on this plane. In both these cases the Cd/S ratios, as determined by auger electron spectroscopy and electron probe micro analyser, were close to 1. For still lower deposition potentials of –1.4 V and –1.6 V the films were found to be amorphous with a high sulphur content (Cd/S ratio of less than 0.33). This is contrary to the findings Sasikala *et al.* (1997) where the more negative deposition potential resulted in a higher cadmium content. Some of the excess cadmium could have been removed in the anodic cycle of the periodic pulse of the electrodeposition, but the excess sulphur was attributed to the deposition mechanism where the sulphur reduction is controlled by electron transfer at the substrate surface, which is governed by the applied potential.

Individual particle size and morphology have been observed by electron microscopy techniques and calculated from x-ray diffraction spectra using the Scherrer equation (Morris *et al.* (1992)). The initial films electrodeposited onto metallic substrates were relatively flat films and exhibited severe cracking (Baranski *et al.* (1981), (1983)) and high porosity (Fatas *et al.* (1986)). No further detail of the microstructure was observed at the scanning electron microscopy magnifications used. More recently, uniform, adherent films have been electrodeposited and, with high resolution SEM techniques, the morphology of the individual particles and grains have been imaged. Morris *et al.* (1992) reported individual particles of 56 nm in size as calculated from the Scherrer equation, which is in good agreement with the SEM image of the film. Ileperuma *et al.* (1998), using very similar electrolytic conditions to Morris *et al.* (1992), found no crystalline features on the film with SEM

studies. Using x-ray diffraction, the deposit was identified as hexagonal CdS, but there was a high background count on the spectra and considerable peak broadening. When electrodepositing from a non-aqueous solution at a higher temperature of 170°C (Ileperuma *et al.* (1998)), well developed grains of > 100 nm were observed and the x-ray diffraction spectra had substantially narrower peaks and lower peak to noise ratio. The broad peaks obtained for the aqueous deposition could have been due to small crystallite size, as reported by Flood *et al.* (1995) and Shirai *et al.* (1996).

The morphology of hexagonal CdS electrodeposited films has been found to be substrate dependent. Yoshida *et al.* (1999) reported that electrodeposition onto ITO substrates, at a pH of 3.2, formed rice-like grains of 100 – 200 nm in length with no obvious preferred orientation. Using a nickel substrate, the grains were much smaller, conical in form and more uniform in size with a diameter of 70 nm. The grains showed strong (002) orientation on the nickel substrate. In both cases, it was seen that the thickness of the films was due mainly to the growth of the individual grains since the height of the grains and the thickness of the film did not differ substantially.

Rami *et al.* (1999) investigated the growth of CdS films by electrodeposition as a function of deposition time, using atomic force microscopy. The deposition conditions were very similar to those used by Morris *et al.* (1992). During the initial stages of film growth, the grains grew independently in three dimensions, increasing in size until interference from adjacent grains occurred. The growth in the horizontal direction during this stage was, however, faster than the vertical growth, with the grains reaching 250 nm diameter and 20 nm thickness after 40 minutes deposition. Once the substrate had been covered by the individual grains, the vertical growth occurred rapidly, without any increase in the grain diameter after 40 minutes, while the thickness increased to 70 nm after 3 hours. During the deposition, the RMS roughness of the surface increased from 5 nm for the clean substrate to 10 nm when the substrate was covered with CdS. As with the grain diameter, the RMS roughness did not increase further with time.

The electrodeposited CdS films are generally not excessively contaminated during the deposition process, since the conditions used are specific for the species in question, namely Cd and S. Specific elements can be incorporated in the film during the electrodeposition process if the electrolyte is tailored in the correct concentrations and the appropriate deposition potential is used, such as the incorporation of thallium in the CdS film by Baranski *et al.* (1981).

Aqueous electrodeposition of CdS at 90°C has been analysed using XPS, Auger electron spectroscopy and EDX methods, and have been found to consist of Cd and S, with oxygen and carbon usually present on the surface (Morris *et al.* (1992), Ileperuma *et al.* (1998)). It was usually necessary to normalize all analyses with respect to a standard CdS sample, due to the sensitivity factors of the instruments (Morris *et al.* (1992), Dahaher *et al.* (1985)). The Cd:S ratio was found to be the same as that of monocrystalline CdS when pulse depositing with an anodic potential of +0.6 V (Morris *et al.* (1992)). Increasing this potential to >0.6 V resulted in poor surface coverage and porous CdS films. The films deposited with an anodic voltage of +0.6 V exhibited a film of uniform composition and a clear CdS/ITO interface when compared to those deposited with higher anodic potential. Contrary to the report by Dennison (1993), who suggested that the electrodeposition of CdS is self-regulatory, the composition of the electrodeposited film was found to be influenced by the deposition potentials used (Raffaelle *et al.* (1999), Rami *et al.* (1999)). Raffaelle *et al.* (1999) found that decreasing the deposition potential from –1.2 V to more negative values resulted in the films changing from having Cd:S ratios of 1:1 to cadmium rich films. On depth profiling, they found an increase in the sulphur content near the molybdenum interface. Rami *et al.* (1999), on the other hand found the opposite, i.e. a decrease in the cadmium and an increase in the sulphur content with a decrease in deposition potential from –0.5 V to –0.64 V. Chlorine was also detected in these films due to contamination from the electrolyte which contained $CdCl_2$. These two studies used the same precursors, but there were differences in the concentrations of the electrolytes and, therefore, differences in the deposition potentials and the resulting observations.

3.4.2. *Other deposition techniques*

Chemical bath deposition has been studied extensively with a view to lowering the cost of processing CdS/CdTe solar cells. There are many studies of the morphology and composition of these films (Kolhe *et al.* (1984), Danaher *et al.* (1985), Al-Jassim *et al.* (1993), Kylner *et al.* (1996), Stoev *et al.* (1996), Mendoza-Galván *et al.* (1996)) and the results show that the morphology and composition of CBD CdS are process dependent.

The crystal structure of the CBD CdS appears to be strongly dependent on the processing solution. Some researchers report the as-deposited film to have a cubic structure (Kolhe *et al.* (1984), Mendoza-Galván *et al.* (1996), Pandey *et al.* (2000)), others report a hexagonal structure (Danaher *et al.* (1985)) while some studies report the as-deposited film to be amorphous (Stoev *et al.* (1996), Al-Jassim *et al.* (1993)). The crystal structure of CBD CdS has been found to be temperature dependent and it has been observed to deposit in the cubic structure at 60°C and the hexagonal structure at 30° (Froment *et al.* (1995)), and to improve in crystallinity as the deposition temperature is increased (Sasikala *et al.* (2000)).

When viewing the films under electron microscopes, researchers have found a wide variety of grain structures in the CBD CdS films. These range from non-oriented polycrystalline films with small grains of ~10 nm in size (Al-Jassim *et al.* (1993)) to highly oriented films with a fibrous, dendritic structure (Al-Kuhaimi (1998), Toušková *et al.* (1998)) to very fine grains with no crystalline features (Ileperuma *et al.* (1998)). The columnar structure of the grains, found also in the electrodeposited films, was also observed in some as-deposited CBD films (Rossetti *et al.* (1983)), but the films were generally fine grained (0.01 μm – 0.5 μm) and exhibited the characteristic broadening of XRD spectra. Danaher *et al.* (1985) reported a combination of two types of structures, namely dense small crystallites (0.1 μm – 0.2 μm in diameter) and larger lumps embedded in the surface (0.5 μm), probably from colloidal particles formed in solution, which are then adsorbed. Similar particles have

Table 3.2: Summary of thin film CdS composition results obtained from XPS and other analytical techniques.

Deposition	Cd:S	Elements present	Comments	Reference
Electrodep.	1 : 1	Cd, S	Stoichiometry not accurate	Power *et al.* (1981)
Electrodep.	<2 : >98		Mo substrate	Fatas *et al.* (1984), (1986)
Electrodep.	10 : 90 58 : 42		Al substrate – S-rich area Longer deposit time	
Electrodep.	1 : 1	Cd, S, O, C	As deposited – O, C on surface only	Morris & Vanderveen (1992)
CBD	Not given	Cd, S, O, C	As deposited	Kolhe *et al.* (1984)
CBD	Not given	Cd, S, O, C	Cd excess after 300°C anneal in air. Less O, C	Kolhe *et al.* (1984)
CBD	1.04 : 1	Cd, S, O, C	As deposited – stoichiometric CdS	Danaher *et al.* (1985)
CBD	1.05 : 1	Cd, S, O, C	450°C anneal in H_2 – not much change in CdS composition	Danaher *et al.* (1985)
CBD	Not given	Cd, S, O, C, N, H	Impurities due to the processing precursors.	Kylner *et al.* (1996)
CBD	~ 2 : 1	Cd : S : Cl : O 48.9 : 25: 0.2 : 25.9	As deposited	Stoev and Katerski (1996)
CBD	~ 3 : 1	Cd : S : Cl : O 31.1:10.6:16.5:41.8	$CdCl_4$ surface treatment and exposure to air increased Cl and O content.	Stoev and Katerski (1996)
CBD	1.2 : 1	Cd, S, O	Only surface oxygen was present after RTA.	Jayakrishnan *et al.* (1996)
Spray Pyrolosis	0.9 – 1.0 : 1	Cd, S, O, C, Cl	There was preferential sputtering of Cd. Oxygen content decreased on sintering.	Kohle *et al.* (1987)

been observed to be adsorbed on the surface and then removed by washing, ultrasonic cleaning or by tapping the substrate against something (Toušková *et al.* (1998), Dennison (1993)).

The compositional analyses of CBD films have been widely studied and it can be concluded that the bath composition and the deposition conditions play a crucial role in the compositional purity of the CBD film. The chemical precursors have been found to introduce impurities into the film, the most common being residual carbon, chlorine and oxygen. Table 3.2 compares some of the compositional studies of as deposited CdS using electrodeposition, CBD and spray pyrolosis deposition techniques.

3.4.3. *Annealing CdS*

Annealing of the CdS layer in a cell usually occurs after the CdTe film has been deposited (Ferekides *et al.* (1993), (Das (1993(a), (b)), Danaher (1985), Jayakrishnan *et al.* (1996), Kolhe *et al.* (1987), Matthew *et al.* (1995), Ebothe (1996), Gallaway *et al.* (1996)), but annealing studies of the CdS films specifically have been undertaken prior to CdTe deposition (Kohle *et al.* (1984), Jayakrishnan (1994),(1996)). The purpose of annealing in the CdS/CdTe solar cell is to encourage grain growth in the CdTe layer, so as to reduce the number of grain boundaries and, hence, the defects associated with these. This then improves the efficiency of the cells (Al-Jassim *et al.* (1993)).

In the CdS film, the annealing process results in grain growth (Lee *et al.* (1987), Morris *et al.* (1992), Al-Jassim *et al.* (1993)), which is sometimes also accompanied by a structural change from cubic or amorphous to hexagonal phase when the annealing temperature is high enough (Kohle *et al.* (1984), Lozada-Morales *et al.* (1996), Mendoza-Galván *et al.* (1996), Stoev *et al.* (1996), Ichimura *et al.* (1999),). These larger grained CdS films form better substrates for junction formation between the CdS and CdTe films (Lee *et al.* (1987)).

After annealing the electrodeposited CdS films at 400°C for 15 minutes in air, Morris *et al.* (1992) found that the film showed less preferred orientation and the peaks of the XRD spectra were narrower and of higher intensity than those of the as-deposited films, indicating improved crystallinity.

Table 3.3: Summary of annealing conditions used after various methods of deposition.

Deposition	Atmosphere	Temperature	Time	Comments	Reference
CBD	N_2	>450°C		Sulphur loss on surface	Al-Jassim *et al.* (1993)
CBD	N_2 + $CdCl_2$	>450°C		Fewer in planar defects Decreases sulphur loss	Al-Jassim *et al.* (1993)
CBD	Vacuum	300-330°	2 hr	Decreased resistivity, not as much as H_2	Danaher *et al.* (1985)
CBD	H_2	450°C	4 hr	O_2 desorption Decreased resistivity No change in Cd/S ratio	Danaher *et al.* (1985)
CBD	Vacuum Air + $CdCl_2$	600°C 400°C	30 min	Rapid thermal annealing Oxygen eliminated Strong (0002) orientation	Jayakrishnan *et al.* (1994, 1996)
CBD	Air	300°C	30 min	Cd-rich after annealing Cd peak shift due to CdO formation	Kolhe *et al.* (1984)
CBD	Air	200°C - 350°C		Decrease in O content	Kylner *et al.* (1996)
CBD	Ar	208°C – 447°C	28 hr	Cubic to hexagonal transition at 260°C	Mendoza-Galván *et al.* (1996)
CBD	Ar+$CdCl_2$	400°C	30 min	Exposure to air increases Cl and O contents. Cd/S ratio increases to 3	Stoev & Katerski (1996)
CBD	Ar	200°C – 450°C	28 hr		Tomás *et al.* (1995)
Electrodep.	Air + $CdCl_2$	400°C	15 min	Well crystalline large grains. Decrease in resistivity	Morris *et al.* (1993), Das (1993(b))
Electrodep.	Air	400°C	15 min	Decrease in resistivity Decrease in band gap	Morris *et al.* (1992)
Electrodep.	N_2	200°C - 500°C	30 min	Rearrangement of Cd and S atoms to form Cd-S bonds. Colour change Brown to yellow Improved crystallinity	Shirai *et al.* (1996)
Evaporation	Air + $CdCl_2$	400°C	20 min		Galloway *et al.* (1996)
Screen Print	N_2-H_2	670°C	120 min	One step in a number of heating steps during the production of a cell.	Yoshida *et al.* (1993)
Spray Pyrolysis	Air, O_2, H_2, N_2, He, Ar, Vacuum	420°C	6hr (2hr in H_2)	2 – 3 mm diameter grains after annealing in air. Small crystallites after O_2 annealing	Ebothe (1996)
Spray Pyrolysis	Air Vacuum (10^{-4} Torr)	100°C – 300°C 350°C	45 min		Matthew *et al.* (1995)
Spray Pyrolysis	Air	200°C – 400°C	10 min	S vacancies increase as annealing temp. increases. Resistivity decreases	Kohle *et al.* (1987)

The grain size was larger than the as-deposited film with an average of 70 nm, compared to 56 nm as-deposited.

A number of atmospheres have been used to anneal the CdS films, with air, nitrogen, nitrogen/hydrogen and argon being the most commonly used (Table 3.3). When annealing in air, there is generally extensive oxidation of the surface if the CdS is unprotected, but when the annealing is done with the CdTe layer in place, this oxidation is significantly less (Basol (1984), Kohle *et al.* (1984)). Kylner *et al.* (1996), on the other hand, did not report any oxide formation after annealing at 350°C, but did report that the water is no longer detected. This discrepancy can be attributed to the different processing techniques used during deposition. Annealing in vacuum, nitrogen or hydrogen (20kPa) results in the desorption of the oxygen in the film (Danaher *et al.* (1985), Kohle *et al.* (1987)). There are some reports of the formation of sulphur vacancies during H_2 annealing (Mitchell *et al.* (1975)) and others where the Cd/S ratio of the films after H_2 annealing did not differ significantly from the as-deposited film (Danaher *et al.* (1985)). Cd-deficient films have also been reported after annealing in a hydrogen atmosphere (Rohatgi *et al.* (1991)). The CdS film can be successfully doped during annealing to improve the electrical properties when using a H_2 atmosphere carrying In or Cd vapour (Danaher *et al.* (1985)).

The presence of $CdCl_2$ during the annealing process has been shown to be essential in producing good quality CdS films and more efficient CdS/CdTe photovoltaic cells. A saturated solution of $CdCl_2$ in methanol can be used to coat the CdS surface prior to annealing (Das (1993(b))). The $CdCl_2$ acts as a flux, resulting in larger well crystalline grains (500nm and larger) in both CdS and CdTe (Lee *et al.* (1987), Al-Jassim *et al.* (1993), Das (1993(b))). It prevents the loss of cadmium and sulphur during heat treatment, thus producing more stoichiometric CdS films, which result in more efficient photovoltaic cells due to few interface states (Danaher *et al.* (1985), Morris *et al.* (1993), Al-Jassim *et al.* (1993)). The presence of the $CdCl_2$ promotes the phase transformation of cubic CdS to hexagonal CdS when annealing under the same conditions (Johnson (2000)).

The specific annealing of electrodeposited CdS films has been reported in a few studies. The electrodeposited CdS is usually deposited as hexagonal CdS and, therefore, does not undergo any re-crystalization, but the microstructure of the film is definitely influenced by the annealing process. There is generally grain growth (Morris *et al.* (1992)), as mentioned previously, accompanied by an improvement in the crystallinity of the film, which is manifested in the x-ray diffraction spectra, which increase in intensity and sharpness (Sasikala *et al.* (1997), Rami *et al.* (1999)) or the decrease in the full width half maximum (FWHM) value of the Raman spectra peaks (Shirai *et al.* (1996)). The films can also have less preferred orientation after annealing compared to the as-deposited films (Morris *et al.* (1992)). Sasikala *et al.* (1997) found that, according to the x-ray diffraction measurements, there was an increase in the unit cell of the CdS which could be attributed to filling of vacancies or the appearance of sulphur interstitials.

In another study, the electrodeposited CdS films were dark brown in colour when deposited, not the conventional clear yellow (Shirai *et al.* (1996)). This colouring was attributed to the presence of elemental Cd in the film. On annealing in N_2 atmosphere for 30 minutes up to 300°C, the films became yellow with some brown areas still present. Having increased the annealing temperature to 400°C, no brown was visible on the films after annealing. Auger electron spectroscopy results showed little change in the composition of the films and it was concluded that the annealing process facilitated a rearrangement of atoms and the formation of Cd-S bonds, which increased the Raman spectra intensity. The crystallinity of the film increased significantly as evidenced by the decrease in the Raman spectra peak widths and confirmed by XRD studies.

The cubic CBD films were found to recrystallize into hexagonal CdS after annealing when the temperature was sufficiently high (Mendoza-Galván *et al.* (1996), Ichimura *et al.* (1999)), or when a chlorine flux such as $CdCl_2$, was used (Johnson (2000)). The phase transition temperature was also found to be atmosphere dependent. Annealing at 300°C in an Ar + S_2 atmosphere led

to hexagonal CdS (Lozada-Morales *et al.* (1996)), while annealing in air at 400°C still resulted in cubic CdS films (Johnson (2000)). In contrast to this, annealing in the presence of $CdCl_2$ or with the CdTe in place in the cell at 400°C, facilitated the transition (Johnson (2000)). Determining the exact point of transition was found to be difficult when the films were highly oriented in the cubic (111) direction or the (0002) hexagonal direction. Due to the coincidence of the interplanar distances of these two planes, identification by x-ray diffraction was difficult (Kohle *et al.* (1984)).

In general, the rate at which the grain growth occurs depends on the temperature used and the atmosphere in which the heat treatment is done (Kolhe *et al.* (1984), Al-Jassim *et al.* (1993)). After annealing spray pyrolised CdS films in air, large crystalline grains of 2 – 3 mm in diameter were formed, while using oxygen atmosphere produced agglomerates of small crystallites (Ebothe (1996)). These differences in the microstructure have also been analysed by determining the roughness of the annealed surfaces and it has been found that nitrogen produces a smoother finish (lower RMS roughness) than helium when annealing spray pyrolised CdS films (Ebothe (1996)). The use of $CdCl_2$ treatment of the surface of the CdS prior to annealing has resulted in fewer defects in the grains after annealing and larger grains (Al-Jassim *et al.* (1993), Morris *et al.* (1993)). Changes in the density gradient and thickness of the films was also found to result after annealing (Mendoza-Galván *et al.* (1996)).

The resistivity of the CdS film changes upon annealing, and the extent of the change is dependent on the atmosphere used and the temperature at which the annealing was done. The oxidation of the CdS film when annealing in air results in a significant increase in the resistivity of the film. This effect is less when the annealing is done with the CdTe layer in place (Basol (1984), Kohle *et al.* (1984)). Contrary to this, Kohle *et al.* (1987) reported that air annealing of spray pyrolysed CdS resulted in sulphur vacancies and, therefore, the mobility increased and resistivity decreased. The resistivity of electrodeposited CdS films was reported to decrease after annealing in air at 400°C for 15 minutes from 700 Ω.cm as-deposited to 300 Ω.cm after

annealing, as measured under AM1 conditions (Morris and Vanderveen (1992)). There was no significant change in the dark resistivities.

Annealing in vacuum, nitrogen or hydrogen resulted in a decrease of the resistivity due to the desorption of the oxygen in the film (Danaher *et al.* (1985), Kohle (1987)). The resistivity could be further reduced by using H_2+In vapour or H_2+Cd vapour during annealing, both of which dope the CdS during annealing, resulting in much reduced resistivities (Danaher *et al.* (1985)).

Annealing has been found to influence the bandgap of the CdS significantly on some occasions (Morris *et al.* (1992), Özsan *et al.* (1994), Lozada-Morales *et al.* (1996)) and on others, there was very little change (Özsan *et al.* (1994)). Morris *et al.* (1992) reported a decrease in the bandgap from 2.53 eV to 2.42 eV after annealing electrodeposited CdS in air at 400°C for 15 minutes. Özsan *et al.* (1994) also reported a decrease of at least 0.1 eV in the bandgap of CBD CdS films annealed in air for 20 minutes at 400°C, from 2.42 eV to 2.31 eV, which is well below the theoretical value of 2.45 eV for CdS. This decrease in the bandgap can be attributed to disorder remaining in the crystal structure after annealing in air (Özsan *et al.* (1994)). When using a $CdCl_2$ treatment, the bandgap did not change after annealing and was close to the theoretical value; this has been attributed to the reduction in the defect density which accompanies the recrystallization of the films (Özsan *et al.* (1994)). Lozada-Morales *et al.* (1996) found that the bandgap of CBD CdS decreased after annealing in Ar + S_2 flux to a minimum value (2.28 eV) at 300°C, which was identified as being the transition point from cubic to hexagonal CdS. At that point, a lot of disorder could be present in the structure due to the above transition. Annealing temperatures below and above 300°C produced higher bandgap values (up to 2.38 eV), due to the gradual increase in disorder as the transition temperature was approached, and the gradual increase in order as the transition temperature was surpassed.

On a similar trend, the bandgap of as-deposited CdS was found to decrease as the cadmium concentration in the chemical bath increased and more hexagonal phase CdS was deposited (Sasikala *et al.* (2000)). When only hexagonal CdS was deposited, the bandgap increased again, thus, during the transition, the bandgap decreased in a similar way to that described by Lozada-Morales *et al.* (1996).

The composition of some CdS films before and after annealing are summarized in Table 3.2. All the reports show that there is surface oxygen present and this is sometimes also present in the bulk film. The impurities found in the films are generally from exposure to the atmosphere (carbon and oxygen), or from elements introduced during the processing from the precursors used (nitrogen and chlorine). The difference between surface oxygen and carbon from atmospheric contamination, and contamination arising from processing conditions can be determined using XPS techniques and depth profiling. The binding energy of the element can be determined and from that the state or states the particular element in the film can be determined (Kohle *et al.* (1984), Kohle *et al.* (1987), Stoev *et al.* (1996) Jayakrishnan *et al.* (1996)). The peak positions of the XPS analysis have been reported to shift to lower energies compared to those obtained from the single crystal reference and it is necessary to normalize the Cd:S ratios with respect to a standard CdS sample in order to get a true reflection of the Cd:S relationship before and after annealing (Danaher *et al.* (1985)).

Rapid thermal annealing (RTA) is a much faster annealing process where the material is heated rapidly (100°C/s) and the annealing times are less than an hour (Jayakrishnan *et al.* (1994), (1996)). This method results in the elimination of oxygen from the bulk of the film, and no detrimental loss of cadmium during the annealing process. Oxygen is only detected on the surface of the CdS films. The CdS films were also found to have a strong (0002) orientation (Jayakrishnan *et al.* (1996)).

3.5. Transmission Spectra

The transmission properties of the CdS window layer in a photovoltaic cell influence the spectral response and the efficiency of the cell, since only that light which is transmitted through the window layer to the CdTe layer can be converted into electrical energy. A number of factors have been found to influence the transmission properties of the CdS films, namely the deposition technique (Ileperuma *et al.* (1998), Al Kuhaimi (1998)), the thickness (Uda *et al.* (1990), Rami *et al.* (1999)), composition of the film (Sasikala *et al.* (2000)), deposition conditions (Sasikala *et al.* (1997), Uda *et al.* (1990)) and annealing conditions (Danaher *et al.* (1985), Lee *et al.* (1987), Morris *et al.* (1992),Rami *et al.* (1999)) to name the most prominent.

A comparison of the transmission spectra of CdS films produced by various techniques has been done and the spectra varied significantly for the as-deposited films with the transmission variations at a wavelength of 600 nm of between 80 % for vacuum evaporated and about 40% for screen printed and CBD CdS (Al Kuhaimi (1998)). In a similar study, Ileperuma *et al.* (1998) showed that the absorbance of the films deposited by different methods differed with the CBD CdS having the highest absorbance (>20%) at 600 nm, with the aqueous and non-aqueous electrodeposition having absorbances of ~10%.

During electrodeposition, the deposition potential has been found to influence the transmission spectra. At more negative deposition potentials the deposition of the films was faster and the as-deposited CdS films had much lower transmission, which was attributed to the increased concentrations of cadmium deposited at these potentials. The absorption edge of the spectra was also not as sharp as was found at less negative potentials (Figure 3.1) (Sasikala *et al.* (1997)). Similar results were obtained by Sasikala *et al.* (2000) using chemical bath deposition. The cadmium concentration in the bath was adjusted and, on increasing the cadmium concentration from 0.4 M to 0.8 M, which in turn increased the growth rate of the film, the transmittance of the films decreased significantly. At higher concentrations of cadmium in the bath, the CdS film no longer deposited in the cubic form, but in

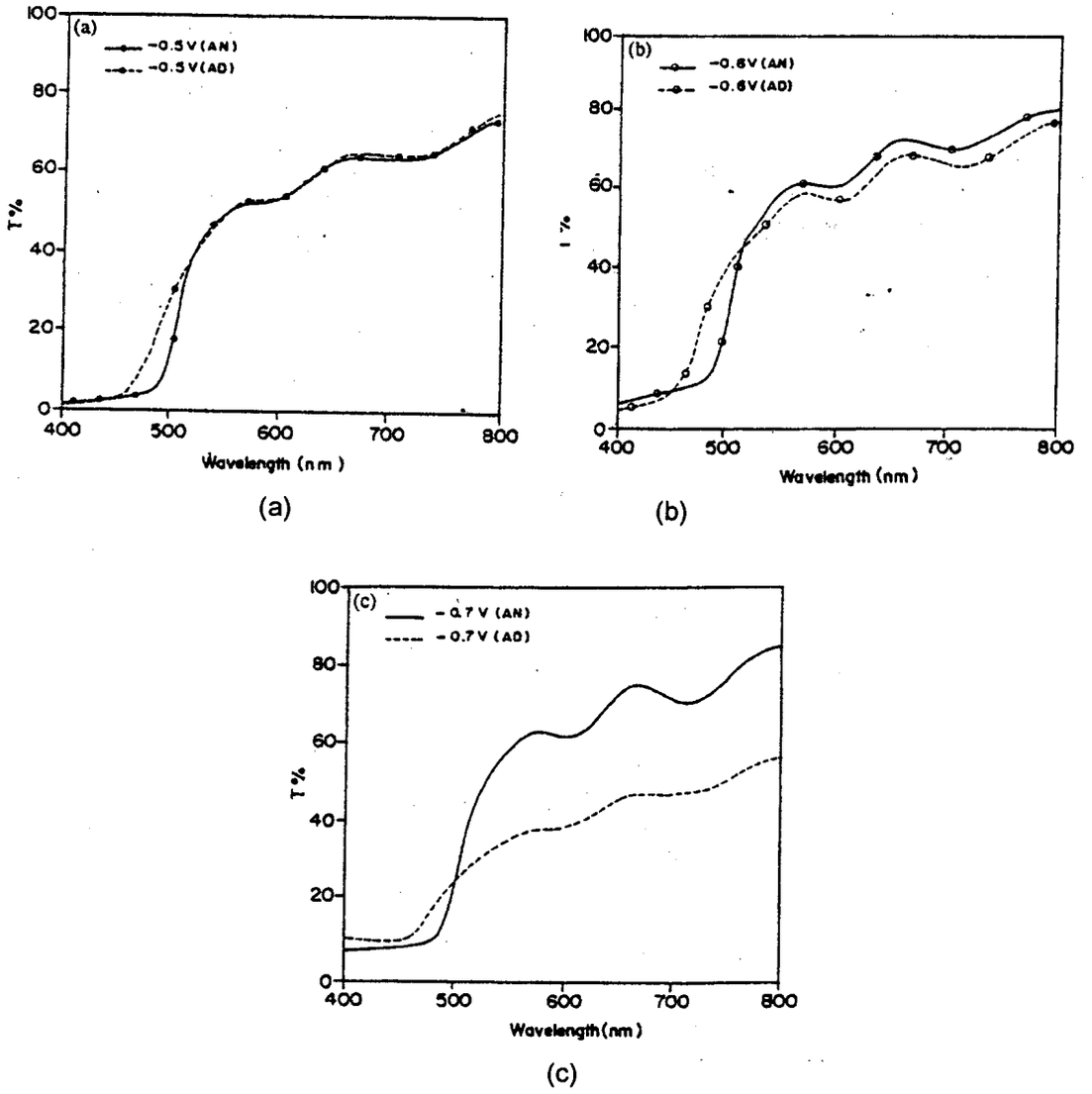

Figure 3.1: The comparison of the transmission spectra of three films, elecrodeposited at potentials of –0.5V, -0.6 V and –0.7 V, before (AD) and after (AN) annealing (Sasikala *et al.* (1997)).

the hexagonal form. The variation of the transmittance during the gradual increase in the concentration of cadmium could be attributed to the transition between these phases, which was also found to influence the band gap.

Annealing of the CdS films influences the transmission, but the conditions of annealing and the original film composition also influence the final transmittance of the film. Sasikala *et al.* (2000) found that annealing CBD CdS films at 350°C for 30 min in hydrogen increased the optical transmittance and the absorption edge became sharper and shifted to a higher wavelength. A similar effect was observed

for the electrodeposited CdS annealed under the same conditions when the as-deposited film was cadmium rich and it was concluded that the improved crystallinity increased the transmittance (Sasikala *et al.* (1997)). For other electrodeposited films which had good transmission prior to annealing, the annealing process did not change the transmission spectra much, except to sharpen the absorption edge and shift it to a higher wavelength (Morris *et al.* (1992), Sasikala (1997)).

The thickness of the CdS films also influences the transmission spectra, with an increase in thickness resulting in lower transmittance (Uda *et al.* (1990), Rami *et al.* (1999)). The presence of larger grains in the film has lead to increased transmittance due to the reduced amount of scattering in the film caused by fewer grain boundaries (Lee *et al.* (1987)). Columnar grains, with few grain boundaries parallel to the film, can also lead to higher transmittance (Uda *et al.* (1990)).

3.6. Raman Spectroscopy

Raman spectroscopy can be used as an easy method to determine the crystal quality and / or the strain of a thin film. This technique has often been used for CdS films using either the 488.0 nm or 514.5 nm lines of an Ar-ion laser. The crystallinity of the material can be deduced from the position of the Raman lines and by the sharpness of the peaks (Chuu *et al.* (1991), Shirai *et al.* (1996), Zhu *et al.* (2000)). The amorphous materials and those with very small crystallites result in a shift to lower frequencies, compared to the spectra obtained for larger crystals with surface modes also being present (Kanellis *et al.* (1980), Veprek *et al.* (1981), Rossetti *et al.* (1983)). This is due largely to the increase in the bond lengths in the less crystalline material. The full width half maximum (FWHM) value of the peaks has been found to relate directly with the extent of crystallinity of a film. As the crystallinity improves the FWHM decreases (Shirai *et al.* (1996)) and this technique has been shown to be more sensitive than XRD techniques in determining the crystallinity of films (Zhu *et al.* (2000)).

When plotting the intensity of the first overtone / fundamental vibrational mode (2LO)/(1LO) against the crystallite size, it has been found to be a straight line with

the ratio increasing with increasing crystallite size (Hayashi *et al.* (1989)). When crystallites become extremely small, surface modes tend to dominate with the spectra having broad indistinct peaks, rather than the typical sharp peaks (Chuu *et al.* (1991)).

When studying the Raman spectra in the range 200 cm^{-1} to 800cm^{-1}, the vibrational modes of the cubic and hexagonal phases coincide. The hexagonal phase has been reported to exhibit more overtones of the 1LO (at 305 cm^{-1}) series (up to nine under the certain excitation conditions) compared to the cubic phase (Briggs *et al.* (1976), Trujillo *et al.* (1996)).

Stresses in materials have been observed to result in shifts of the Raman lines. In CdS these shifts have been found to be proportional to the applied uniaxial stress (Briggs *et al.* (1976)).

Thin films also exhibited a shift toward lower frequencies compared to thicker films (Kanellis *et al.* (1980)).

3.7. Motivation for this study

A thorough study of electrodeposited cadmium sulphide thin films is necessary to understand more fully the effect that the sulphide layer can have on photovoltaic cells.

The effect of the substrates on the cells has been documented, but the possible causes of these differences have not been examined and as far as the cadmium sulphide layers are concerned, have not been thoroughly investigated.

The effect of the deposition conditions, such as temperature, in the range from room temperature to 90°C, and deposition potential, need to be studied in more detail. The literature in this regard is contradictory in that some report deteriorating quality, amorphous films at deposition temperatures less than 90°C, while others report good quality, crystalline films deposited at 25°C.

The initial cleaning of the substrate has not been documented in detail previously for the various conducting oxide layers. This is a crucial step in the processing, since poor cleaning techniques can result in poor substrate coverage and therefore poor cell quality in the final applications.

Little has been reported on the effect of annealing in the presence of $CdCl_2$ on CdS composition (Al-Jassim et al (1993), Lee et al (1987)), particularly on electrodeposited films. The microstructure of $CdCl_2$ treated films after annealing has also not been studied extensively.

Very little has been published on how the microstructure of electrodeposited CdS films develop from the early nucleation stages through to the final deposits. Such studies could contribute to a better understanding of how certain structural features are generated and how to control or avoid undesirable structures.

4. Experimental Methods

4.1. Substrates

Two different substrates were used, namely indium tin oxide (ITO) on glass obtained from Donnelley Corp. (USA) and fluorine doped tin oxide (FTO) obtained from Asahi (Japan). Various methods were used to remove surface particles and organic contaminants from the transparent conducting oxide layers.

4.1.1. Cleaning

Various solvents were used near boiling point in an ultrasonic bath to remove surface particles and organic contaminants from the transparent conducting oxide layers. The four cleaning procedures considered were:

Method 1: Five minutes in TCE followed by 5 minutes in isopropanol followed by 3 consecutive washes in water of 5 minutes each.

Method 2: Acetone, methanol and isopropanol washes of 5 minutes each.

Method 3: Acetone, methanol and isopropanol washes of 5 minutes each followed by a water wash of 5 minutes.

Method 4: Hexane, isopropanol and water washes of five minutes each.

Method 2 is based on that used by Das *et al.* (1993(b)) with the elimination of their last step of isopropanol vapour degreasing. In method 3, the additional water wash was included to determine whether any isopropanol residue which might be present was removed. In all cases the solvents used were analytical grade and the water was deionised water with a 18 MΩ.cm resistivity.

4.1.2. Resistivity

The sheet resistance of the two substrate conducting oxide films was determined by the standard 4-point probe method. The thicknesses of the two films used in the calculation were those given by the suppliers.

4.2. Electrodeposition

The electrodeposition of the CdS films was carried out using a three electrode configuration, as sketched below (Figure 4.1). This is similar to that described by Pandey *et al.* (1996)(Chapter 4). The bridge between the electrolyte and the reference electrode was part of the solution which was drawn up into a U-tube. The reason for this is to keep the reference electrode at room temperature, while the electrolyte temperature was varied between 30°C and 90°C.

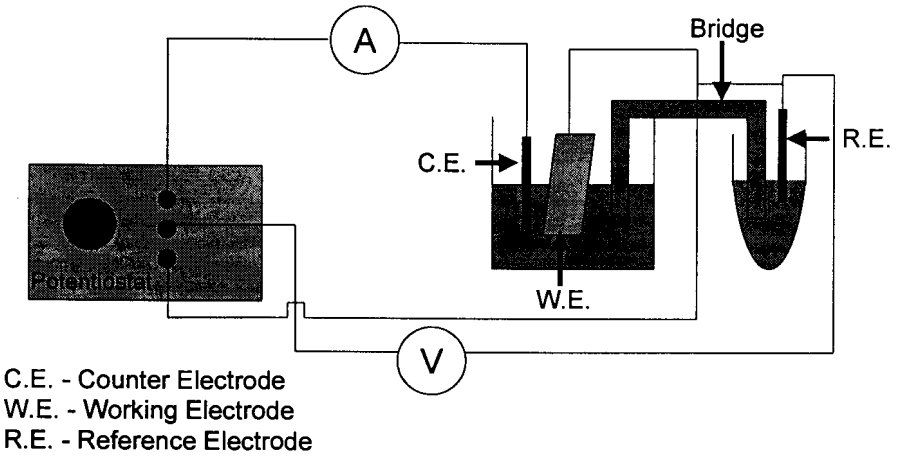

Figure 4.1: A sketch of the electrodeposition set-up used during the study.

The cathodic deposition of the CdS took place from an acidic (pH 2) aqueous solution of 0.2 M $CdCl_2$ and 0.02M $Na_2S_2O_3$. This solution was first used by Basol (1988) and subsequently by Das (1993(a)) and Das *et al.* (1993(a)). A potential of 600 mV with respect to the standard Ag-AgCl electrode was used. Constant voltage was used rather than constant current to ensure that the conditions remained conducive for co-deposition (illustrated in Figure 2.2). The solution was stirred vigorously throughout the deposition process.

CdS films were deposited at temperatures ranging from 30°C to 90°C and times of 90 minutes to 4 hours to determine the effect temperature and substrate had on the deposited film. The temperature of the electrolyte was automatically controlled using a water bath (not shown in Figure 4.1).

The deposition times were varied between 1 minute and 90 minutes at 60°C and 90°C to examine the differences in the deposition on the two substrates at the two temperatures.

4.3. Annealing

The as-deposited films were annealed in a tube furnace at temperatures ranging from 300°C to 460°C in a flowing Ar atmosphere (4 litres/min) for times of 15 minutes and 30 minutes. Some of the films were treated prior to annealing with a saturated solution of methanol and $CdCl_2$. The films were introduced to the heat zone once the temperature had been reached, thus resulting in a rapid heating rate of the film.

4.4. Microstructural and compositional evaluation

4.4.1. Atomic Force Microscopy

Atomic force microscopy (AFM) has been used to investigate the surfaces of polycrystalline films and single crystals for various reasons.

- Yoshino *et al.* (1997) studied the Cd and S polar surfaces of the CdS bulk single crystal.
- Carter *et al.* (1994) used the AFM to monitor the RMS roughness of the Si-SiO_2 surface before and after H_2-plasma cleaning. This was to determine whether any reaction occurred during the cleaning process.
- In another application, AFM was used to study the surface roughness and the affect of crystallite size on raman lines in nanocrystallite CdS films (Nanda *et al.* (1997)).

- AFM has also been used to compare the surfaces after heat treatments (Al-Jassim *et al.* (1993)) and during growth stages of films on different substrates (Ihanus *et al.* (1997), Rami *et al.* (1999)).

Atomic force microscopy allows the precise measurement of contamination layer heights and particle dimensions with angström resolution (Binnig (1986)). Lateral force microscopy (LFM) is sensitive to the difference in friction between the Si_3N_4 scanning tip and the surface. The amount of friction is monitored as the twisting of the cantilever supporting the tip while the sample is scanned in the direction normal to the cantilever main axis. A contrast in the LFM images indicates differences in surface composition (Colchero *et al.* (1992)). By modulating the vertical position of the sample by a displacement of the order of 1nm at a frequency of about 1kHz and recording the resulting flexion of the cantilever, an image is produced where the contrast is due to differences in the sample surface compliance (Force modulation) (Maivald *et al.* (1991)). The simultaneous acquisition of AFM (topography) and LFM images, or AFM and force modulation (Fmod) images allows direct correlation of the features seen in the images.

Topography, friction and force modulation information of the atomic force microscope (AFM) were utilised to determine the efficiency of the cleaning methods and to study the microstructure of the thin films.

A Park Scientific Autoprobe CP (Park Scientific Instruments, Sunnyvale, CA) equipped with an AFM/LFM head was used for the measurements. The topography images were acquired in the constant force mode using the minimal force to keep the tip in contact with the sample. A rectangular cantilever ("Microlever") of nominal force constant of 0.02 N/m and nominal 0.008 N/rad. torsion force constant with a sharpened tip of nominal radius of 20 nm was used for all experiments. For the force modulation images, a sinusoidal signal of amplitude 0.6nm was applied to the scanner at a frequency of 1 kHz. The 10 μm piezo scanner had been calibrated using a

standard calibration grid supplied by the manufacturer in the X and Y direction and using a VLSI standard for the Z direction.

Root mean square (RMS) roughness values were calculated for both the conducting oxide surfaces and the CdS films and the values quoted are the average of RMS values obtained from at least four 4.4 x 4.4 μm^2 areas in different regions on each surface.

Atomic force microscopy (AFM) can therefore be used to verify the cleanliness of a surface after cleaning procedures and provides additional information regarding the structure and morphology of the contaminants and the substrate surface.

4.4.2. *Electron Microscopy*

The structure of the films grown were determined using a Jeol JSM 6000F field emission scanning electron microscope. The samples were cut to fit into a standard holder and were examined as-deposited or as-annealed, without coating in secondary electron imaging mode. An accelerating voltage of 5kV was used, unless otherwise stated.

A conventional scanning electron microscope, Jeol 5800LV, was also used for some studies with an accelerating voltage of 10 – 20 kV.

A Philips EM 301 transmission microscope, operated at 80kV, was used to obtain diffraction patterns of the deposited CdS films. The films were scraped off the substrate onto thin carbon films floating on distilled water and then scooped up onto electron microscope grids for examination.

4.4.3. *Thickness determination of deposited films*

The thickness profiles of the deposited films were determined using a stylus method on an Alpha-Step 2000 (Tencor Instruments). For a specific film, the average thickness of 5 measurements over the width of the film was

calculated. In some cases these measurements could be compared to those obtained from AFM studies.

4.4.4. X-ray photoelectron spectroscopy (XPS)

The composition of the electrodeposited films was determined on a Quantum 2000 XPS. The surface carbon at 284.8 eV was used as an internal standard and a CdS standard was used to normalize the data obtained from analysis of the films. Surfaces were sputtered for 5 seconds using 2kV argon ions to remove excess contamination from the surfaces. Both as deposited and annealed films deposited onto both the ITO and FTO substrates were analysed. Compositional depth profiles were obtained for some of the as deposited and annealed films.

4.5. Raman spectroscopy

Raman spectra were recorded using a XY Dilor multi-channel Raman spectrometer in the range 100 cm^{-1} to 800 cm^{-1} using the 514.5 nm and 488.0 nm lines of an Ar-ion laser. The laser power was varied between 1 mW to 500 mW to determine whether the laser caused any structural change during the acquisition of the spectra. The acquisition time ranged from 30 s to 120 s and a 100 μm aperture was used for all spectra. The spectra were obtained in a backscatter configuration in air from the thin films, which were deposited at various temperatures, ranging from 30°C to 90°C. According to Zhu *et al.* (2000) and Shirai *et al.* (1996), the extent of crystallinity can be qualitatively deduced and compared to other films. This analysis technique appears to be more sensitive than XRD, according to Zhu *et al.* (2000), when the crystallites are small.

4.6. Transmission properties

The transmission of light through the substrates and various CdS films of varying thicknesses was determined using white light from a tungsten source in the wavelength range 400 nm – 800 nm. An S20 photomultiplier was used. In order to eliminate the properties of the light source and the variations in the setup conditions, a set of data from only the source was collected at the beginning of each batch of data collected. The signal from the source was then divided into the signal from the transmitted light through the sample, in order to obtain the transmittance of the sample.

5. Results

5.1. Effective cleaning of the different substrates

5.1.1. Introduction

The first step in the production of CdS thin films by electrodeposition was to determine the most effective and appropriate method to clean the surfaces prior to deposition.

The two substrates (indium tin oxide (ITO) and fluorine doped tin oxide (FTO)) were vastly different in surface morphology and are dealt with separately. The same cleaning methods were used on both substrates.

5.1.2. ITO substrate cleaning

AFM, LFM and force modulation (Fmod) images of the as-received ITO substrate surfaces were acquired. Figure 5.1, a three dimensional topographical image of the indium tin oxide (ITO), shows the surface to be relatively smooth with a few protruding features resulting in a RMS roughness of 5 nm. Figure 5.2 is a multi-image representation of the three scanning modes on the as-received ITO. Figure 5.2(a) is the 2-dimensional equivalent of Figure 5.1 with the light parts of the image corresponding to the higher features and the darker areas corresponding to the

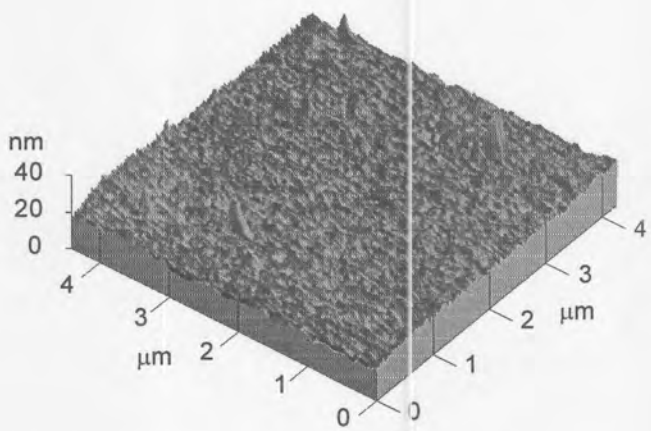

Figure 5.1: Three dimensional topographical image of the as received ITO layer.

lower parts of the surface. The grey scale extends from 0 nm to 40 nm due to the particles present on the surface. Figure 5.2 (b) and (c) are the LFM images taken simultaneously with the topography image from left to right and right to left respectively. The images show a reversal in signal, i.e. features that appear dark grey in one image, appear light in the other due to different forces experienced by the cantilever when scanning from the two directions. This indicates that the contrast is due to contaminant materials on the surface which affect the friction. Apart from confirming the features seen in the topography images, the LFM also shows features that are not visible in the topography image. This is due to the additional lateral force localised at step edges, making the LFM more sensitive than the topography mode in certain instances. These additional features could be organic contamination on the surface. The topography and LFM images were taken simultaneously. The sensitivity of the LFM was not only used to determine that the height of the protruding contamination particles was greater than 30 nm, but also that most of the other contamination seen in the LFM images did not rise significantly above the natural roughness of the surface (Figure 5.1 and 5.2). The Fmod image of the same region (Figure 5.2(d)) shows a map of compliance of the surface of the sample. The contamination patches appear darker since they are softer and, therefore, the tip penetrates further than in the conducting layer, which appears much lighter.

Studying the topography and LFM images on an as-received ITO surface (Figure 5.2(a), (b) and Figure 5.3), it was often observed that the protruding particles in AFM topography mode were accompanied by patches of contamination around and possibly under the particle. The contamination appears to act as a "glue" for these particles as seen in the topography image (Figure 5.3 (a)) and the LFM image (Figure 5.3 (b)) of the surface. Removing the patches of contamination would therefore enable the removal of the particles thus yielding a cleaner surface.

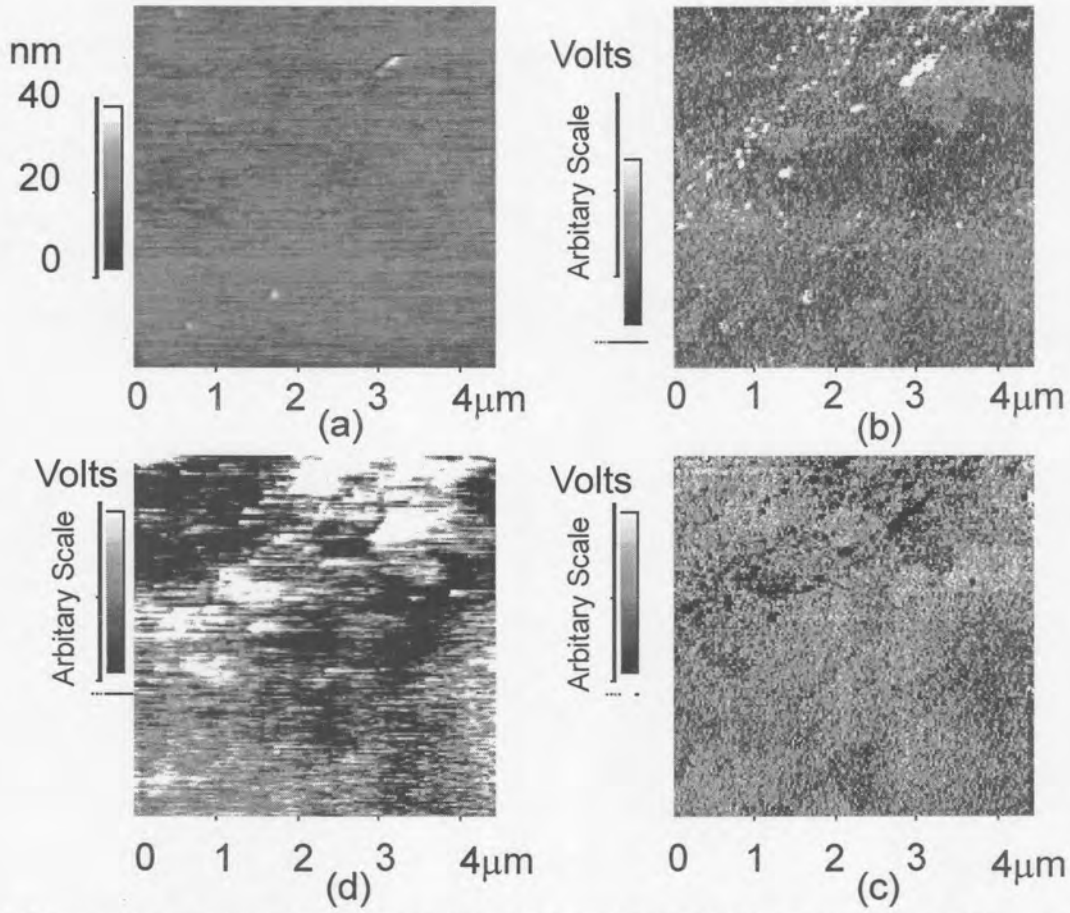

Figure 5.2: A multi-image representation of the as received ITO layer, showing a) the topography image b) the left to right scanned LFM image, c) the right to left scanned LFM image, and d) the Fmod image of the same region.

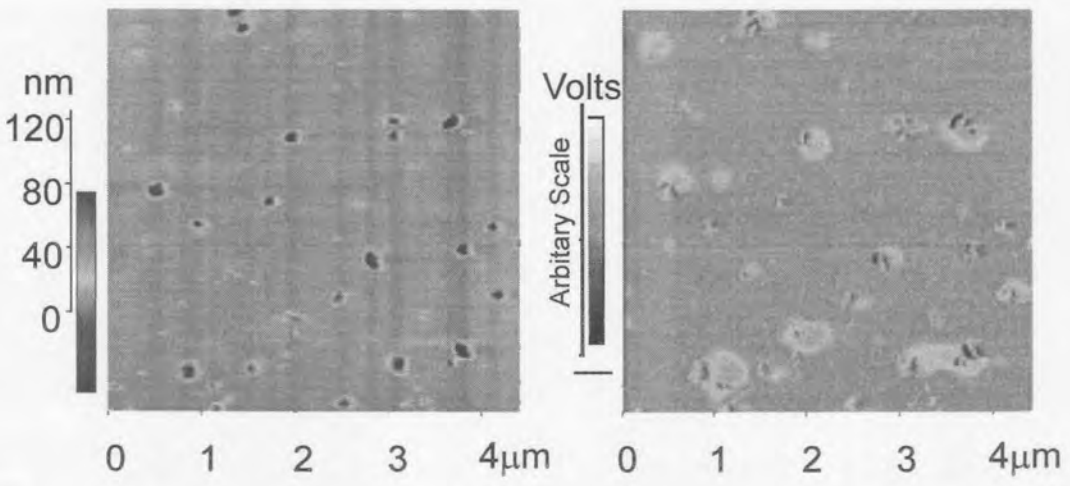

Figure 5.3: (a) Topography image of the ITO layer as received and (b) LFM image of the same area showing patches of contamination around the particles.

Apart from the qualitative AFM, LFM and Fmod images, the particles on each surface were also quantitatively analysed after cleaning, using the line profile provided in the instrument's image analysis software. In the histograms of particle heights and widths on the as received and the cleaned ITO surfaces (Figure 5.4), it can be seen that all cleaning methods removed the high (1400 – 1600 Å) protruding particles from the surface, but only methods 1 (TCE, isopropanol, water) and 2 (acetone, methanol, isopropanol) removed the wide (3000 – 3500 Å) particles from the surface. Cleaning method 4 (hexane, isopropanol, water) left the least average number of particles on the surfaces after cleaning, while method 2 left the most. Remnant particles were the narrowest (<2000 Å) following washing method 2, while they were the flattest (<400 Å) following method 2 and 4.

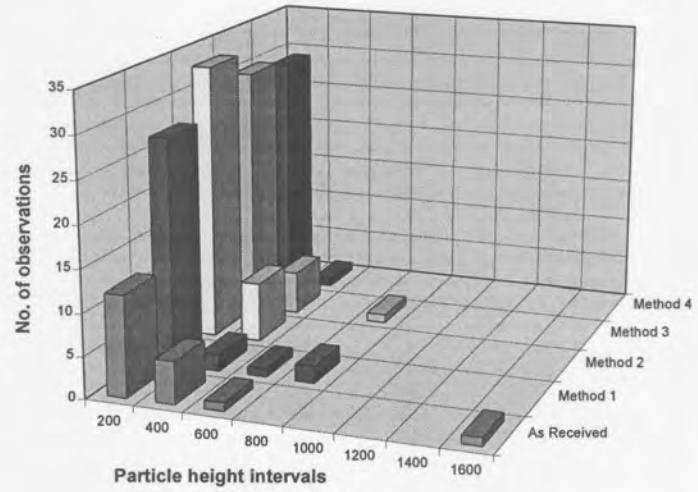

(a)

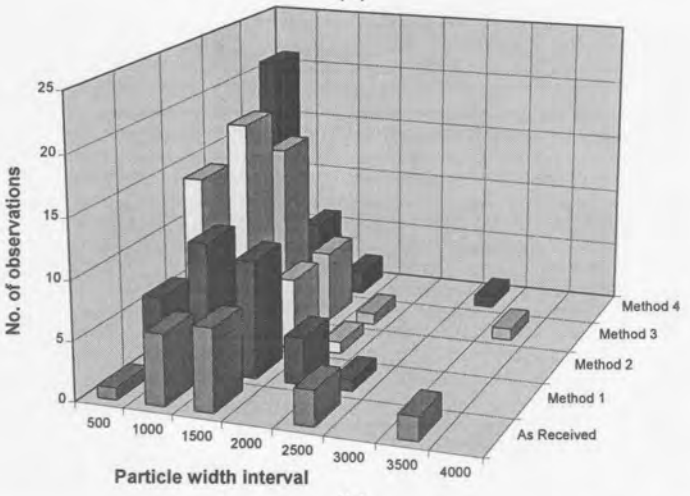

(b)

Figure 5.4: Histogram showing the particle (a) heights (Å) and (b) widths (Å) on the as received ITO surface and those remaining on the surfaces after the various cleaning methods.

Comparing the topographical images (Figure 5.5) of the ITO as received and cleaned surfaces (method 4 - hexane, isopropanol and water), it can be seen that larger particles have been removed reducing the RMS roughness values from 5 nm to 2 nm before and after cleaning respectively. In Figure 5.5, in order to observe any features on the cleaned surface, it was necessary to use a finer grey scale compared to the as received sample. Using the same grey scale would have masked all the small surface features left after cleaning since these are all less than 10 nm in height. The reduction in the roughness values is ascribed to contamination and particles being effectively removed during the cleaning procedure.

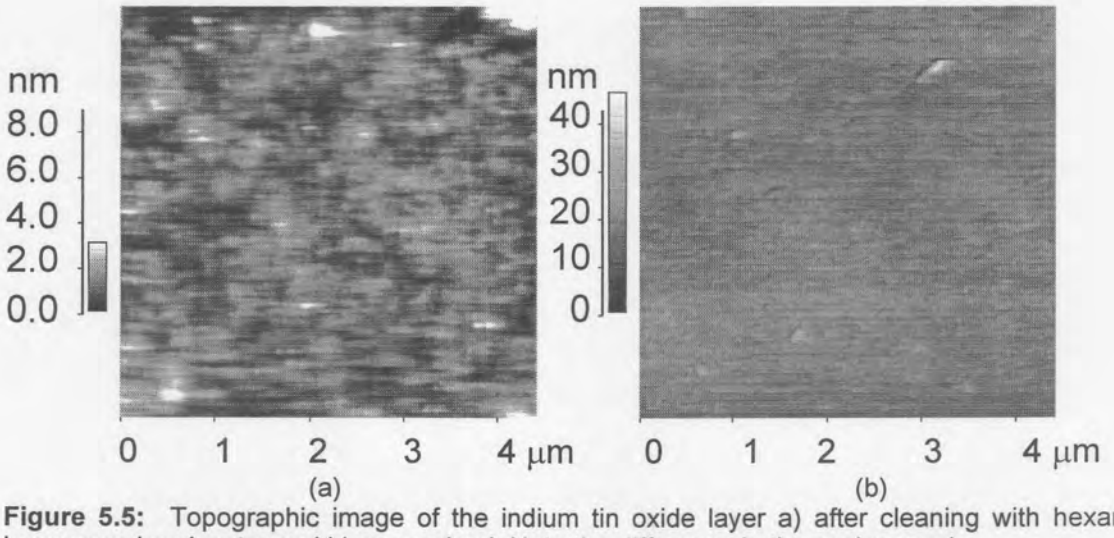

Figure 5.5: Topographic image of the indium tin oxide layer a) after cleaning with hexane, isopropanol and water and b) as received. Note the difference in the scales used.

5.1.3. *FTO substrate cleaning*

AFM, LFM and Fmod images of the as received FTO surfaces were acquired. As seen in the 3-dimensional topographical image, the FTO surfaces (Figure 5.6(a)) were much rougher than the ITO surfaces. The LFM images (Figure 5.6(b)) show the influence of the topography rather than that of contrast due to contaminant materials, since there was no signal reversal when scanning in opposite directions. Grain boundaries can clearly be seen in the LFM image and the average grain size was found to be 258 nm. The methods used previously on the ITO substrates could not be used as effectively to investigate the effectiveness of the cleaning methods.

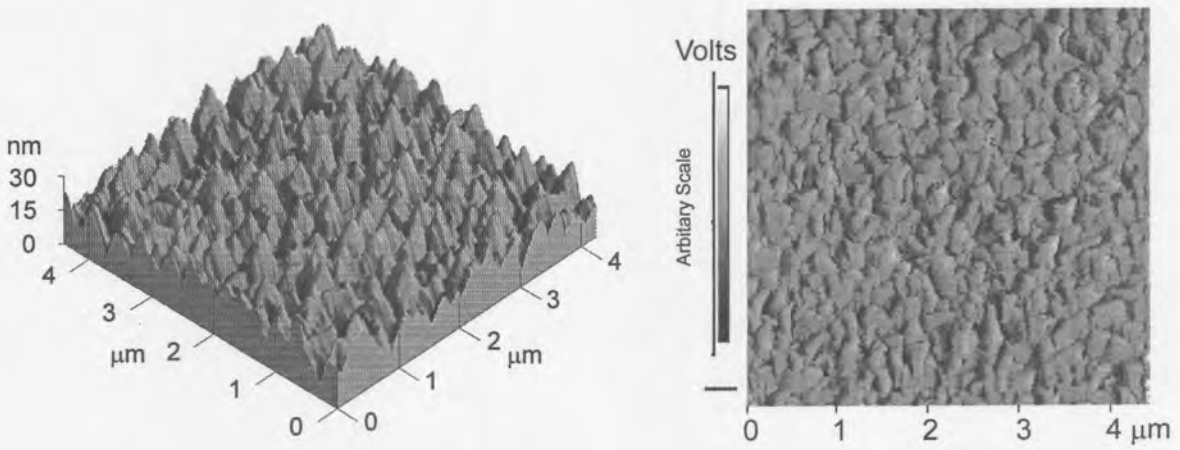

(a) (b)

Figure 5.6: (a) Three dimensional topographic image of the FTO layer as received (b) LFM image of the same area showing grain boundaries.

5.1.4. *Surface Roughness*

RMS roughness values were determined for all the cleaned surfaces, and they were found to be influenced by the cleaning procedures. The presence of contamination between topographical features and particles on the surface affects the RMS roughness values. This was used as an indication of the effectiveness of the cleaning procedures on the substrates, particularly those of the FTO. Although it should not be taken as an absolute measurement of the surface cleanliness, it can be used in conjunction with other qualitative descriptions. These results are summarised in Figure 5.7.

The ITO surfaces showed a reduction in the RMS roughness values after cleaning, with wash methods 2 and 4 giving the lowest values of approximately 2 nm compared to 5 nm as received. This decrease in the RMS roughness is ascribed to the removal of particles and contamination from the relatively smooth surface. This corresponds to information gleaned from the AFM images of the various surfaces discussed previously, where the residual particles on the surface were the smallest after cleaning methods 2 and 4 had been used.

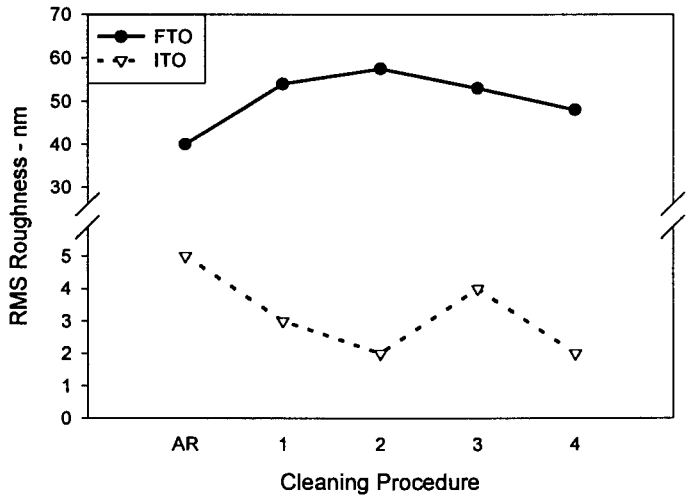

Figure 5.7: The RMS roughness values for the different cleaning procedures under investigation. AR = as received.

The FTO surfaces, on the other hand, showed a significant increase in RMS roughness values after cleaning, with wash method 2 giving the highest value of 60 nm compared to 40 nm as-received. It is assumed that during cleaning, particles are removed from the surface and it would appear that these particles were predominantly in-between the grains on the surface, hence the increase in the RMS roughness values. This assumption is further supported by topographical images such as in Figure 5.6, where no particles were observed on top of peaks on the surface which would result in a decrease in RMS when removed.

5.1.5. Conclusions

The AFM lends itself ideally to analysing the effectiveness of the cleaning methods used on substrates. The LFM images differentiate clearly between contamination and topography differences on the surface, provided the surface is not too rough. The RMS roughness of the surfaces were determined and used in conjunction with qualitative AFM and LFM images to determine the efficiency of the cleaning methods.

The two substrates have different topographies and the efficiency of the cleaning methods differed for each substrate. Both wash method 2 (acetone, methanol, isopropanol) and method 4 (hexane, isopropanol, water) were effective in removing contamination and particles from the surface of the ITO, which is a relatively smooth surface. The FTO surface was much rougher, and wash method 2 appears to be effective in removing the contamination and particles while wash method 4 was not as effective. It would appear that the cleaning of the surfaces depends on the initial topography of the surface and therefore an investigation into the most efficient cleaning procedure needs to be done on all new types of substrates prior to deposition of the thin films.

In all further work, both the substrates were cleaned using method 2, namely consecutive near boiling point acetone, methanol and isopropanol washes in an ultrasonic bath.

5.2. Rate of Deposition

The initial deposition currents for the two substrates were fairly similar with the ITO being slightly higher than the FTO (Table 5.1). This can be attributed to the lower sheet resistance of the ITO (17.3 Ω/□) compared to the FTO (21.8 Ω/□). The deposition current density decreased significantly as the temperature decreased. The deposition rate of the cadmium sulphide decreased significantly from an average of approximately 30Å/min at 90°C to approximately 1Å/min at 30°C. A reduction in deposition rate as a function of temperature has been previously reported and attributed to the reduction in the rate of disproportionation of the $S_2O_3^=$, making less sulphur ions available in the electrolyte for deposition at lower temperatures (Basol (1988), Morris *et al.* (1992), Dennison (1993), Sasikala (1997)).

Table 5.1: Summary of initial deposition currents for the temperature range 30°C to 90°C on areas of approximately 1 cm^2. (Deposition potential = 600 mV)

Temperature	Deposition current	
	ITO	FTO
30 °C	0.02 mA	0.02 mA
60 °C	0.31 mA	0.19 mA
90 °C	1.56 mA	1.03 mA

Morris *et al.* (1992) reported a "poorer quality" film when studying the microstructures of films deposited at 60°C compared to 90°C, but no specific detail was given for these films. Other studies have shown that CdS films were successfully deposited at temperatures as low as 25°C using similar electrolytes (Power *et al.* (1981), Fatas *et al.* (1984), Shirai *et al.* (1996)).

5.3. Composition of As Deposited CdS

XPS studies of the CdS layers were done after electrodepositing CdS films at temperatures ranging from 30°C to 90°C. The films analysed were a transparent bright yellow colour. A CdS powder standard was analysed and it was found to give a Cd/S ratio of 1.293. This was used as the standard for comparison of the XPS analysis of the electrodeposited layers. All Cd/S ratios were normalised with respect to the standard CdS powder sample, similar to Danaher *et al.* (1985), who normalised the Cd/S ratios with respect to a single crystal. The normalised results of

the deposited CdS films at different deposition temperatures are shown in Table 5.2 for both substrates. All the as-deposited layers are slightly cadmium rich, with Cd/S ratios ranging from 1.01 to 1.15. On average, the films deposited on the smoother ITO substrate had less excess cadmium than those deposited on the FTO. The variation in the ratios were random and no trends were observed as a function of temperature.

Table 5.2: Summary of cadmium / sulphur ratio for the electrodeposited CdS films deposited in the temperature range from 30°C to 90°C. The CdS power standard was used to normalise the data.

	Standard	
Powder	1.00	
Deposition Temperature	Normalised Cd/S	Normalised Cd/S
	ITO	FTO
30	1.149	1.086
40	1.033	1.120
50	1.055	1.111
60	1.142	1.154
70	1.136	1.086
80	1.009	1.064
90	1.008	1.076
Average	1.076±0.059	1.099±0.029

Studying the cadmium and sulphur peaks more closely did not reveal any significant shift in peak position compared to the standard CdS powder (Table 5.3). These positions correspond well to those peak positions reported for CdS by Kohle *et al.* (1987) and Bhide *et al.* (1981). There were no significant differences in the peak shapes for the cadmium and the sulphur between the standard CdS powder, the thin films deposited on ITO and those deposited on FTO. It can, therefore, be concluded that the Cd/S ratio and the bonding states of the Cd and S in the electrodeposited layer did not change as a function of temperature in the range 30°C - 90°C and also did not differ significantly from the standard CdS powder. On comparing these peak positions to those obtained after annealing (Table 5.3), there was no significant shift in the peak positions and, therefore, it can be concluded that the bonding states of the Cd and S in the as-deposited yellow CdS films and those of the annealed CdS are the same.

Table 5.3: Summary of peak positions of the cadmium and sulphur peaks for deposition temperatures ranging from 30°C to 90°C. The peak positions of the CdS powder standard and films annealed at 300°C in argon for 15 minutes are included for comparison.

Deposition Temp. - °C	ITO		FTO	
	Cd (eV) 3d 5/2	S (eV) 2p	Cd (eV) 3d 5/2	S (eV) 2p
30	405.8	161.7	405.6	162.6
40	404.8	160.8	405.7	162.7
50	405.8	162.3	405.9	162.8
60	404.9	161.8	405.8	162.8
65	405.8	162.4		
70	405.4	161.8	405.8	162.8
75	405.3	161.8	404.8	161.8
80			404.9	161.8
85			404.8	161.9
90	405.8	162.7	405.8	162.8
Annealed 300°C	405.3	161.8	405.2	162.0
Std. Powder	405.6	161.9		

A typical XPS spectrum is shown in Figure 5.8, showing some of the common impurities found in the films, such as chlorine in the chloride form (from the electrolytic solution used), oxygen (from exposure to the air and water) and carbon (from exposure to air). The levels of chlorine were low, below 7 at%, for films on

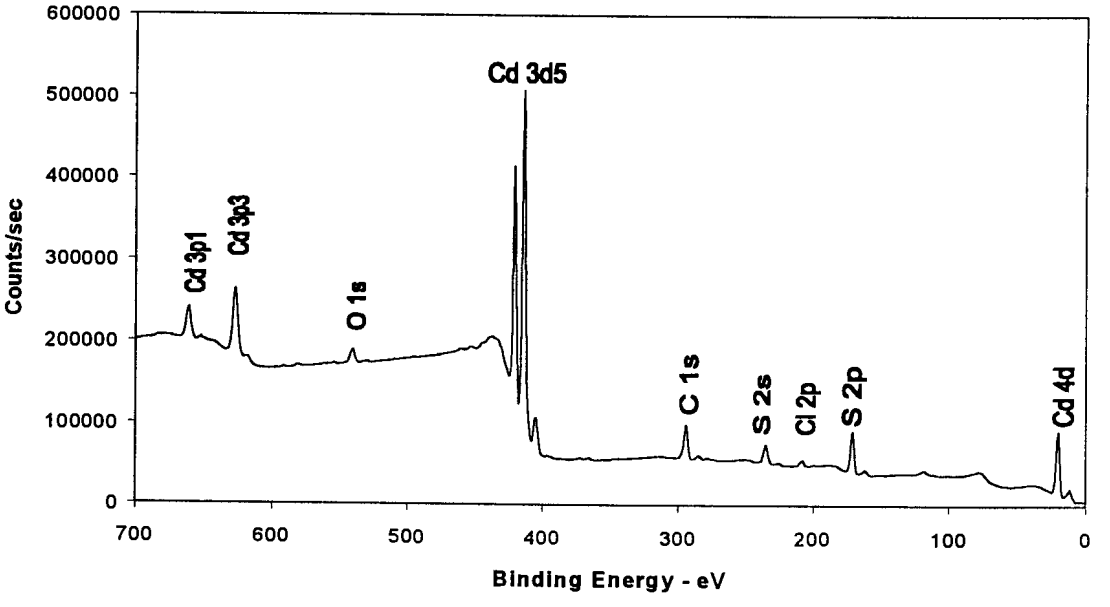

Figure 5.8: X-ray photoelectron spectrum of a typical CdS film deposited on the conducting oxide layer, in this instance, ITO.

both the substrates. The carbon and oxygen contents on the surface were found to vary depending on the length of time of the exposure to the atmosphere between processing and analysis. There was no correlation between the deposition temperature and the oxygen and carbon content (Figure 5.9). The carbon content on the surface varied from 5 at% to 25 at%, but once the surface layer had been removed (~200 Å) the carbon content decreased to <2 at%. Similarly the high (up to 30 at%) oxygen content was limited to the surface layer and, when removed, the oxygen content was <5 at%. Other impurities found in the very thin films were sodium (typically less than 5 at%), indium and tin from the substrates.

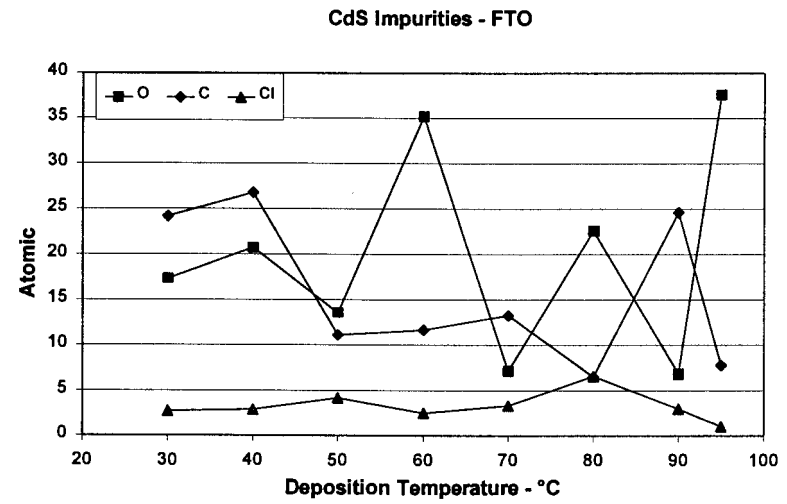

Figure 5.9: Graphical representation of the carbon, oxygen and chlorine impurities present in the films deposited at different temperatures on (a) FTO and (b) ITO substrates.

Composition profiles of the films deposited at various temperatures were studied by sputtering away the CdS layer using argon ions. The sputtering removed the layers at a rate of ~4 Å/s. The films deposited at 30°C for 4 hours were very thin (240 Å) and, due to incomplete coverage in places, the substrate was detected through the CdS film for the smooth ITO. This was even more prominent for the rougher FTO substrate. There was no clear distinction between the CdS film and the substrate, since the film was essentially little more than an interface layer. The Cd/S ratio was found to increase slightly from the surface (Cd/S = 1.07) to the last 100 Å (Cd/S = 1.29).

Films deposited at 60°C and 90°C were thicker than those deposited at 30°C and, therefore, the surface layer, film and interface were more distinct in the depth profiles. From Figure 5.10 it can be seen that the carbon and oxygen are limited to the surface of the films, with their concentrations decreased significantly once the first 200Å had been removed. The cadmium and sulphur concentrations increased as the surface layer was removed and were then constant until the interface between the CdS and the substrate was reached. The Cd/S ratios on the depth profiles of the films deposited at 60°C and 90°C were within the range obtained for the films listed in Table 5.2. On studying the sulphur and cadmium peaks on depth profiles, there was no change in the position of the peaks with depth into the film and there was also no change in the shape of the peaks.

The high roughness (RMS value = 600 Å) of the FTO substrates results in a thinner uniform concentration region in the film where only Cd and S are detected, since the FTO protrudes into the CdS film (Figure 5.11). The Cd/S ratios remain relatively constant in the depth profiles, but these films were slightly richer in cadmium than the as deposited films on the ITO substrates with a Cd/S ratio at the interface of 1.3 for both the 60°C and 90°C deposition temperatures. The higher cadmium content on the FTO was also found for the surface layers (Table 5.3). The higher Cd/S ratio associated with the FTO could be due to the roughness of the surface, which could result in preferential deposition of one of the species. Despic *et al.* (1968) have shown that on a rough surface, the height of the deposit depends on the initial height of the substrate multipied by an exponential dependence on the molecular mass of the depositing species (Equations 17 and 18 in Section 2.4). In the case of

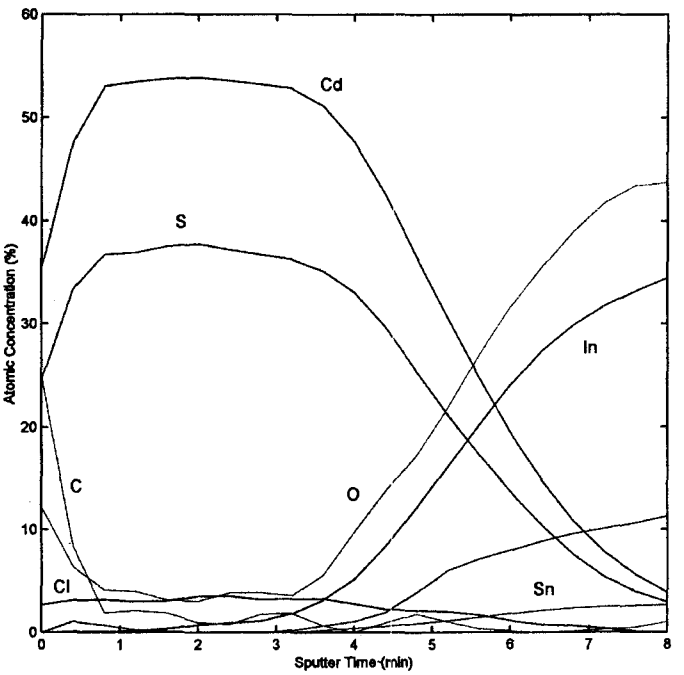

Figure 5.10: XPS depth profile of a typical CdS film deposited on ITO substrate. The film was 2000Å thick, deposited at 60°C.

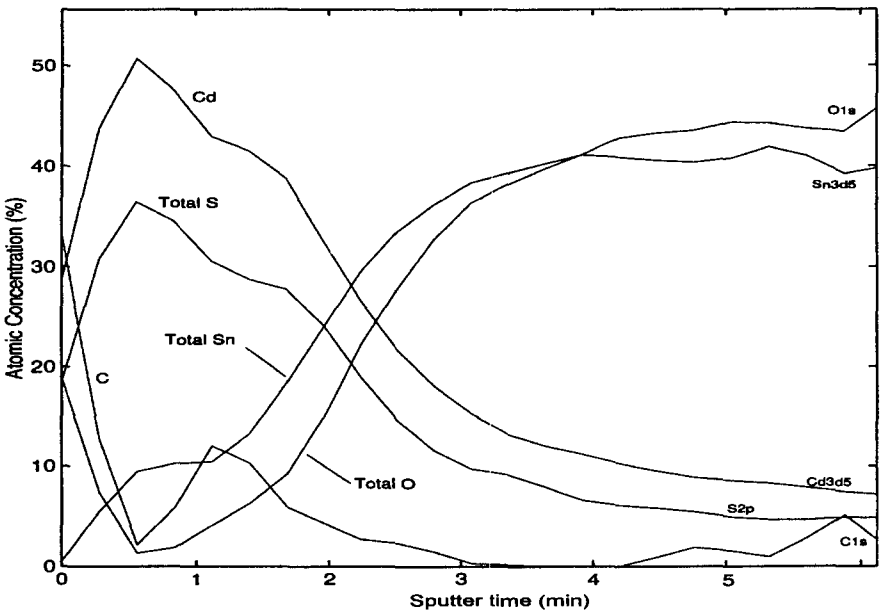

Figure 5.11: The typical XPS depth profile of a CdS film deposited on the rough FTO surface. The film thickness was ~600Å, and was deposited at 90°C.

CdS, the two components deposit separately and, since Cd^{2+} has a higher atomic mass than S^{2-}, this could be a cause for the higher Cd content in the films deposited on the rougher FTO substrates.

5.4. Composition of Argon Annealed CdS

The CdS films were annealed at temperatures between 300°C and 450°C in a flowing argon atmosphere for 15 – 30 minutes. The film compositions were again analysed using XPS techniques. It was found that for both substrates, there was a significant decrease in the cadmium content on the surface of the film as the annealing temperature increased (Figure 5.12). Cadmium loss on annealing has been previously reported when annealing CdS (Ferrer *et al.* (1989), Rohatgi *et al.* (1991)). There are, however, not many studies of compositional evaluation after annealing of electrodeposited CdS films. Shirai *et al.* (1996) report no change in the Cd/S ratio of the electrodeposited film, but a change in the bonding of the Cd and S after annealing in nitrogen atmosphere. Sulphur loss and the production of sulphur vacancies in CdS has been reported after annealing the films in various atmospheres (Mitchell *et al.* (1975), Kohle *et al.* (1987), Ferrer *et al.* (1989)).

When annealing for 30 minutes there is less decrease in the Cd/S ratio on the surface compared to annealing for 15 minutes (Figure 5.13). This may be an indication that the excess cadmium is initially more volatile than the sulphur, but that

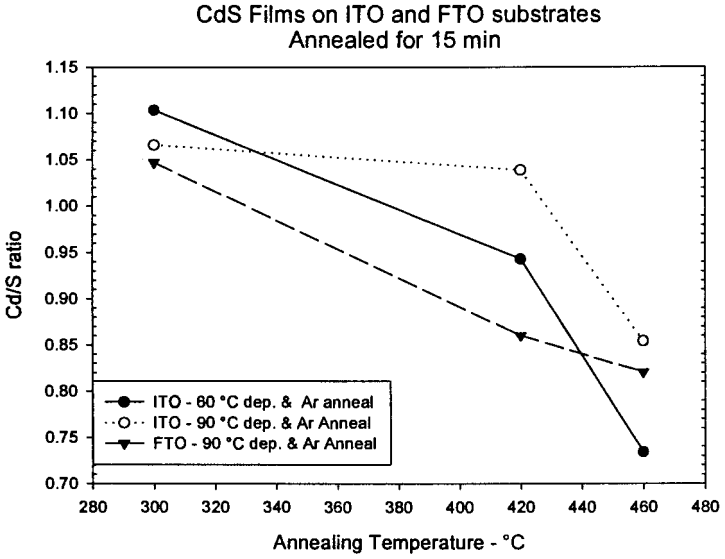

Figure 5.12: The Cd/S ratios of the films after annealing in a flowing argon atmosphere. The films were deposited at 60°C and 90°C on the two substrates.

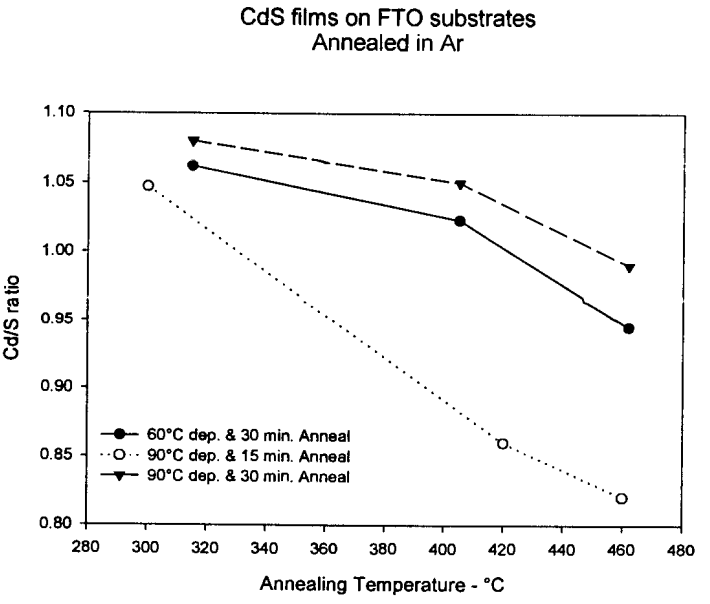

Figure 5.13: The effect of annealing time on the Cd/S ratio of films annealed in flowing Ar atmosphere. The films were deposited at 60°C and 90°C and annealed for 15 minutes or 30 minutes.

for longer annealing times, some sulphur is also lost. This results in the decrease of the Cd/S ratio not being as high and, therefore, the appearance that less Cd is lost.

On investigating the depth profiles of the films after annealing in an argon atmosphere, it was found that only the surface was cadmium deficient. Once the surface layer was removed, the ratio of the Cd/S was very similar to that obtained in the depth profiles for the as deposited films, with ratios ranging from 1.02 to 1.3.

5.5. Composition after Annealing with $CdCl_2$

The annealing in the presence of $CdCl_2$ has been shown to improve the electrical properties of CdS/CdTe solar cells as well as the microstructure of CdS and CdTe films (Lee *et al.* (1987), Morris *et al.* (1993), Johnson (2000)). Little has been reported on the effect of the heat treatment on the CdS composition after annealing in the presence of $CdCl_2$ (Al-Jassim *et al.* (1993), Lee *et al.* (1987)), particularly on electrodeposited films.

Figure 5.14 shows the relationship between the annealing temperature and the Cd/S ratio on the surface after annealing in the presence of $CdCl_2$. The significant decrease in the cadmium content observed previously (Figure 5.13) did not occur

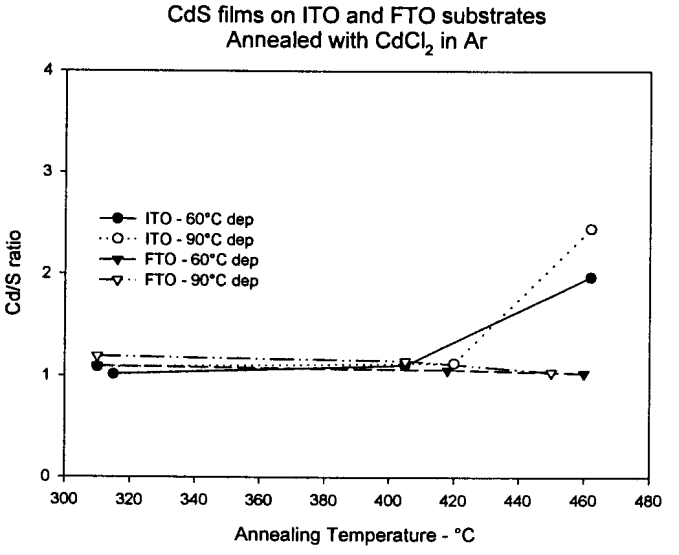

Figure 5.14: Cd/S ratio of films with $CdCl_2$ treatment after 30 min annealing for both substrates and films deposited at 60°C and 90°C.

and, in some instances, the cadmium content increased with respect to the sulphur content, indicating either the infusion of cadmium into the film or the loss of sulphur from the film. $CdCl_2$ has been previously reported to inhibit the loss of sulphur from the CdS films (Al Jassim *et al.* (1993)). The increase in the Cd/S ratio can more likely be attributed to the incorporation of Cd into the CdS film from the $CdCl_2$ than the loss of sulphur during annealing. The chlorine content of these films was also monitored after annealing and found to be very low (less than 5 at% (average of 3 at%)) which is not significantly different to that obtained on the surfaces of the as deposited films due to the electrolyte used. The increase in Cd content cannot, therefore, be attributed to poor cleaning of the surface after annealing, since there is no corresponding increase in the chlorine content. Lee *et al.* (1987) found that $CdCl_2$ content (monitored by chlorine presence) in slurry deposited CdS films decreased on heat treatment due to evaporation of the $CdCl_2$, confirming that chlorine content should not increase significantly due to the $CdCl_2$ treatment. It was not clear whether the cadmium content decreased in proportion to the chlorine in Lee *et al.* (1987). In this study it would appear that the CdS films deposited on the ITO substrate were Cd-rich after annealing at 460°C with $CdCl_2$ treatment, whereas the

CdS on the FTO substrates were close to stoichiometric. This could be due to differences in the thickness of the CdS layers and sputtering of the surface layer prior to XPS analysis, since subsequent depth profiles show close to stoichiometric compositions once the surface layer was removed.

On studying the depth profiles of these annealed films, it became apparent that only the surface layer of the film was Cd-rich. Once the surface layer had been removed (approximately 200 Å) the CdS was close to stoichiometric, with a Cd/S ratio of approximately 1. This ratio was then constant throughout the film, Table 5.4 giving an example of a CdS film deposited on ITO substrate at 90°C and annealed at 460°C for 15 minutes.

Table 5.4: Cd/S ratios calculated from the depth profile of a film deposited on an ITO substrate at 90°C and annealed at 460°C for 15 minutes after $CdCl_2$ treatment.

Sputter Time	Cd/S ratio
0	1.07
0.4	0.98
0.8	0.96
1	0.96
2	0.97
5	0.96

There was no diffusion of chlorine into the film, as seen by the depth profile of a thick film which was annealed at 460°C for 15 minutes with $CdCl_2$ treatment (Figure 5.15). From this profile, it is clear that the CdS film is comprised of Cd and S, with very low amounts of C, O and Cl below the surface layer. Similar profiles with constant Cd/S ratios below the slightly Cd-rich surface were obtained for films annealed for 30 minutes. $CdCl_2$-containing slurry deposited CdS films have been found to not retain the chloride in the film due to evaporation during annealing for 60 minutes at 600°C, with the Cl content significantly lower after just 5 minutes (Lee *et al.* 1987). In the current study, the annealing temperature is much lower than 600°C, but the $CdCl_2$ was only applied to the surface of the film and appears to have evaporated and not diffused into the film during annealing. Any $CdCl_2$ remaining after annealing could also have been removed from the surface during rinsing in

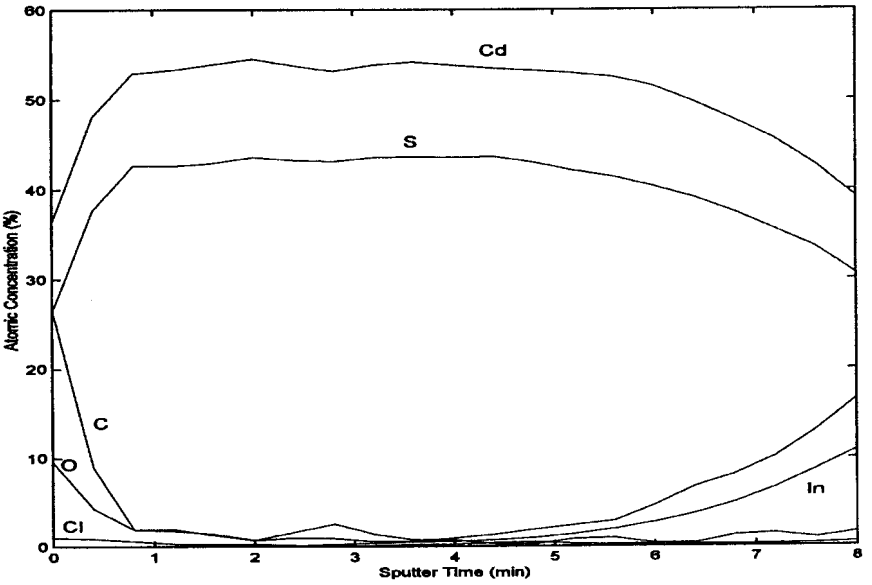

Figure 5.15: Depth profile of a CdS film deposited on an ITO substrate at 90°C and annealed at 460°C for 15 minutes after $CdCl_2$ treatment.

deionised water, since it is soluble in water. The as-annealed, unrinsed films were not analysed by XPS, and therefore it is not certain whether the elimination of the $CdCl_2$ occurred during the annealing or the rinsing process.

From the various studies undertaken previously, it can be concluded that the heat treatment environment of the CdS films, be it as part of a solar cell or as an isolated film, influences the final composition of the film and the cell properties. Previous studies of exclusively CdS films (Kohle (1987),Tomás *et al.* (1995), Stoev *et al.* (1996)) have concentrated on the effect of heat treatment on the composition of CdS films which were deposited from solutions containing various Cd and S species (spray pyrolysis and CBD). These chemical deposits require conversion to CdS, which can result in residual impurities in the film. This is not the case with electrodeposited films, since this method deposits specific ions (Cd and S) at specific potentials, thus making this process less prone to impurity inclusions.

5.6. Raman Spectroscopy

Raman spectra have previously been used to determine the crystallinity of thin films (Campbell *et al.* (1986), Chuu *et al.* (1991), Shirai *et al.* (1996)). The full width half maximum values of the peaks found at the characteristic frequencies are indicative of the extent of crystallinity of the films under examination. In the case of CdS thin films, the dominant peaks in the spectra are the longitudinal optical (LO) vibrational modes at frequencies of 305 cm^{-1} (single crystal) for the fundamental mode, and the first overtone near 605 cm^{-1} (Rossetti *et al.* (1983), Zahn *et al.* (1991), Chuu *et al.* (1991)). The position of the fundamental peak is usually lower for polycrystalline materials (Shirai *et al.* (1996)).

The Raman spectra were obtained using the 514.5 nm and 488.0 nm lines from an argon ion laser as excitation sources. Spectra were obtained for a series of films deposited at temperatures ranging from 30°C to 90°C. All the films showed clear peaks at $\leq$ 300 cm^{-1}. The position of the peaks obtained for the films deposited at the various temperatures using both excitation lines are given in Table 5.5. There are small differences in the peak positions obtained from films deposited across the temperature range, but these peaks are in the same range as reported in the literature for electrodeposited CdS (Shirai *et al.* (1996)). Veprek *et al.* (1981) reported a shift to lower frequencies, with a decrease in crystallite size. The above results contradict this, in that the film deposited at 30° has a higher peak position

Table 5.5: Table summarising peak positions of the fundamental peak for the different deposition temperatures used.

Temperature (°C)	Peak Position (cm^{-1}) 514.5 nm	Peak Position (cm^{-1}) 488.0 nm
30	300.0	299.2
40	298.4	299.8
50	294.8	298.7
60	296.1	296.5
70	297.1	295.4
80	297.5	297.5
90	297.3	296.4
Sputtered film	298.3 (Thick) 299.5 (Thin)	

than those deposited at 90°C, and yet microstructural studies showed that the films deposited at 90°C had larger particles (Section 5.9.1). Raman spectra were also recorded from CdS films which were evaporated onto glass slides, and the fundamental peak was found to be between 298.3 cm^{-1} and 299.5 cm^{-1} for thick and thin areas respectively on the film (Table 5.5). These peak positions are also lower than those obtained for single crystal spectra with peak position of 305 cm^{-1} (Rossetti *et al.* (1983), de Tacconi *et al.* (1993)). The change in the position of the peaks could, therefore, not be attributed to the thickness of the films, since the thickness of the films is closely related to the deposition temperature. There is also no significant difference in the peak positions obtained using the two laser wavelengths, but the scatter in the peak positions when using the 488.0 mn line is slightly less than for the 514.5 nm line.

Previous studies of CdS electrodeposited films have concluded that films deposited at temperatures below 90°C were of poor microstructural quality (Morris *et al.* (1992)) or amorphous (Rami *et al.* (1999)). Raman spectroscopy can be used to evaluate qualitatively the crystallinity of the CdS films deposited by evaluating the full width at half maximum (FWHM) (Shirai *et al.* (1996)). The FWHM of the Raman spectra of the films deposited between 30°C and 90°C are shown for both the fundamental peak (~300 cm^{-1}) and the first overtone (~600 cm^{-1}) in Figure 5.16. When using the 514.5 nm exciting line, there is a gradual decrease in the FWHM of

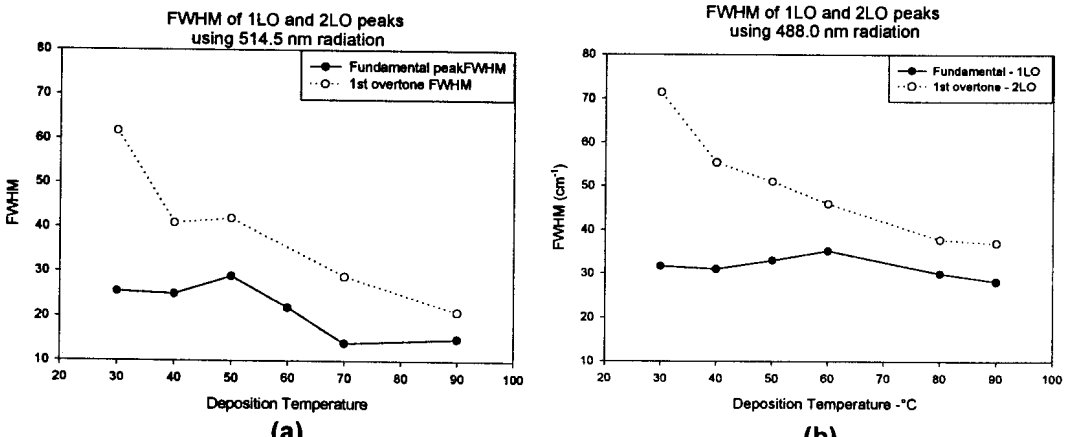

Figure 5.16: FWHM of the fundamental and first overtone peaks as a function of deposition temperature with radiation of (a) 514.5 nm and (b) 488.0 nm from an argon ion laser.

the fundamental peak from between 25 cm^{-1} and 29 cm^{-1} for films deposited below 60°C to between 20 cm^{-1} and 15 cm^{-1} for films deposited at 60°C and higher. There is a much more significant decrease in the FWHM of the first overtone as a function of deposition temperature. When using the 488.0 nm exciting line, the fundamental FWHM remained relatively constant (between 28 cm^{-1} and 35 cm^{-1}), but the first overtone exhibited a significant decrease in the FWHM as the deposition temperature increased from 30°C to 90°C. According to Shirai *et al.* (1996), the decrease in the FWHM of the fundamental peak is an indication of an improvement in the crystallinity of the film. The FWHM are higher than those obtained by Shirai *et al.* (1996), but the trend observed is similar. The thickness of the film is not thought to influence the FWHM to any great extent, since Zahn *et al.* (1991) report that the thinner layers do not exhibit very much broader peaks in comparison to thicker layers when using the 514.5 nm excitation line.

It would appear that the energy of the exciting line used to obtain the spectra plays a role in these comparisons. The intensity of the fundamental peaks in the spectra obtained with the 514.5 nm excitation line were higher than for those obtained with the 488.0 nm excitation line for the whole deposition temperature range. The photon energy of the 514.5 nm excitation line is 2.41 eV, which is close to the band gap of CdS, 2.42 eV. Resonance Raman effects can therefore occur, thus increasing the intensity (Zahn *et al.* (1991)) and sharpness of the peaks obtained with this excitation line in comparison to the 488.0 nm excitation line with a photon energy of 2.55 eV. These resonance effects may improve the sensitivity of the technique with the 514.5 nm excitation line in comparison to the 488.0 nm excitation line, hence the more prominent decrease in the FWHM of the fundamental peak with the former excitation line.

In order to investigate whether the exposure of the film to the laser resulted in localised annealing of the film during the acquisition of the spectra, spectra were obtained for varying laser powers (the source was varied between 1 mW and 100 mW) on different areas of the sample. There was no sign of localised annealing taking place in the film which would have been evidenced by a growth in the grain size and a decrease in the values of the FWHM. Figure 5.17 shows the relationship between the laser power and the FWHM of the spectra obtained, and it can be seen

that the FWHM does not significantly differ from those obtained across the temperature range. All these spectra were obtained on the same film on different areas, thus eliminating the possible effects of differences in processing conditions which could influence the spectra.

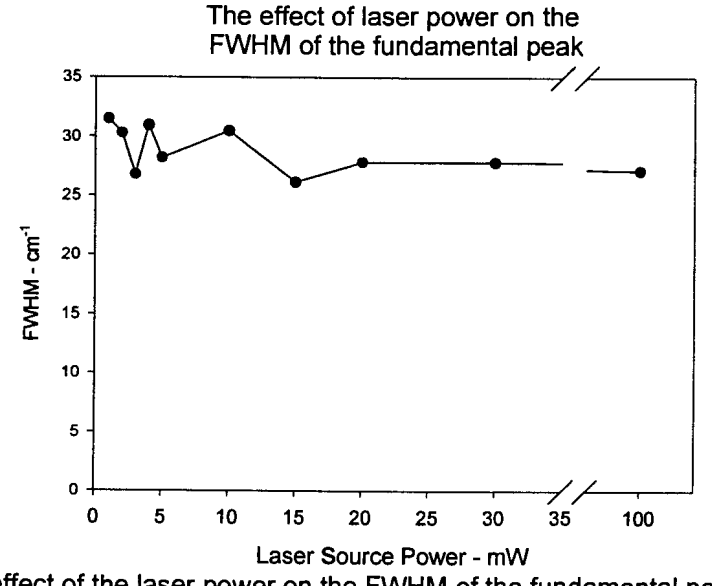

Figure 5.17: The effect of the laser power on the FWHM of the fundamental peak of spectra obtained using the 514.5 nm line. (Experimental error = ± 5 cm^{-1}.

There was a slight shift in the position of the peak from ~302 cm^{-1} to ~295 cm^{-1} as the power increased from 30 mW to >100 mW. This shift is within the range of the 1LO peak for films deposited in the temperature range 30°C to 90°C (Table 5.5). Shifts in the peak positions have been reported to occur due to stresses in the film (Briggs *et al.* (1976)) and crystal size (Veprek *et al.* (1981), Campbell *et al.* (1986)). There is no visible annealing taking place and, therefore, the crystal size does not contribute to this peak shift. There is a possibility that defects could have been annealed out of the CdS film, thus resulting in some stress relief. Another possibility is that the shift could be due to the increase in the bond length of the Cd-S (Veprek *et al.* (1981)) as the intensity of the laser imparts more photons to the specific area, resulting in more vibrational energy in the bond due to localised heating. These possible reasons were not examined further since the main aim of the Raman spectroscopy was to determine some correlation between the spectra and the crystallinity of the films.

A significant decrease in the FWHM was observed when spectra were recorded from annealed CdS films (460°C for 30 minutes after $CdCl_2$ treatment). The peak position of the spectra of annealed CdS films were between 299 cm^{-1} and 297 cm^{-1}. The FWHM decreased from 15 cm^{-1} for the as deposited films deposited at 90°C to 9 cm^{-1} for a 1mW source focused with a 100-times objective lens. This improvement in the crystallinity was evident when examining the microstructure of the films in more detail and the particle size of the CdS increased on annealing (This is discussed in more detail in Section 5.9.4 and 5.9.5).

From this study of the Raman spectra, it can be concluded that the films deposited in the temperature range 30°C to 90°C are crystalline and that the long range order of the film increased as the deposition temperature increased, thus resulting in the decrease in the FWHM of the peaks. The exposure of the film to the laser did not appear to influence the crystallinity of the CdS and no sign of localised annealing due to the exposure was observed. Annealing the CdS films did result in an improvement of the crystallinity of the film as evidenced by a decrease in the FWHM of the fundamental peaks of the annealed films.

5.7. Transmission Properties of Electrodeposited CdS Films

The transmission of the two substrates without CdS films were investigated initially as a reference with which to compare the electrodeposited CdS films. Figure 5.18 shows the transmission of the two films used across the visible spectrum. The ITO/glass substrate has a higher transmittance for the whole range compared to the FTO/glass substrate, with the ITO/glass having a transmittance of > 74% and the FTO/glass having a transmittance of > 62% for the whole visible range. The transmittance increases for wavelengths of 500 nm with the ITO being ~80% and the FTO ~ 70%. The lower transmittance of the FTO is due to the thickness of film which is 800 nm compared to the ITO film of approximately 150 nm (Manufacturers' statistics).

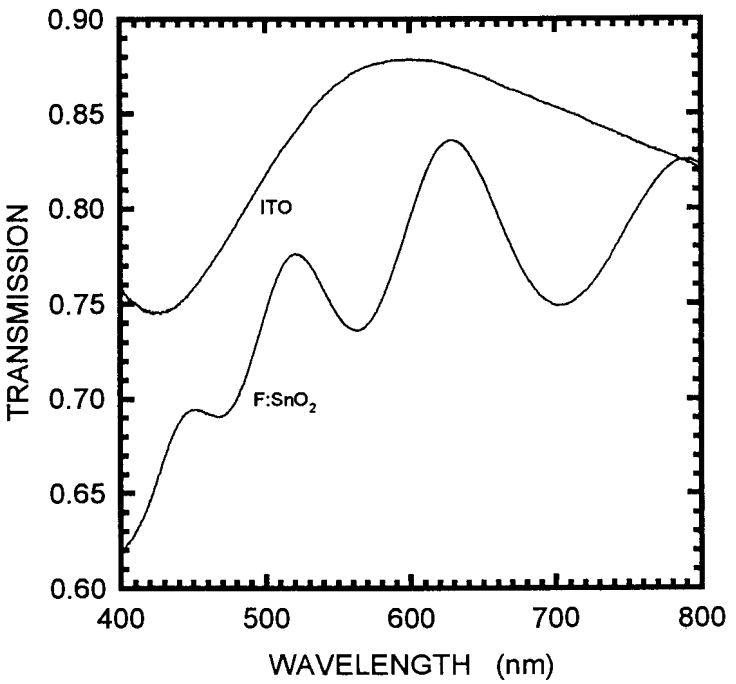

Figure 5.18: Transmission spectra of the two transparent conducting oxide films on the glass substrates. The ITO has an average thickness of 150 nm and the FTO ($F:SnO_2$) 800 nm.

The electrodeposited CdS films on the substrates were examined, and the transmittance was evaluated as a function of CdS thickness. The ITO substrates gave higher transmission of the visible spectrum than the FTO substrates for films of similar thickness. The transmittance of the films on both substrates decreased as the films increased in thickness, which is in agreement with the previous reports (Higuchi *et al.* (1993), Matthew *et al.* (1995)). From Figure 5.19, it can be seen that the 700 Å films on the ITO substrates had approximately 10% higher transmission than the 700 Å films on the FTO substrates for wavelengths higher than 5000 Å. Below 500 nm, the low transmittance of the FTO substrate reduces the effective transmittance of the CdS/FTO/glass significantly compared to the ITO substrate. As the thickness increased, it was found that the transmittance of the CdS films on the ITO remained much higher than those on the FTO. The 1200 Å CdS on FTO had only a slightly higher transmittance than the 3000 Å CdS on ITO. The 3000 Å FTO film is shown in Figure 5.19 for comparison. The lower transmittance of the FTO/CdS films can be attributed mainly to the lower transmittance of the FTO/glass substrate (Figure 5.18).

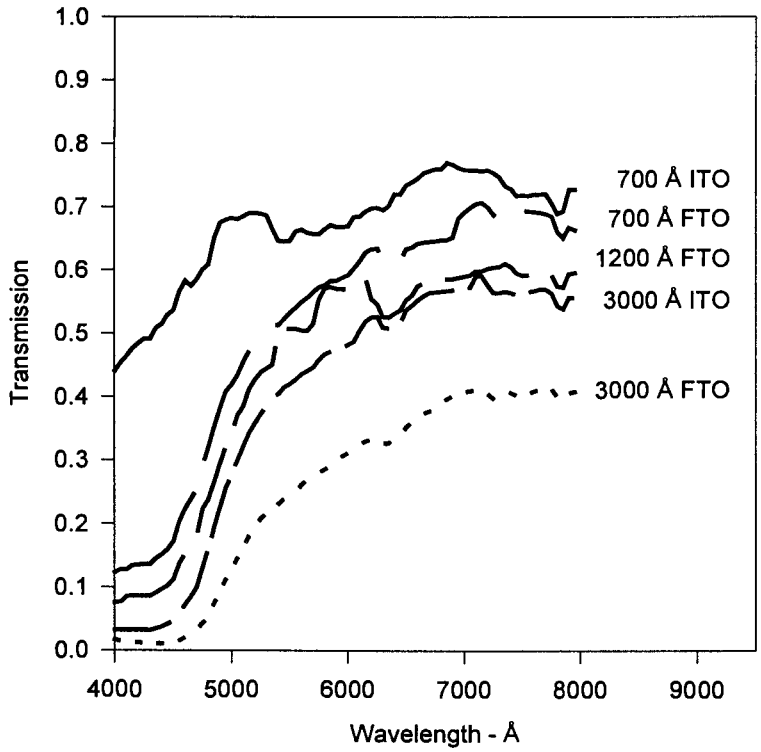

Figure 5.19: A comparison of the transmission of white light through films of different thicknesses on the ITO and FTO substrates.

An absorption edge (a sharp decrease in the transmission) is observed for all the films at wavelengths below 500 nm (Figure 5.19). The absorption edge of the 700Å CdS on ITO was less prominent than the other films in Figure 5.19 and was also at a lower wavelength than the other films. The position of the absorption edge is in agreement with those obtained previously for yellow electrodeposited CdS films (Morris *et al.* (1992), Rami *et al.* (1999)). There is a direct correlation between the absorption edge and the band gap of the CdS (Lind and Bube (1962), Tujillo *et al.* (1996), Shirai *et al.* (1996)). The absorption edge showed a shift to longer wavelengths, i.e. lower optical band gap as the film thickness' increased on both ITO and FTO substrates. These transmission curves are similar to those obtained in previous studies, but the percentage transmission was lower (Morris and Vanderveen (1992), Rami *et al.* (1999)). This could be due to the thickness of the films in this study, since no mention was made of the thickness of the films in the above reports. These transmission values are, however, higher than those obtained by Shirai *et al.* (1996) after annealing electrodeposited CdS films.

After annealing, the transmittance decreased in comparison to a film of similar thickness on the same substrate prior to annealing. Figure 5.20 shows the transmittance of CdS films after annealing at different temperatures and for different times in comparison to an as deposited film of 800Å. The transmittance of the annealed films increased as the annealing temperature increased. The length of the annealing process does not appear to be as influential as the temperature, but, for longer annealing times, the lower wavelengths (below 500 nm) were transmitted less efficiently than for shorter annealing times (Figure 5.20) (462°C for 30 min vs. 460°C for 15 min.). The absorption edge was sharper for the longer annealing times. This unexpected decrease in the transmittance after annealing was previously reported by George *et al.* (1996(b)) for chemical bath deposited CdS, but it is not typical for electrodeposited CdS. The transmission of electrodeposited films usually remains relatively similar to the as deposited film or improves after annealing (Morris *et al.* (1992), Shirai *et al.* (1996), Rami *et al.* (1999)). The reason for the decrease in the transmittance of the annealed films in relation to the as deposited films is not clear, but could be due to scattering effects.

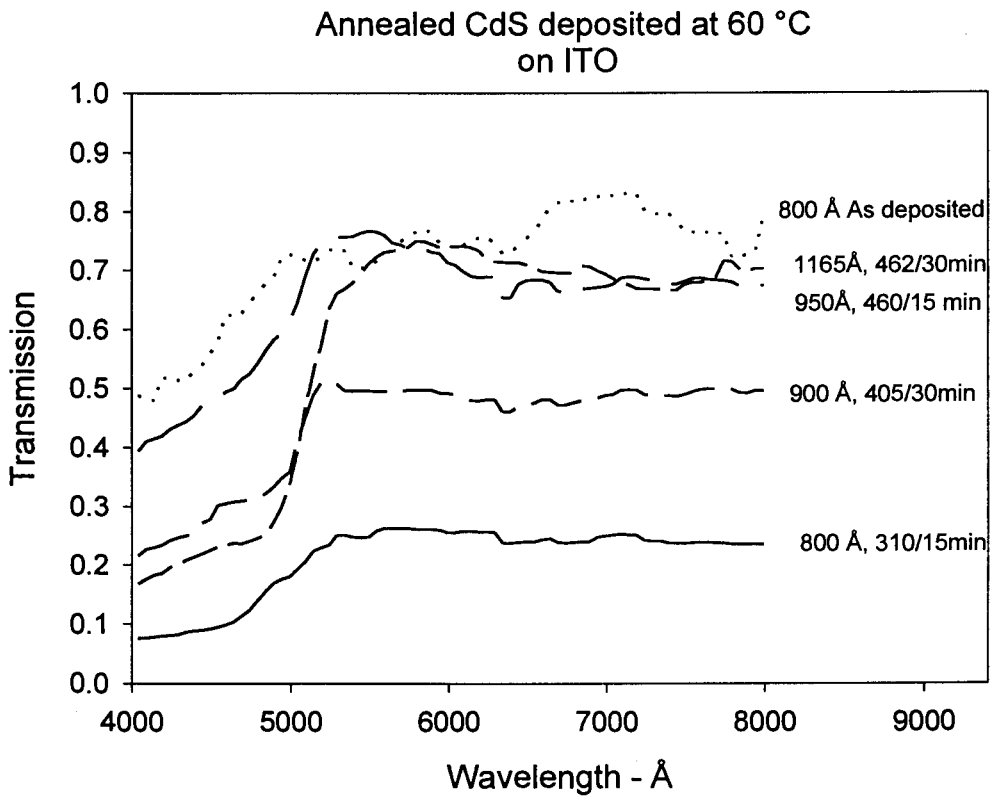

Figure 5.20: Transmittance of visible light through the CdS films on ITO substrates after annealing at various temperatures and times.

The expected increase in the transmittance of the films as the annealing temperature increases is observed (Shirai *et al.* (1996), George *et al.* (1996(a))). The sharpening of the absorption edge and its shift to longer wavelengths which is evidence of a decrease in the band gap of the CdS has also been previously reported (George *et al.* (1996(b)), Sasikala *et al.* (2000)). A correlation between the grain size of the film and the transmittance has been shown to exist, with the larger grains after heat treatments resulting in higher transmittance (Lee *et al.* (1987), George *et al.* (1996(b))). It would appear that the same phenomenon is seen here, since the higher annealing temperatures and the longer annealing times resulted in larger grains/particles in the films (Section 5.9.4) and higher transmission.

Annealing CdS films in the presence of $CdCl_2$ has been found to be advantageous in the improvement of the efficiency of the solar cells (Morris and Das (1993), Ferekides *et al.* (1993)). There is vast improvement in the microstructure of the CdS films after $CdCl_2$ treatment and annealing (Morris and Das (1993), Johnson (2000)).

The effect of annealing after treating the CdS surface with $CdCl_2$ on the transmittance of the films in this study is shown in Figure 5.21. Despite the differences in thickness of the films, it can be concluded that the $CdCl_2$ treatment increases the transmittance of the film, since the $CdCl_2$ treated films are thicker than the non-treated films and yet they have higher transmittance after annealing at the same temperature. The longer annealing time seems to be more crucial when annealing after $CdCl_2$ treatment compared to the untreated films, since the 30 minute annealing has a higher transmittance across the visible spectrum (4000 Å to 8000Å). Unlike the untreated films, the absorption edge shifted to lower wavelengths with longer annealing times. The absorption edge is also shifted to lower wavelengths after 30 minutes annealing at 400°C in comparison to the annealed films that were not treated with $CdCl_2$, but is still at a higher wavelength in comparison to an unannealed film of similar thickness.

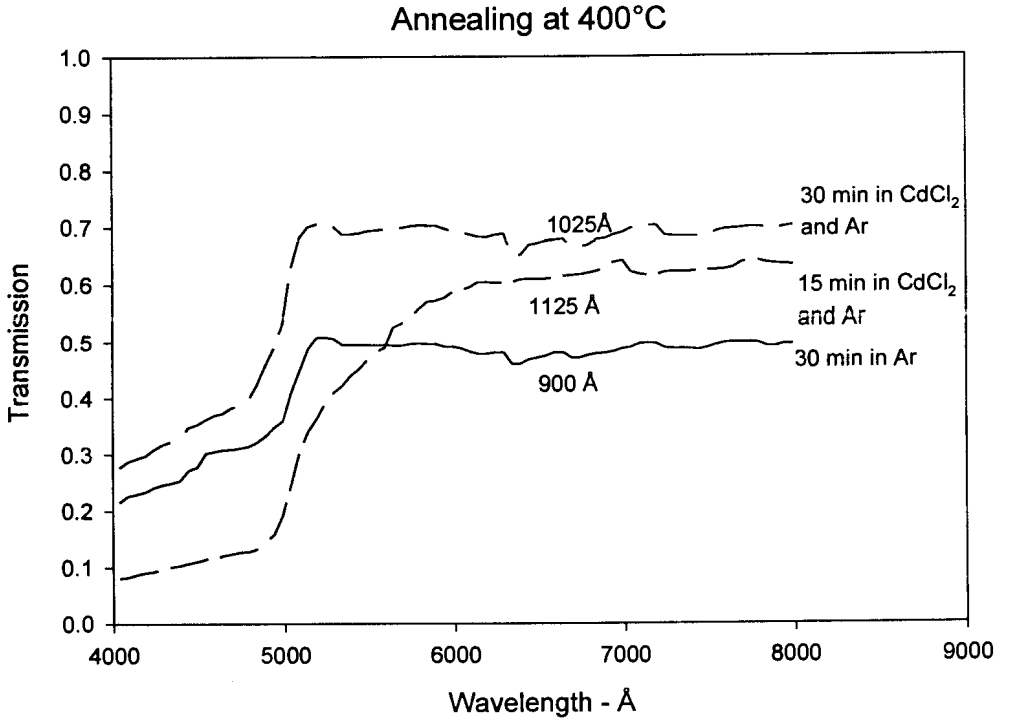

Figure 5.21: The transmittance of CdS films with $CdCl_2$ treatment after annealing compared to a film annealed in Argon without $CdCl_2$ treatment at 400°C.

Morris and Das (1993) reported that the $CdCl_2$ treatment resulted in increased transmission at wavelengths lower than 4000Å. This range was not investigated in this study, but it does appear that, for the same heat treatment conditions (30 minutes annealing at 400°C in Figure 5.21), the $CdCl_2$ treated film had almost 10% higher transmission for wavelengths below 5000Å in comparison to those films which were not treated.

Adhesion of the Films

The average CdS layers were transparent and bright yellow in colour. The films exhibited strong adhesion to the substrates for the entire temperature range (30°C – 90°C). They were not lifted off with the scotch tape test (Dini (1993)). In order to remove the films for further examination in the transmission electron microscope, they had to be scratched off with a diamond scriber.

5.9. Microstructural Development of CdS films

CdS films have been successfully electrodeposited at temperatures ranging from 25°C to 90°C (Fatas *et al.* (1986), Morris *et al.* (1992), Shirai *et al.* (1995)), but information regarding the effect of temperature on the microstructure of the CdS films is not available. During this investigation, CdS films were electrodeposited between 30°C and 90°C on the two substrates for times of 90 minutes unless otherwise stated. The microstructures of the films were studied in the SEM and TEM. CdS films were also deposited on the two substrates for times ranging from 1 minute to 90 minutes at deposition temperatures of 60°C and 90°C. These films were used to determine the microstructural development of the electrodeposited CdS films on the surfaces with significantly different morphologies and roughness values. Films were also annealed in a flowing argon atmosphere between 300°C and 460°C for 15 or 30 minutes with and without $CdCl_2$ treatment. The microstructures of the annealed films were also evaluated.

5.9.1. Effect of deposition temperature on microstructure

CdS is typically electrodeposited at 90°C from the aqueous solutions (Morris *et al.* (1992), Pandey (1996)), with some studies depositing at room temperature, (Fatas *et al.* (1986), Shirai *et al.* (1995), Nishino *et al.* (1999)). Thin films of CdS were electrodeposited on to the two substrates previously discussed (Section 5.1) for 90 minutes unless otherwise stated. The microstructure of the final films is shown in Figure 5.22 for both substrates. The CdS film is comprised of particles which are agglomerates of platelets and elongated grains. The microstructural development of these films is discussed in more detail in Sections 5.9.2 and 5.9.3. The size of the agglomerates varied and the smooth ITO substrate had agglomerates of approximately 300 nm (Figure 5.22 (a)) while the FTO agglomerates ranged from 300 nm – 400 nm with smaller particles of approximately 100 nm and less between the larger ones (Figure 5.22 (b)).

Decreasing the deposition temperature resulted in slower deposition rates and consequently thinner films for the same deposition times. This has been previously attributed to the decrease in the rate-controlling step involving the dissociation of the thiosulphate ions in solution (Morris *et al.* (1992)).

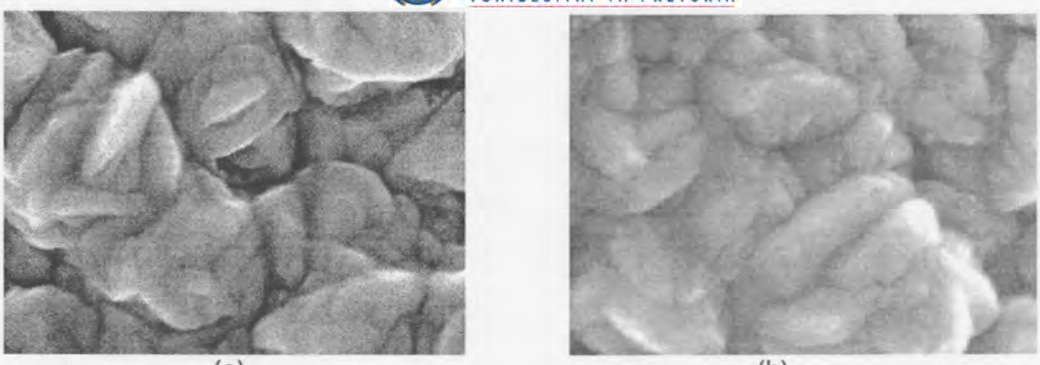

Figure 5.22: A SEM image of the films deposited at 90°C on (a) the ITO and (b) the FTO substrates.

Lowering the deposition temperature to 60°C and depositing for 90 minutes resulted in thinner films due to the lower deposition rates, but the microstructure of the films were similar to those deposited at 90°C, Figure 5.23 The packing of the agglomerates was, however, not as dense as at 90°C. The agglomerate sizes were smaller than those deposited at 90°C in that the agglomerates ranged between 100 nm and 300 nm in diameter for the two substrates. It can be seen from the micrographs, that at a deposition temperature of 60°C, the deposited particles are still clearly crystalline.

After only a few minutes deposition at bath temperatures ≥60°C the deposited particles are clearly composed of an agglomeration of grains (Figure 5.24). The substrate was completely covered after about 30 – 40 minutes deposition at 60°C, and in less than 5 minutes at 90°C.

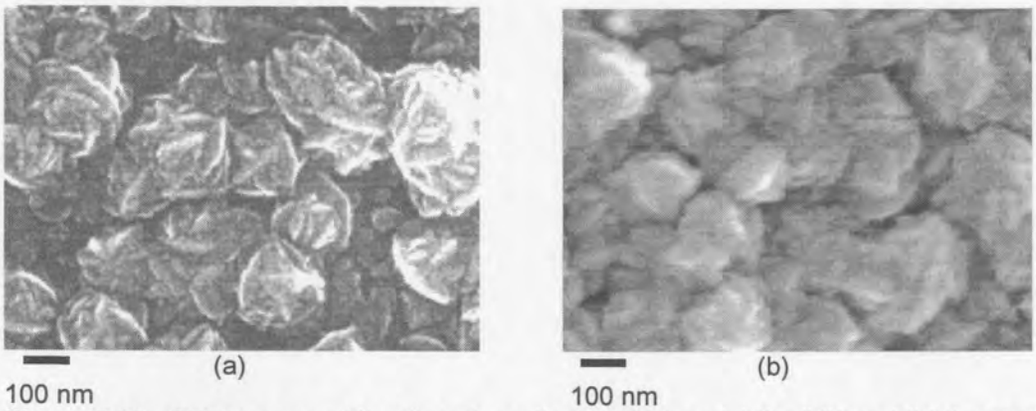

Figure 5.23: SEM images of the films deposited at 60°C on (a) the ITO and (b) the FTO substrates.

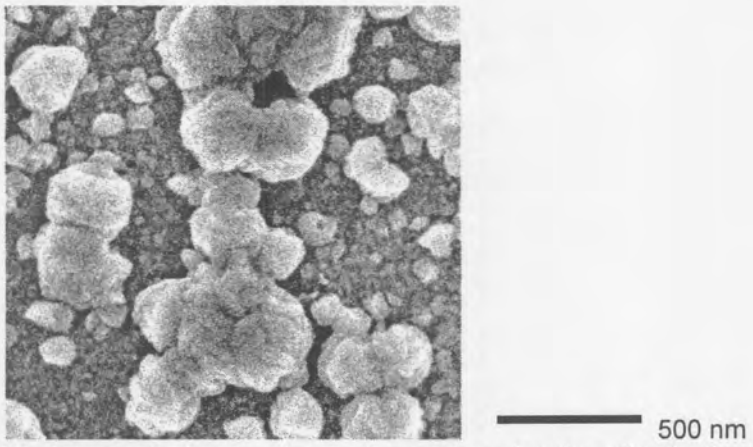

Figure 5.24: SEM micrograph showing the agglomeration of grains after 1 minute depositing at 90°C.

When deposition is carried out at 50°C the substrate is not completely covered after 90 minutes deposition (Figure 5.25(a)). The grain substructure of the particles is still clearly visible (Figure 5.25(b)) but smaller compared to deposits formed at higher temperatures.

The deposition at 30°C was extremely slow in comparison to higher temperatures, and the substrate was just barely covered after 4 hours of deposition. Featureless particles with no resolvable substructure were observed. The particles on the FTO substrate were larger than those on the ITO substrate (Figure 5.26). It was only after

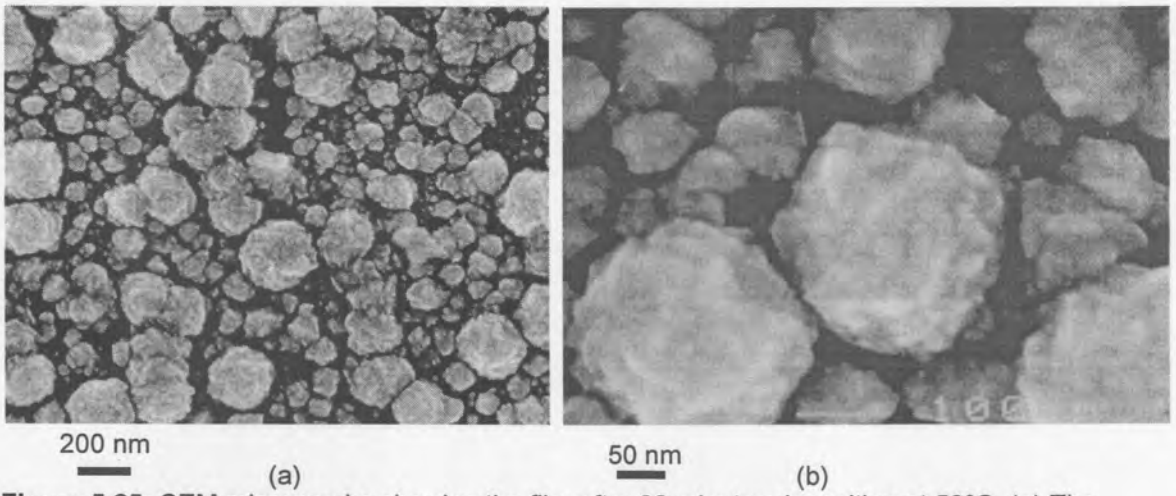

Figure 5.25: SEM micrographs showing the film after 90 minutes depositing at 50°C. (a) The substrate is not yet completely covered at this time, although it can be seen (b) that the particles are comprised of grains agglomerated together.

15 hours deposition that the grains constituting the particles developed into sizes of about 10 – 100 nm which could be resolved in the SEM (Figure 5.27(a)). Dark field electron microscopy, however, revealed predominantly small grains, mostly with sizes ≤ 10nm (Figure 5.27(b)). This implies that most of the apparently large particles (~100nm) observed by FESEM actually had a much finer substructure of smaller grains.

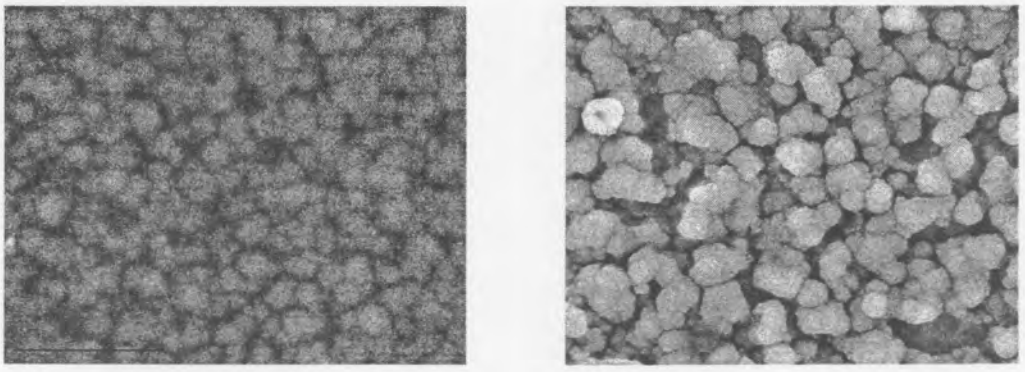

Figure 5.26: A SEM image of the films deposited at 30°C on (a) the ITO and (b) the FTO substrates after depositing for 4 hours.

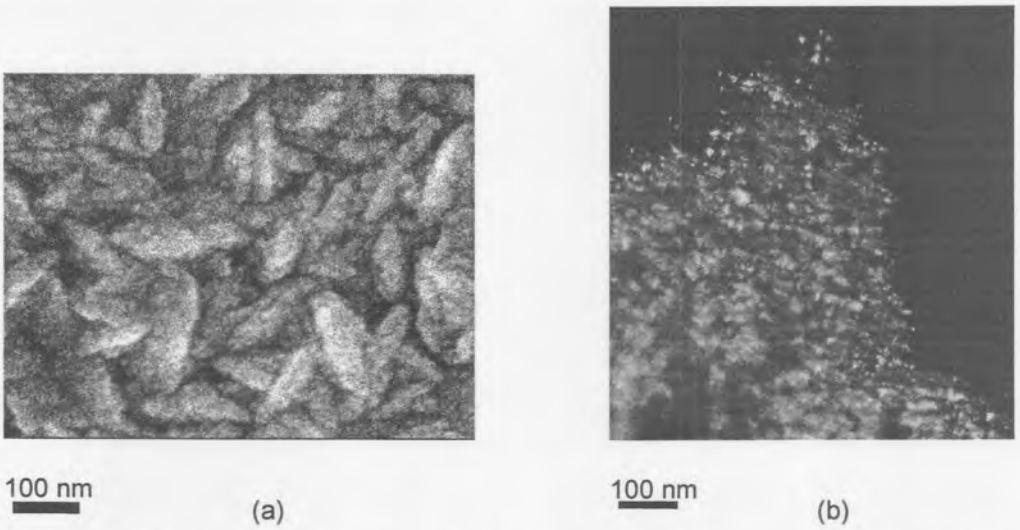

Figure 5.27: After 15 hours deposition at 30°C, the FESEM micrograph (a) of the film showed particles/grains of 10 – 100 nm had formed, while the dark field transmission electron micrograph (b) showed a high density of much smaller grains.

The films deposited in the temperature range from 30°C to 90°C were scraped off the substrates and collected on electron microscope grids for transmission electron microscope examination. Transmission electron diffraction (TED) patterns of films which were deposited at bath temperatures ≥ 60°C consisted of sharp rings, indicating well crystallized, polycrystalline deposits (Figure 5.28(a)). All the diffraction patterns are consistent with the hexagonal (wurtzite) phase of CdS. The three closely spaced inner rings are characteristic and correspond to the 100, 002 and 101 reflections of hexagonal CdS. No evidence for the cubic phase could be found in any of the patterns. The presence of all allowed reflections, together with the absence of intensity variations on the circumference of the rings, indicates that the grains have no preferred orientation. These results concur with those of Rami *et al.* (1999) who found electrodeposited CdS films to be hexagonal by x-ray diffraction (XRD).

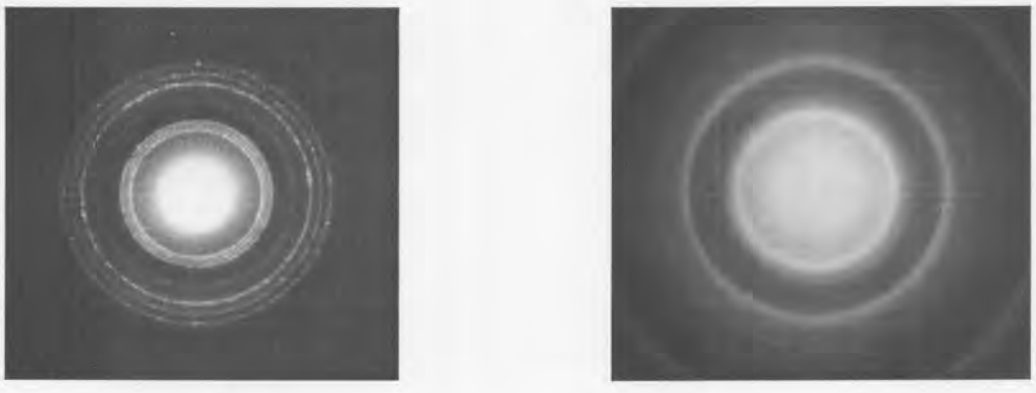

(a) (b)

Figure 5.28: A typical TED pattern of film deposited at bath temperature (a) ≥ 60°C and (b) < 60°C

For deposits formed at bath temperatures < 60°C the TED patterns consisted of a few relatively broad, diffuse rings (Figure 5.28(b)). The broad rings indicate that the grain size is very small. Although the broadening of the rings precludes accurate measurement of lattice spacings, the patterns are more in agreement with the hexagonal phase. Assuming the camera constant, which was previously established for exactly the same diffraction conditions, the three prominent rings in Figure 5.28 (b) correspond satisfactorily to the 100, 110 and 200 reflections of hexagonal CdS. Despite the broadening of the rings, the presence of the strong 002 and 101

reflections should easily have been observed. The absence of these reflections could be explained if it is assumed that the grains have a preferred orientation with the c-axis perpendicular to the substrate, but there is no preferred alignment in any direction in the plane of the film. This preferred orientation is not uncommon and has, for example, been reported for thin CdS films on InP substrates (Froment *et al.* (1995)).

In a previous study (Rami *et al.* (1999)), XRD was used to determine the crystallinity of electrodeposited CdS films. According to the XRD patterns the deposits formed at 20°C were found to be amorphous. In the SEM and dark field TEM images of the films deposited below 60°C, very small grains were observed. These grains have been shown, by XPS, to be close to stoichiometric CdS for all deposition temperatures (Section 5.3). The small size of the crystallites was also evidenced by the diffraction ring broadening. The Raman investigations (5.6) have shown clear, characteristic peaks for all deposition temperatures. Together these findings show unequivocally that the films, even those deposited at 30°C, are indeed crystalline. There have been other studies that have shown that X-ray diffraction is not necessarily sensitive enough to determine the crystallinity of very small crystallites, but that Raman spectra can more accurately reflect the crystalline state of small particles (Veprek *et al.* (1981), Zahn *et al.* (1991)).

The lowest deposition temperature at which a continuous, well crystalline film can be obtained in a reasonable deposition time ($\leq$ 90 minutes) can as a rough guide be taken as about 60°C. An XPS study of the composition (Section 5.3) of the deposited films has shown that the Cd/S ratio was not significantly influenced by deposition temperature. All the temperatures produced films close to stoichiometric composition, yet slightly cadmium rich.

Qualitatively, the microstructure of deposits obtained from baths at temperatures in the range 60°C to 90°C was found to be very similar for a particular substrate. We will now discuss the results for deposition at 60°C and 90°C as representative examples of the effect of bath temperature and different substrate morphologies on the microstructural development of CdS.

5.9.2. *CdS films deposited on the ITO substrate*

The microstructural development of CdS films on the smooth ITO substrate was studied at regular intervals during deposition. The temperatures used during deposition were 60°C, which has been identified as the lower limit for efficient deposition of CdS films (Section 5.9.1) using the conditions described in Section 4.2, and 90°C, a commonly used temperature in the production of relatively high efficiency solar cells (Morris *et al.* (1992)).

After depositing at 90°C on the ITO for 1 minute the AFM and SEM showed three distinct regions in the samples (Figure 5.29). In the AFM image (Figure 5.29 (b), the darkest regions correspond to the substrate, the intermediate grey levels correspond to smaller particles, while the lightest regions correspond to higher, usually larger, particles. At this stage the particles were evenly distributed across the surface and large areas of the surface were not covered by the CdS, which is consistent with the findings of Rami *et al.* (1999). It is, however, evident that, even at this early stage, coalescence had already occurred in local areas. From SEM images the small particles were found to have diameters of less than 50nm and the large ones up to 100 nm (Figure 5.29 (a)). From both the AFM and SEM images, it was clear that the larger diameter particles were higher than the smaller diameter particles. When analysing the height distribution of the particles, there were two distinct particle height ranges, with averages of 25 nm (for the small particles) and 40 nm (for the

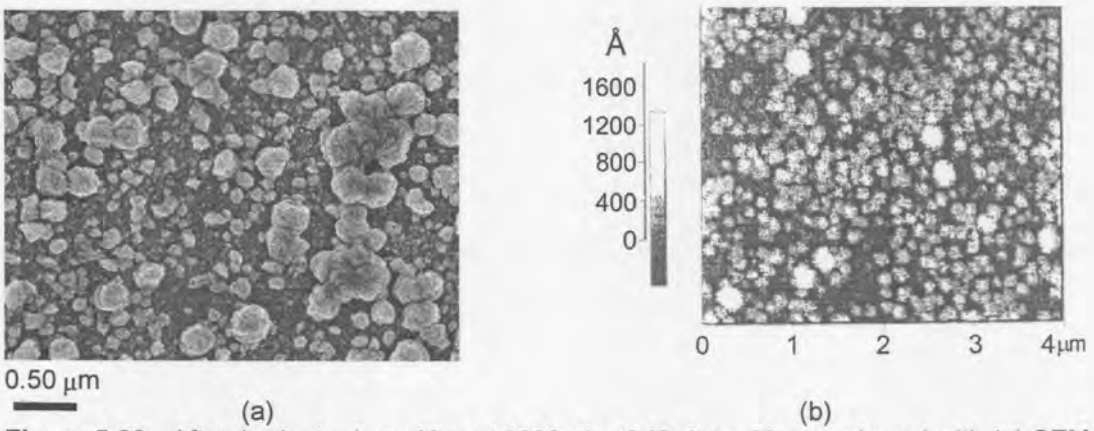

Figure 5.29: After 1 minute deposition at 90°C, the CdS deposition as viewed with (a) SEM and (b) AFM. (Note: the areas imaged are not the same.)

larger particles). Lateral growth, therefore dominated in the initial stages of deposition on the ITO substrates, which agrees with findings by Rami *et al.* (1999).

Viewing the deposited particles at higher magnifications (Figure 5.30 (a)), it can be seen that they are generally not single crystal grains, but agglomerates of grains. This was also evident in the high magnification AFM image of a single agglomerated particle (Figure 5.30 (b)).

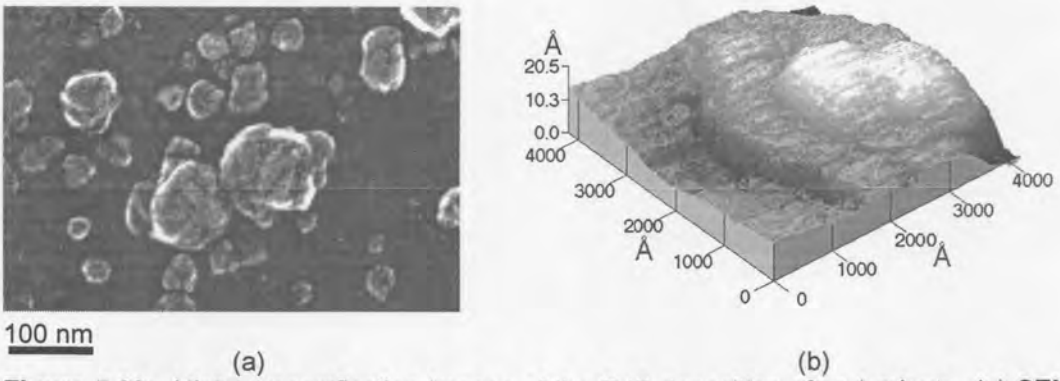

(a) (b)

Figure 5.30: Higher magnification images of the CdS deposition after 1 minute. (a) SEM image showing the agglomerate nature of the particles and (b) an AFM image of one of the smaller agglomerates.

The composite structure is more pronounced in the SEM images after longer deposition times. Figure 5.31 (a) shows aggregates of elongated grains and flat, plate-like grains. These platelets were 100 – 200 nm in diameter and the elongated grains up to 200 nm long. There is no evidence from these images of any preferred orientation of the grains. Similar elongated particles and platelets were also seen in the AFM images presented by Rami *et al.* (1999) after 40 minutes electrodeposition of hexagonal CdS films. As deposition proceeded, the agglomerates grew by further nucleation and growth of the grains. After about 4 – 5 minutes deposition, coalescence of the particles had occurred to the extent that the substrate was essentially covered by the agglomerates (Figure 5.31 (a)). The average particle diameter after 5 minutes was about 250 nm and the average thickness 35 nm. The agglomerates grew predominantly horizontally (parallel with the substrate) with time, until interference from neighbouring agglomerates occurred. After 20 minutes deposition, the typical agglomerates of the as deposited CdS film are seen (Figure

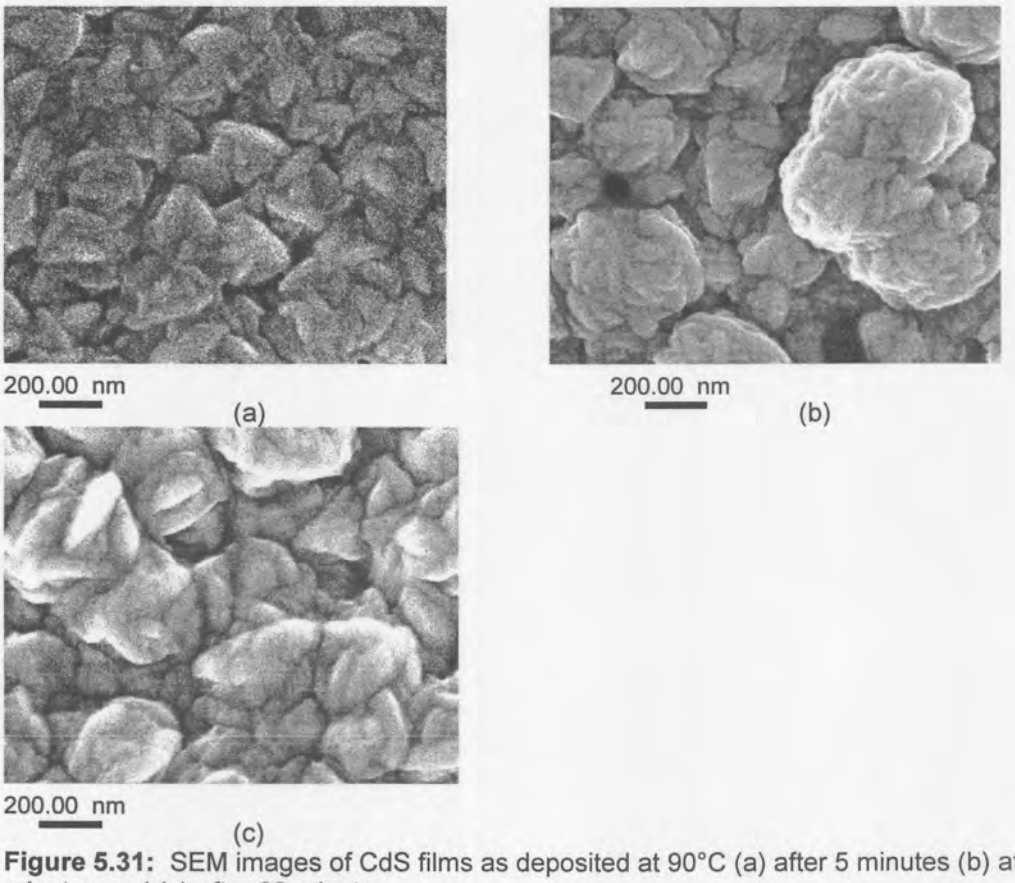

Figure 5.31: SEM images of CdS films as deposited at 90°C (a) after 5 minutes (b) after 20 minutes and (c) after 90 minutes.

5.31 (b)). The general morphology and diameter of the particles did not change significantly as the deposition time increased from 20 minutes to 90 minutes (Figure 5.31 (b) and (c)). The agglomerates in the final films deposited at 90°C were approximately 400 nm in diameter with no signs of preferred orientation (Figure 5.31 (c)), which is in agreement with the TED patterns obtained (Section 5.9.1, Figure 5.28(a)).

Cross-sectional SEM of the 90°C deposits (Figure 5.32) showed that the particles had a columnar structure. Although there were places where the deposit was two, and occasionally more, particles thick, in general, the height of a single, composite particle corresponded to the local thickness of the deposit, similar to that reported by Yoshida *et al.* (1999). Apart from occasional, localised voids, the deposit had good contact and conformity with the substrate surface.

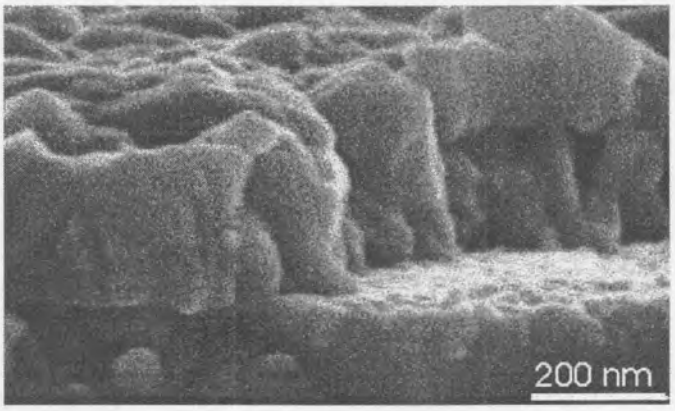

Figure 5.32: Cross-sectional SEM image showing the columnar structure of a CdS film elecrodeposited at 90°C.

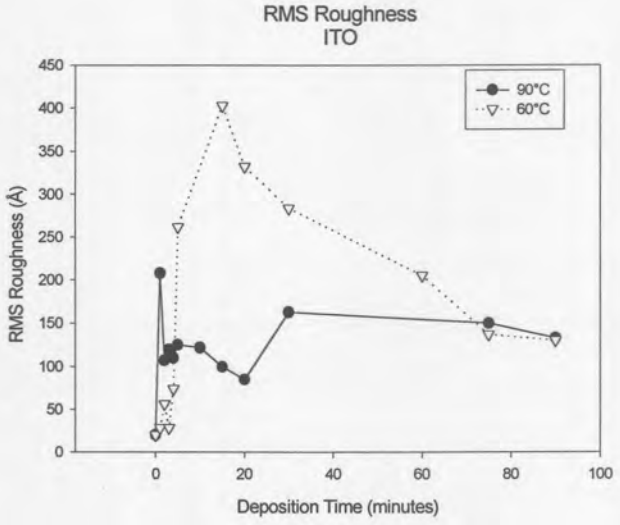

Figure 5.33: RMS roughness values of CdS films deposited on ITO substrates at 90°C and 60°C as a function of deposition time.

The surface roughness of the films is of considerable practical importance for the deposition of subsequent films, such as CdTe. The RMS roughness values of the surfaces were found to decrease after an initial significant increase (Figure 5.33) due to the evenly distributed CdS deposits on the surface. The average peak to valley distance decreased as more of the surface was covered as a result of lateral growth of the composite particles with deposition time. The RMS roughness values of the films deposited at 90°C increased after 30 minutes to approximately 150 Å. There was little change in the RMS roughness values as the deposition times increased to 90 minutes. This increase can be attributed to the larger particles in the agglomerates, compared to 20 minutes deposition. As the particles grew in height,

there was also lateral growth so that the RMS roughness remained constant as the average thickness of the films increased with times longer than 30 minutes.

When the deposition temperature was lowered to 60°C, the current density and hence the deposition rate decreased significantly (Morris *et al.* (1992), Pandey *et al.* (1996)). After 1 minute deposition, there were small particles on the surface <40 nm wide (Figure 5.34 (a)). After 3 minutes deposition, these particles were larger (>50 nm) and more numerous, compared to 1 minute (Figure 5.34 (b)). The microstructure and coverage of the surface after 5 minutes deposition at 60°C (Figure 5.34 (c)) was comparable to that after 1 minute deposition at 90°C (Figure 5.29). The major difference was that the particles were more uniform in size, although a few smaller particles were visible. This implies that most of the nucleation occurred within a short space of time (less than 5 minutes) across the surface and very little after this. The particles found on the surfaces were also agglomerates of smaller grains, as found in the films deposited at 90°C. Full

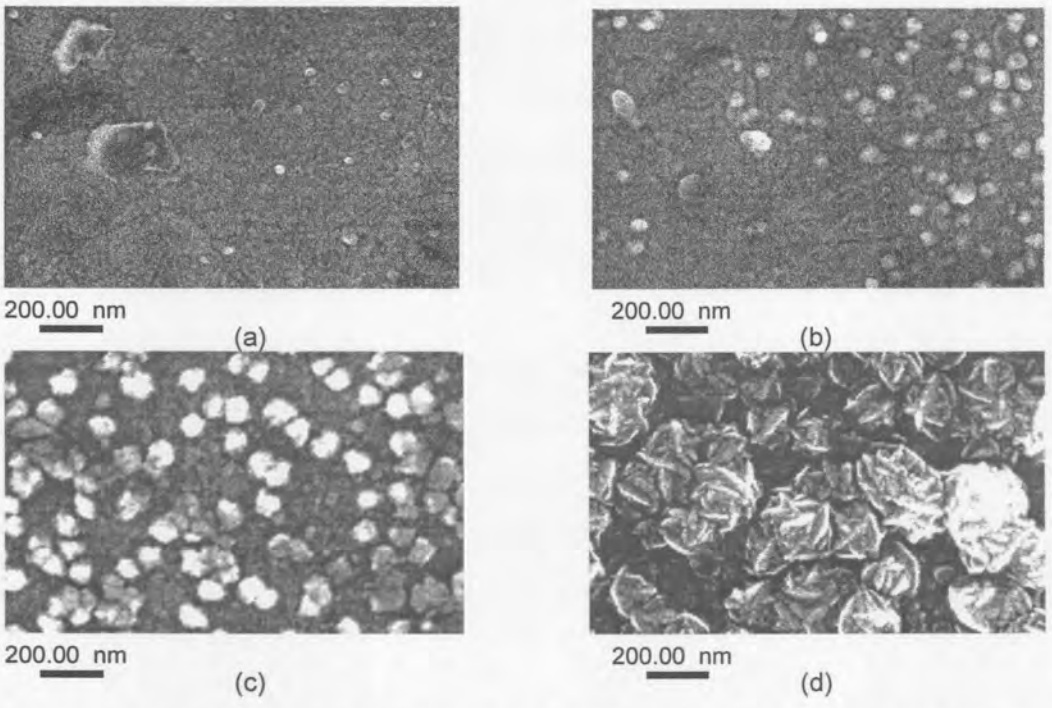

Figure 5.34: SEM images of CdS deposited at 60°C on ITO substrate after (a) 1minute, (b) 3 minutes, (c) 5 minutes and (d) 90 minutes.

coverage of the surface occurred only after 30 – 40 minutes. The final film deposited for 90 minutes at 60°C had particles of approximately 200 nm diameter (Figure 5.34 (d)).

Cross sectional views of the films deposited at 60°C show that even after 90 minutes deposition, there were still relatively deep cusps between some of the particles (Figure 5.35). The columnar particles extended through the thickness of the film, as was found for films deposited at 90°C. Excellent conformal coverage of the substrate was observed with very few voids at the interface.

Figure 5.35: Cross-sectional SEM image of a film deposited at 60°C for 90 minutes on an ITO substrate.

Figure 5.33 also shows the variation of the RMS roughness values with deposition time at a deposition temperature of 60°C. The roughness increased from 2 nm for the clean substrate to a maximum of about 40 nm after 15 minutes deposition. This initial increase is, as for the 90°C deposits, due to the formation and growth of isolated, three dimensional particles prior to coalesence. After coalescence, lateral growth, which is much slower compared to deposition at 90°C, leads to a gradual decrease in the roughness.

The final RMS roughness values of the films after 90 minutes deposition at both 60°C and 90°C were approximately 150Å, which were significantly rougher than the clean ITO substrates prior to deposition, thus exhibiting surface roughness amplification (Pandey (1996)). Although the particle size of the final films deposited at 60°C were smaller than those deposited at 90°C (200 nm and 400 nm

respectively), the RMS roughness values of the films were the same. This can be attributed to the closer packing of the larger agglomerates deposited at 90°C, compared to the smaller, less closely packed agglomerates deposited at 60°C.

5.9.3. CdS films deposited on FTO surfaces

The microstructural development of electrodeposited CdS films on the rough FTO substrate was also studied at regular intervals during the deposition process at temperatures of 60°C and 90°C.

Initial deposits on the rougher FTO surfaces after 1 minute deposition at 90°C showed agglomerated particles, mostly between 100 nm and 200 nm, which were evenly distributed across the substrate surface. The particles deposited non-preferentially on the surface and were found in the valleys, on the peaks and on the inclined slopes of the substrate (Figure 5.36 (a)). After 3 minutes deposition, the larger agglomerates were between 150 nm and 200 nm and many smaller particles of less than 100 nm were observed between the larger agglomerates, indicating that further nucleation had taken place (Figure 5.36 (b)). As with the 90°C deposits on the ITO substrate, typical agglomerate structure with elongated and plate-like grains

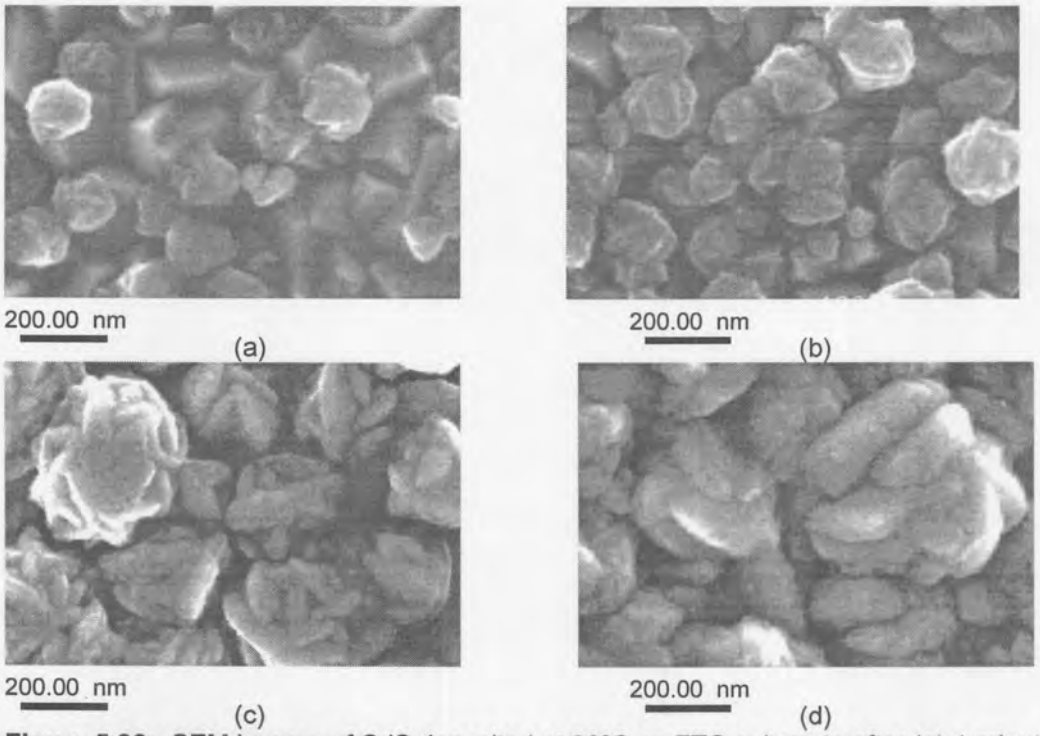

Figure 5.36: SEM images of CdS deposited at 90°C on FTO substrate after (a) 1 minute, (b) 3 minutes, (c) 15 minutes and (d) 90 minutes.

could be seen in both large and small agglomerates (Figure 5.36 (c)). After 4 – 5 minutes deposition, the surface was completely covered by agglomerates of 150 nm – 200 nm. Very few particles of significantly smaller size were observed, indicating that nucleation of the initial particles occurred during the first few minutes of deposition, after which growth of existing particles tended to dominate over the nucleation process. The coalescence of the particles occurred with time and, after 90 minutes (Figure 5.36 (d)), the denser packing of larger particles could be seen when compared with 15 minute deposition (Figure 5.36 (c)). After 90 minutes deposition, the agglomerates were between 350 nm and 500 nm in diameter (Figure 5.36 (d)), while the average thickness of the final deposit was between 150 nm and 250 nm. As with the films deposited on the ITO, the lateral growth occurred preferentially to the vertical growth (height) of the particles.

For deposition at 60 °C, the CdS is initially a thin, flakey deposit with particle size ≤ 100 nm (Figure 5.37 (a)). After 3 minutes the number of the deposited particles has increased significantly (Figure 5.37 (b)). There are nucleation sites distributed evenly across the surface and there appears to be two size ranges, larger agglomerates of up to 90 nm and smaller particles of less than 30 nm. As at 90°C, the particles are not preferentially deposited on any particular site of the substrate. There is a gradual increase in the particle size of the CdS deposit with time and, after 5 minutes, the typical agglomerate structure becomes more prominent. The larger particles are approximately 100 nm wide, with smaller particles of less than 40 nm also present between the larger agglomerates (Figure 5.37 (c)). These are in the particle size range observed after 1 minute deposition at 90°C. This follows a similar trend to that observed with the ITO substrates. After longer deposition times, the deposited film continues to exhibit two agglomerate size ranges and it appears that, unlike at 90°C, nucleation continues on the FTO surface at 60°C until the surface is covered. The growth of the particles continues (Figure 5.37 (d) and (e)) and, after 90 minutes, there are larger particles of up to 300 nm with numerous small particles, < 100 nm, between the larger ones. The elongated grains and platelets which form the agglomerates are clearly visible in the thicker deposits (Figure 5.37 (d) and (e)).

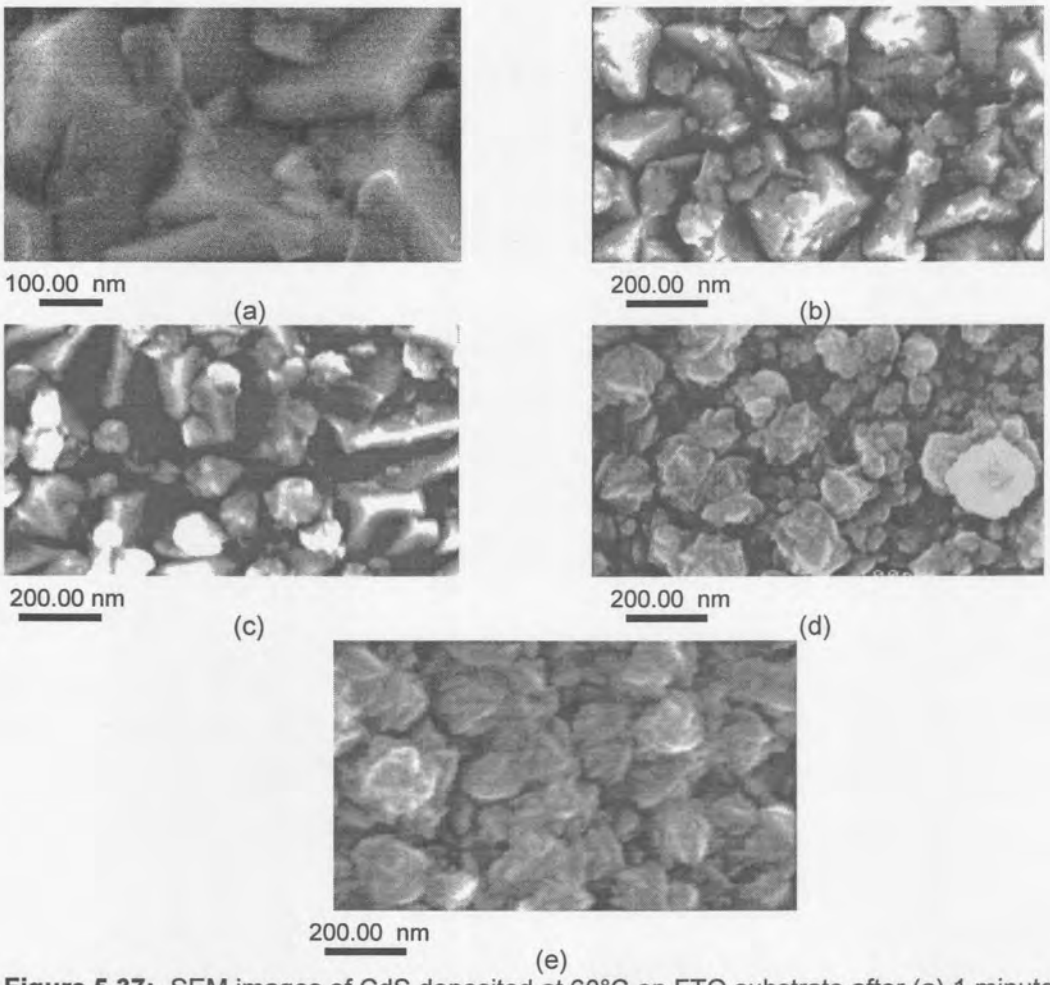

Figure 5.37: SEM images of CdS deposited at 60°C on FTO substrate after (a) 1 minute, (b) 3 minutes, (c) 5 minutes (d) 15 minutes and (e) 90 minutes.

As on the ITO substrates, the cross-sectional views of the CdS films on the FTO substrates showed the films to have formed good contact with the substrate, with a few localized voids visible, Figure 5.38.

Figure 5.39 shows the change in the RMS roughness values for the CdS deposited on the FTO substrate as a function of deposition time at the two deposition temperatures used. For depositions at both 60°C and 90°C, there is an initial significant decrease (after approximately 1 minute of deposition) in the RMS roughness. Although it appears from the SEM micrographs (Figures 5.36 and 5.37) that the initial deposited particles were distributed uniformly over the substrate surface, the roughness data indicated that there must have been significant deposition in the valleys, thus reducing the depth of the valleys and hence the roughness.

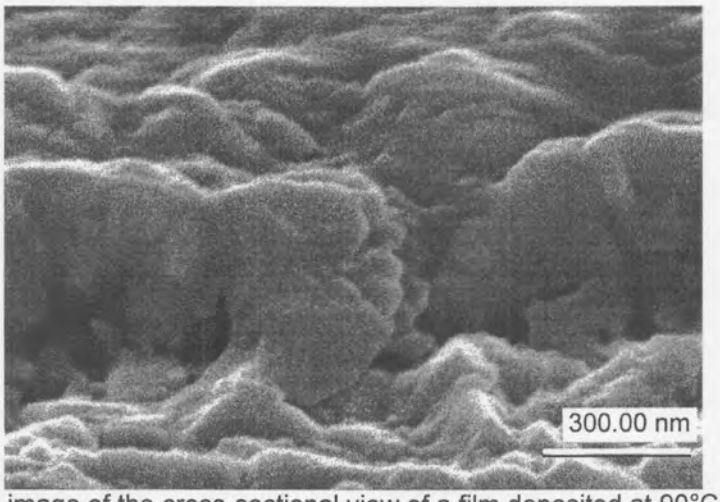

Figure 5.38: SEM image of the cross-sectional view of a film deposited at 90°C on the FTO substrate.

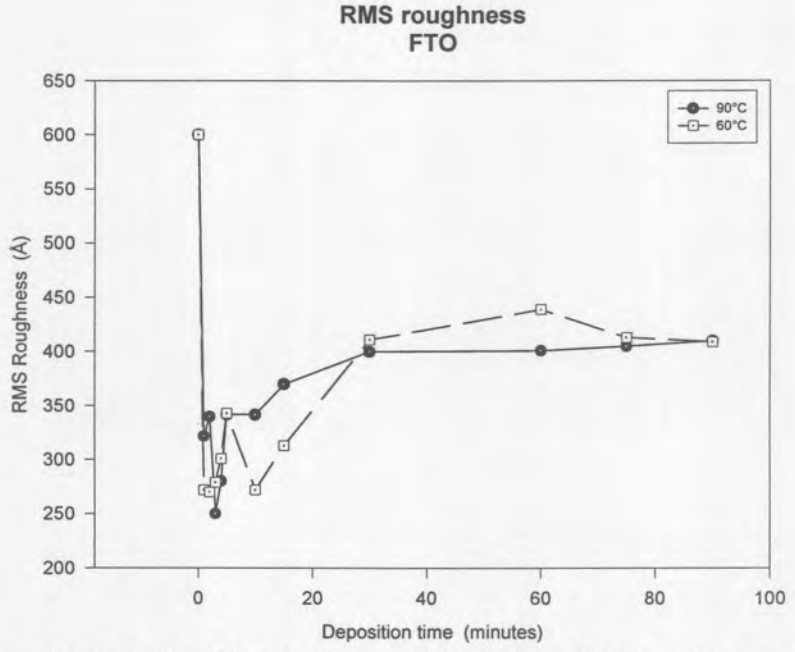

Figure 5.39: The change in the RMS roughness of the FTO and CdS surfaces as a function of deposition time at 60°C and 90°C.

The final roughness values for both the deposition temperatures after 60 minutes deposition are about 400 Å. Although the agglomerates deposited at 60°C are smaller than those deposited at 90°C, the roughness values are in the same range. This is due to the denser packing of the agglomerates after 90 minutes at 90°C, Figure 5.36 (d) compared to 60°C, Figure 5.37 (e). There were more spaces between the agglomerates deposited at 60°C, which increased the RMS roughness

values. This could possibly be decreased to some extent with longer deposition times at 60°C, which should result in further lateral grain growth and hence denser packing.

The final RMS roughness values were significantly lower than the initial roughness of the clean substrate surface. Therefore the surface roughness amplification did not occur on the FTO surface. The reason for this is possibly due to the size of the features on the substrate being comparable to the size of the agglomerates deposited on the surface. The film, therefore, has a smoothing effect on the extreme surface roughness which was initially present. The final roughness (400 Å) of the films deposited on the FTO substrates were, however, much higher than for the films deposited on the ITO substrate which have a final roughness of 150 Å.

5.9.4. Influence of annealing in Argon Atmosphere

Post-deposition treatment of thin film II-VI compounds has long been used to induce good crystallite formation (Feldman and O'Hara (1957)). In this study, the electrodeposited films were annealed between 300°C and 460°C in a flowing argon atmosphere. The annealing has been shown to influence the electrical properties (Basol (1984), Danaher *et al.* (1985), Kohle *et al.* (1987), Lozada-Morales *et al.* (1996)) and result in grain coarsening (Lee *et al.* (1987), Morris *et al.* (1992)). The larger grains have been reported to produce better quality junctions between the CdS and CdTe layers in the solar cells (Lee *et al.* (1987)).

The microstructures of the annealed films were examined in the field emission SEM at the various temperatures. After annealing at 300°C in the flowing argon atmosphere for 15 minutes, there was not much visible difference compared to the as deposited films, Figure 5.40(a). There are some signs of annealing, in that the edges of some of the agglomerates are more rounded than in the as deposited films, Figure 5.40(b). The particles (both large and small) forming the agglomerates are still distinguishable. Increasing the annealing time from 15 minutes to 30 minutes also exhibits the rounding of the edges of the agglomerates, but it is not much more pronounced than that for 15 minutes annealing.

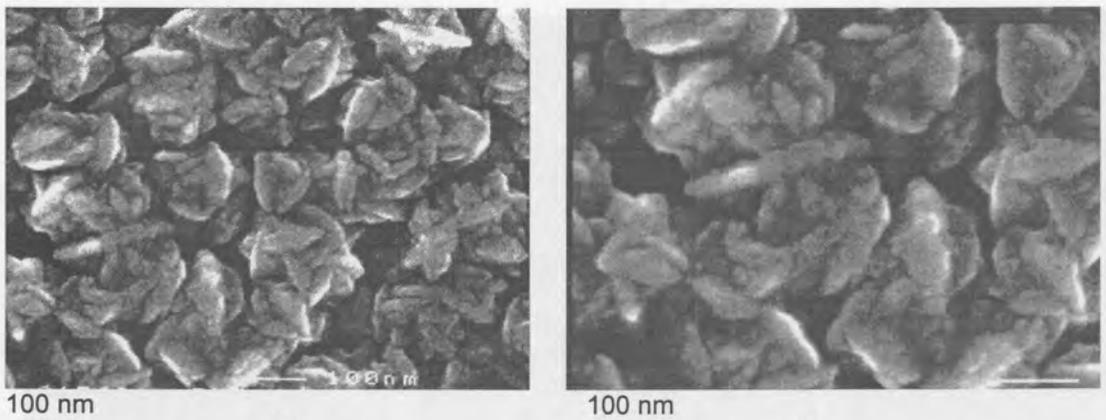

(a) (b)

Figure 5.40: (a) A typical SEM micrograph of a CdS film annealed at 300°C for 15 minutes in argon atmosphere. (b) A higher magnification of an area showing the first signs of annealing which produce rounding of the edges between grains.

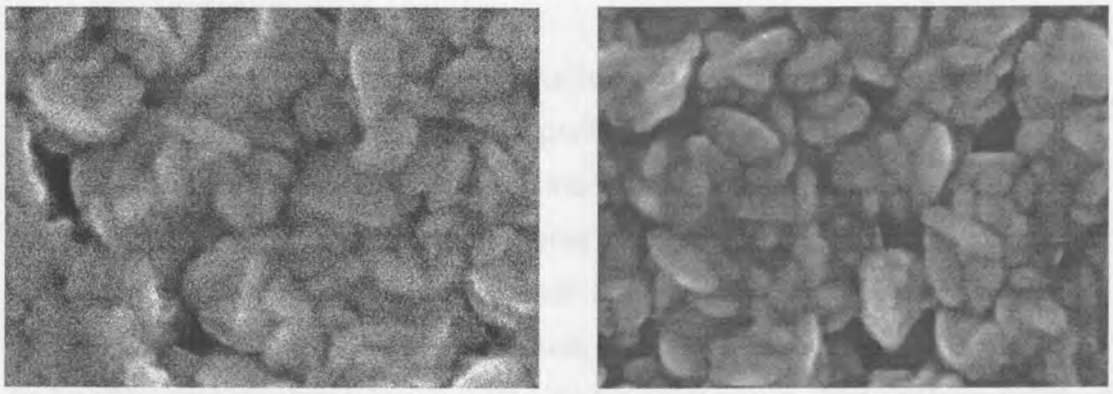

(a) (b)

Figure 5.41: Typical annealed films after (a) 15 minutes and (b) 30 minutes annealing at 400°C in argon atmosphere.

The microstructure was significantly modified after annealing at the higher temperature of 400°C (Figure 5.41) compared to 300°C. The agglomerates showed a more advanced stage of annealing, with the grains in the agglomerates being more coalesced and the agglomerates themselves starting to coalesce to a certain degree. It could be seen that, in the agglomerates, the smaller grains had been incorporated into the developing grains and that the larger grains still protruded from the surface. Comparing the films annealed for 15 minutes and those annealed for 30 minutes, the grains were more prominent in the agglomerates after 15 minutes (Figure 5.41 (a) and (b)).

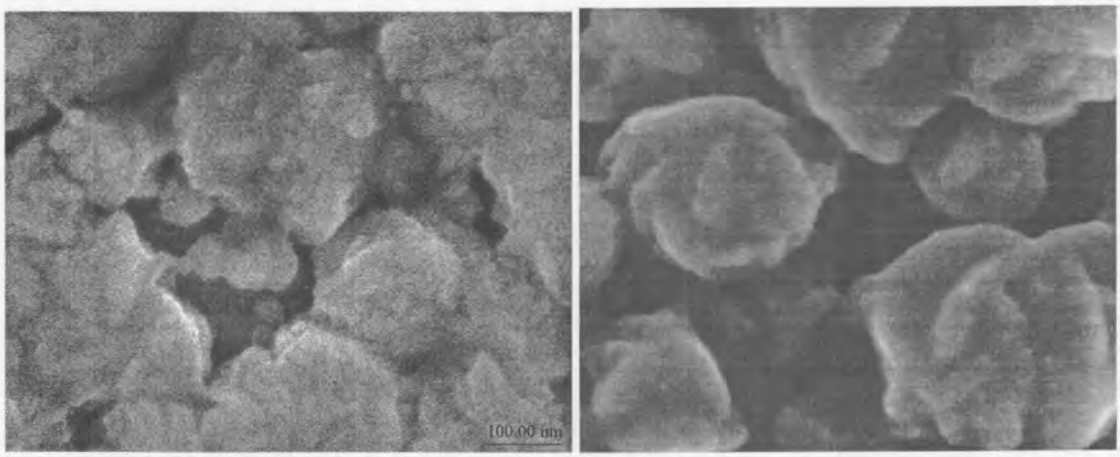

(a) (b)

Figure 5.42: The microstructures of film annealed at 460°C for (a) 15 minutes and (b) 30 minutes.

Increasing the temperature still further to 460°C resulted in further coalescence of the agglomerates (Figure 5.42). After 15 minutes annealing, the agglomerates comprised of a coalesced mass of the forming grain with a few distinguishing characteristic features that were seen in the as deposited films (Figure 5.42 (a)). It would appear that, with flowing argon atmosphere and no pre-treatment of the CdS surface, the longer annealing times show the beginning stages of the film ceasing to be continuous. The melting point of CdS is 1750°C (CRC Handbook of Chemistry and Physics (2000)) and, therefore, it is not expected that copious amounts of CdS evaporate below 600°C – 700°C (Vecht (1966)). The layer was initially 1200 Å thick, which would have resulted in good coverage of the surface. After annealing, however, there was a significant amount of the surface visible, much more than when compared to films annealed for 15 minutes at 460°C or at lower temperatures. It is well known that, when thin films are annealed, agglomeration occurs, i.e. the separation of the film into separate islands (Kane *et al.* (1966)). The observation made in Figure 5.42 is probably attributable to the initial phase in the island formation process that occurs during the annealing of thin films. This process has been characterised into three steps, namely hole formation, hole enlargement and separation into islands; of these, the hole formation is probably what is being observed in Figure 5.42.

5.9.5. *Influence of annealing after $CdCl_2$ treatment*

It is known that the use of $CdCl_2$ during the annealing process of the solar cell improves the electrical properties significantly compared to cells which are untreated (Lee *et al.* (1987), Morris *et al.* (1992), Das (1993(b))). The microstructure of the $CdCl_2$ treated films in the cells has not been studied extensively, in particular the CdS films (Lee *et al.* (1987), Morris *et al.* (1993), Johnson (2000)). In this study the $CdCl_2$ treated films were annealed in the same temperature range as the untreated films and then compared.

After annealing at 300°C there was already a significant difference between the microstructures of the treated and untreated films. The treated films showed characteristic signs of annealing occurring after 15 minutes (Figure 5.43 (a)), with the particles in the agglomerates coalescing in some areas and other areas showing hole formation, which is similar to untreated films after 400°C annealing. Increasing the annealing time from 15 minutes to 30 minutes shows signs of the films loosing the continuous surface coverage, in that the hole formation has taken place after annealing for 15 minutes and hole enlargement occurs for longer annealing times, namely 30 minutes (Figure 5.43 (b)). This is similar to the effect observed after annealing at 460°C for 30 minutes (Figure 5.41 (b)).

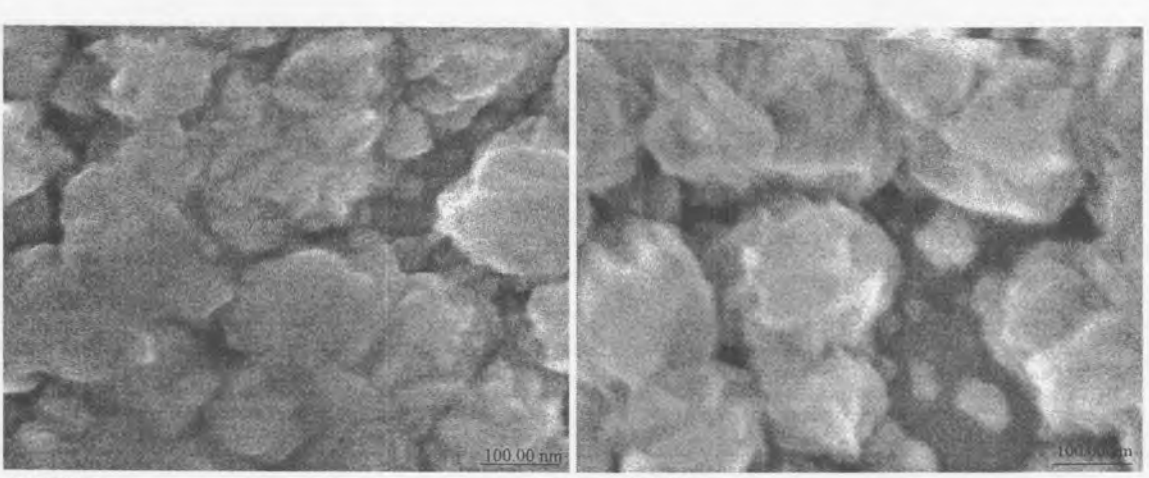

Figure 5.43: The microstructures of CdS films pretreated with $CdCl_2$ after annealed at 300°C for (a) 15 minutes and (b) 30 minutes.

At higher annealing temperatures of 400°C, the particles making up the agglomerates were no longer clearly distinguishable, due to the extent of coalescence of the particles. The coalescence of the agglomerates with each other was also more obvious (Figure 5.44). After longer annealing times, these characteristics were more advanced (Figure 5.44 (b)), although the hole formation and hole enlargement at the grain boundaries can also be seen to be more prominent than at lower annealing temperatures and shorter annealing times.

Annealing at 460°C resulted in the agglomerate structure of the original deposited film being no longer distinguishable, due to grain coarsening and the coalescence of the agglomerates with each other is in an advanced state after annealing (Figure 5.45). This particular film was originally much thicker than the others discussed in this annealing study (~1600 Å) and yet the substrate was also visible in many places. This was an indication of the advanced state of the annealing process in that the hole formation had progressed considerably to the hole enlargement stage. After annealing at 460°C for 30 minutes, the grain size of the film was 150 nm – 250 nm in diameter.

In previous studies, it was reported that $CdCl_2$ treatment prevented the loss of Cd and S from the films and enhanced grain growth during annealing. When studying the XPS results in conjunction with the annealed microstructures, the XPS composition profile studies did not show significant losses of cadmium or sulphur after annealing, except in the surface layers. The composition of the non-surface CdS after annealing with and without the $CdCl_2$ treatment was near stoichiometric. Studying the microstructrures, on the other hand, showed significant differences in the annealing of the CdS when using the $CdCl_2$ treatment. The $CdCl_2$ was found to lower the temperature for the onset of the annealing process by approximately 100°C (300°C for $CdCl_2$ treated films vs. 400°C for untreated films). The treated films were also in a more advanced state of annealing after shorter annealing times in comparison to the untreated films.

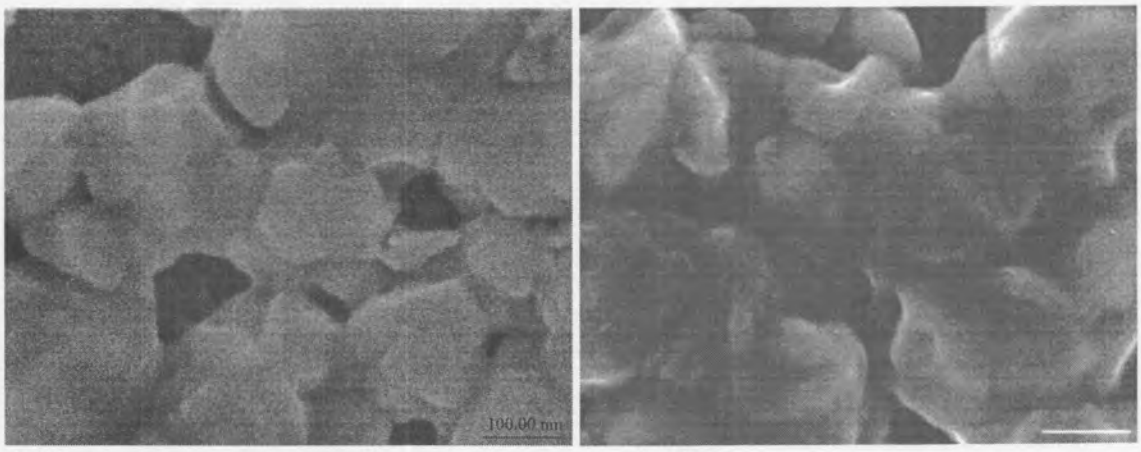

(a) (b)

Figure 5.44: Microstructures of CdS films treated with $CdCl_2$ after annealing at 400°C for (a) 15 minutes and (b) 30 minutes.

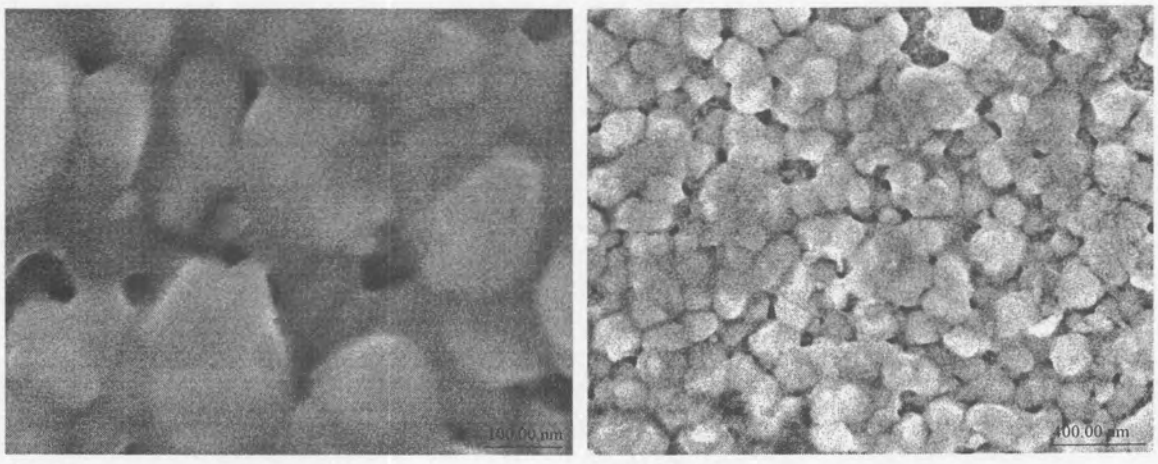

(a) (b)

Figure 5.45: After annealing at 460°C for 30 minutes, the treated CdS films showed (a) microstructures without any of the distinguishing characteristic agglomerates of grains and (b) signs of hole enlargement through which the substrate was visible.

6. Conclusions

The following conclusions were drawn from this study:

6.1. Substrates

- Atomic force microscopy was effectively used to verify the cleanliness of a surface after solvent cleaning, while simultaneously supplying additional information regarding the structure and morphology of the contaminants and the substrate surface.
- RMS roughness can be used as an indication of cleaning efficiency when used in conjunction with the AFM images.
- The efficiency of the cleaning methods used depended on the substrate. The acetone, methanol, isopropanol wash (Method 2) was found to be efficient in cleaning both the ITO and FTO substrates.
- The thinner ITO substrates exhibited higher transmittance across the visible spectra compared to the thicker FTO due the difference in the thickness.

6.2. Effect of deposition temperature on CdS

- Transmission electron diffraction showed that all CdS films electrodeposited in the temperature range 30°C – 90°C had the hexagonal (wurtzite) structure.
- Electrodeposition of CdS between 60°C and 90°C resulted in continuous, well crystalline films in a reasonable time (namely 90 minutes) with no preferred orientation.
- CdS films deposited between 30°C and 50°C were made up of very small crystalline grains with possible preferred orientation, with the c-axis perpendicular to the substrate.
- Raman spectroscopy was successfully used, in conjuction with electron microscopy, to verify the crystallinity of the deposited films.
- Deposition (nucleation and growth) kinetics are influenced by the deposition temperature and the substrate.

- Deposition rate decreases with the deposition temperature.
- Transmittance of white light through the CdS films decreases with an increase in the thickness of the films.
- The CdS films deposited on the ITO substrates had higher transmittance values across the visible spectrum for films of similar thickness deposited on the FTO. This is mainly due to the initial higher transmittance of the thinner ITO layer compared to the FTO layer.
- The XPS results showed that the films were close to stoichiometric CdS and tended to be slightly Cd-rich. There was no significant change in the composition of the CdS films as the deposition temperature was varied from 30°C to 90°C.
- XPS results also showed that there was no change in the oxidation state of the cadmium or the sulphur in the deposition temperature range 30°C – 90°C.
- FTO substrates resulted in, on average, slightly more Cd-rich CdS surfaces in comparison to the ITO substrates for all temperatures. The depth profiles of films deposited at 60°C and 90°C also showed the same phenomenon.

6.3. Microstructural Development

- At both 60°C and 90°C, lateral growth of the grains/particles dominated the initial stages of deposition on both substrates, with the grain diameter being much larger than the height.
- Agglomerates deposited onto the substrates and consisted of elongated grains and flat plate-like grains with no preferred orientation.
- All films deposited onto both substrates at 60°C and 90°C showed good contact and conformity with the substrate.
- Cross-sections of the films showed the CdS particles to have a columnar structure with the thickness of the film typically being the height of a single agglomerated particle.
- Final RMS roughness values of the CdS films deposited at 60°C and 90°C were dependent on the substrate used and independent of the deposition temperature.
- The RMS roughness values of the final CdS films deposited on the ITO films were much higher than those of the clean substrate, indicating that surface roughness amplification does take place on these relatively smooth substrates.

- The RMS roughness values of the final CdS films deposited on the FTO films were much lower than those of the clean substrate, indicating that, on the rough FTO substrates, the electrodeposited CdS had a smoothing effect on the roughness.

6.4. Effect of annealing

- The composition of the CdS film surfaces showed a decrease in Cd content after annealing in argon atmosphere, giving a S-rich surface layer. Below the surface layer, the Cd:S ratio was near stoichiometric for both substrates used.
- The composition of the CdS film surfaces treated with $CdCl_2$ showed an increase in Cd content in some films after annealing in argon atmosphere, giving a Cd-rich surface layer. When removing the surface layer, the Cd:S ratio was again found to be near stoichiometric for both substrates used.
- The use of $CdCl_2$ treatment on the surface prior to annealing caused the temperature at which a visible onset on annealing could be seen in the SEM to be lowered by about 100°C.
- The annealing of the CdS films was characterised by grain coarsening where the smaller grains were incorporated into the larger grains to form even larger grains. Hole formation and hole enlargement were also observed in the films.
- The transmittance of the films increased with an increase in annealing temperature. This could be due to the non-continuous nature of the films after annealing.
- Annealing for a longer period of time in argon atmosphere resulted in a sharper absorption edge and a higher transmittance.
- After $CdCl_2$ treatment, the absorption edge of the annealed films shifted to lower wavelengths and, therefore, higher band gaps, in comparison to the untreated films under the same annealing conditions.
- The Raman spectra indicated that annealing at 460°C for 30 minutes resulted in a more crystalline film since the FWHM of the peak at 300 cm^{-1} decreased from 15 cm^{-1} after deposition to 9 cm^{-1} after annealing.

7. Recommendations

- Investigate effects of substrates on the electrical properties of the CdS film before and after annealing at the different temperatures.
- Correlate these results with the microstructures of the CdS films to determine the optimum microstructure.
- Investigate the effect of intensiostatic electrodeposition and periodic pulsed deposition on the microstructure and electrical properties of the CdS films.
- Investigate the effect of the CdS microstructure on the microstructure of the subsequently deposited CdTe film and the electrical properties and efficiency of the complete CdS/CdTe photovoltaic cell.

8. Acknowledgements

My sincere thanks go to:

- Prof. Danie Auret and Prof. Kappie Gaigher for their supervision during this study.
- Mr. Chris van der Merwe and Mr. Andre Botha of the EM department at the University of Pretoria of assistance with the SEM work.
- The late Prof. Demanet and Mr. Thembile Hillie for the AFM studies undertaken at the University of Transkei.
- Mr. Prem Premachandra for additional AFM studies.
- NRF for financial support via mobility grants for XPS studies.
- Mr. Wynand Louw and Mr. Martin van Staden of MATTEK, CSIR (Pretoria) for the XPS studies and discussions.
- Prof. Johann Brink for assistance with the transmittance experiments and useful discussions.
- Prof. Gerrit Myburg for many insightful discussions.
- Miss Elmarie Oosthuyzen for the many hours she spent cleaning substrates and electrodepositing CdS films.
- Mrs. Linda Prinsloo for assistance and discussions regarding the Raman spectroscopy.
- Mr. Daniel Surridge for proof-reading this manuscript.
- Prof. Deon Raubenheimer and members of the Physics Department at Vista University for the encouragement and interest shown during the duration of this project. Thank you for affording me the time to do the research.
- Mr. Quintin Odendaal for the many welcome interruptions and coffee at La Pat.
- All members of the Physics Department, University of Pretoria for all the small and not so small things you have done for me in the past few years and for always making me feel like one of the department, even when the time between visits was exceptionally long.

9. List of Publications and Conference Presentations

Papers submitted for publication

1. Microstructures of Electrodeposited CdS layers
   J. M. Nel, H. L. Gaigher and F. D. Auret.
   Submitted to Thin Solid Films – September 2000.

Papers published/Conference Proceedings

1. Using scanning force microscopy to investigate various cleaning procedures of different transparent conducting oxide substrates
   J. M. Nel, C. M. Demanet, K. T. Hillie, F. D. Auret and H. L. Gaigher.
   Applied Surface Science, Vol. 134, Issue 1 – 4, pages 22 — 30, 1998

2. Influence of substrate on the morphology of electrodeposited CdS
   J. M. Nel, F. D. Auret, H. L. Gaigher, G. Myburg, Proceedings of the International Conference: 2nd World Conference and Exhibition on Photovoltaic Solar Energy Conversion, Vienna, Austria, 6-10 July 1998, Published by the European Commission, page 1051, 1998.

National and International Conference Presentations

1. Electroplated CdS-films on conducting glass substrates (poster)
   J. M. Nel, F. D. Auret, H. L. Gaigher and A. Botha,
   41st Annual Conference of the South African Institute of Physics, Pretoria, 2-5 July 1996

2. Atomic Force Microscopy investigation of the efficiency of various cleaning methods of glass substrates for photovoltaic cells (poster)
   K. T. Hillie, C. M. Demanet and J. M. Nel,
   41st Annual Conference of the South African Institute of Physics, Pretoria, 2 -5 July 1996

3. Effect of deposition and annealing temperature on the composition of electrodeposited CdS (poster)
   J. M. Nel, G. Myburg, P. Stoddart, M. van Standen, C. W. Louw,
   43nd Annual Conference of the South African Institute of Physics, Cape Town, 6-10 July 1998

4. Influence of substrate on the morphology of electrodeposited CdS (poster)
   J. M. Nel, F. D. Auret, H. L. Gaigher, G. Myburg,
   2nd World Conference and Exhibition on Photovoltaic Solar Energy Conversion, Vienna, Austria, 6 - 10 July 1998

5. Influence of substrate morphology and temperature on electrodeposited CdS thin films (poster)
   J. M. Nel, H. L. Gaigher and F. D. Auret,
   44th Annual Conference of the South African Institute of Physics, Port Elizabeth, 5 - 9 July 1999.

6. The effect of temperature and deposition time on the morphology of electrodeposited CdS thin films (poster)
   J. M. Nel, H. L. Gaigher and F. D. Auret,
   45th Annual Conference of the South African Institute of Physics, Johannesburg, 4 - 8 July 2000.

7. An introduction to CdTe-based thin film solar cells **(Invited talk)**
   J. M. Nel, H. L. Gaigher and F. D. Auret,
   Winter school at the 45th Annual Conference of the South African Institute of Physics, Johannesburg, 4 - 8 July 2000.

10. References

M. I. Abdalla, D. B. Holt and D. M. Wilcox (1973), *J. Mater. Sci.* 8, 590.

M. M. Al-Jassim, F. S. Hasoon, K. M. Jones, B. M. Keyes, R. J. Matson and H. R. Moutinho (1993), *Conference Record of the 23rd IEEE Photovoltaic Specialists Conference*, 459.

S. A. Al Kuhaimi (1998), *Vacuum* 51, 349.

R. D. Armstrong, M. Fleischmann and H. R. Thirsk (1966), *J. Electroanal. Chem.* 11, 208.

R. D. Armstrong and A. A. Metcalfe (1975), *J. Electroanal. Chem.* 63, 19.

P. W. Atkins (1995), in: Physical Chemistry – 5th Edition (Oxford University Press, Oxford).

A. S. Baranski and W. R. Fawcett (1980), *J. Electrochem. Soc.* 127, 766.

A. S. Baranski, W. R. Fawcett, A. C. McDonald, R. M. De Nobriga and J. R. McDonald (1981), *J. Electrochem. Soc.* 128, 963.

A. S. Baranski, M. S. Bennett and W. R. Fawcett (1983), *J. Appl. Phys.* 54, 6390.

B. M. Basol (1984), *J. Appl. Phys.* 55, 601.

B. M. Basol (1988), *Solar Cells* 23, 69.

D. Bhattacharyya and M. J. Carter (1996), *Thin Solid Films* 288, 176.

V. G. Bhide, S. Salkalachen, A. C. Rastorgi, C. N. R. Rao and M. S. Hegde (1981), *J. Phys. D: Appl. Phys.* 14, 1647.

G. Binnig, C. Quate, and G. Gerger (1986), *Phys. Rev. Lett.* 56, 930.

W. H. Bloss and F. Pfisterer (1983), *Proc. 5th E. C. Photovoltaic Solar Energy Conf.,* (D Reidel Publishing Co., Dordrecht) 728.

D. Bonnet and H. Rabenhorst (1972), *Proc. 9th IEEE Photovoltaic Spec. Conf.,* (IEEE), 129.

R. J. Briggs and A. K. Ramdas (1976), *Physics Review B* 13, 5518.

J. Britt and C. Ferekides (1993), *Appl. Phys. Lett.* 62, 2851.

R. Brown (1970) in: Handbook of Thin Film Technology, Eds. L. I. Maissel and R. Glang (McGraw-Hill, New York) , Chapter 6.

R. F. Bunshah (1986), in: Deposition Technologies for Films and Coating: Development and Applications (D Reidel Publ. Co., Dordrecht).

R. J. Carter, T. P. Schneider, J. S. Montgomery and R. J. Nemanich (1994), *J. Electrochem. Soc.* 141, 3136.

I. H. Campbell and P. M. Fauchet (1986), *Solid State Communications* 58, 739.

T. L. Chu, S. S. Chu, N. Schultz, C. Wang and C. Q. Wu (1992), *J. Electrochem. Soc.* 129, 2443.

D. S. Chuu, C. M. Dai, W. F. Hsieh and C. T. Tsai (1991), *J. Appl. Phys.* 69, 8402.

J. Colchero, H. Bielefeldt, A. Ruf, M. Hipp, O. Marti and J. Mlynek (1992), *phys. stat. sol. (a)*, 131, 73.

CRC Handbook of Chemistry and Physics (2000), Edited by D. R. Lide.

W. J. Danaher, L. E. Lyons and G. C. Morris (1985), *Solar Energy Materials* 12, 137.

S. K. Das (1993(a)), *Thin Solid Films* 226, 259.

S. K. Das (1993(b)), *Solar Energy Materials and Solar Cells*, 29, 277.

S. K. Das and G. C. Morris (1992), *J. Appl. Phys.* 72, 4940.

S. K. Das and G. C. Morris (1993(a)), *Solar Energy Materials and Solar Cells* 28, 305.

S. K. Das and G. C. Morris (1993(b)), *Solar Energy Materials and Solar Cells* 30, 107.

S. das Neves and M-A. De Padi (1994), *Semicond. Sci. Technol.* 9, 1719.

N. R. de Tacconi and K. Rajeshwar (1993), *J. Phys. Chem.* 97, 6504.

R. C. DeMattei and R. S. Feigelson (1992), in: Electrochemistry of semiconductors and electronics – Processes and Devices, Editors John McHardy and Frank Ludwig (Noyes Publications, Park Ridge, New Jersey)

S. Dennison (1993), *Electrochim. Acta*, 38, 2395.

A. R. Despic, J. Diggle and J. O'M. Bockris (1968), *J. Electrochem. Soc.: Electrochemical Science* 115, 507.

A. R. Despic and M. N. Djarovic (1984), *Electrochim. Acta*, 29, 131.

J. W. Dini (1993), Electrodeposition: The materials science of coating and substrates, (Noyes Publications, Park Ridge, N.J., USA).

A. J. Ebothe (1996), *Semicond. Sci. Technol.*, 11, 1096.

E. Fatas, R. Duo, P. Herrasti, F. Arjona and E Garcia-Camarero (1984), *J. Electrochem. Soc.*, 131, 2243.

E. Fatas, P. Herrasti, F. Arjona, E Garcia-Camarero and M. Leon (1986), *J. Mater. Sci.* 5, 583.

E. Fatas, P. Herrasti, F. Arjona and A. J. Parker (1987), *J. Electrochem. Soc.*, 134, 2799.

C. Feldman and M. O'Hara (1957), *J. Opt. Soc. Am.* 47, 300.

C. Ferekides, J. Britt, Y. Ma and L. Killian (1993), *Conference Record of the 23rd IEEE Photovoltaic Specialists Conference*, 389.

C. S. Ferekides, K. Dugan, V. Ceekala, J. Killian, D. Oman, R. Swaminathan and D. L. Morel (1994), *Conference Record of the 24th IEEE Photovoltaic Specialists Conference*, 99.

C. S. Ferekides, D. Marinskiy, V. Viswanathan, B. Tetali, V. Palekis, P. Selvaraj and D. L. Morel (2000), *Thin Solid Films*, 361-362, 520.

I. J. Ferrer and P. Salvador (1989), *J. Appl. Phys.* 66, 2568.

M. Fleischmann and H. R. Thirsk (1963), *Adv. Electrochem. Electrochem. Eng.*, 3, 123.

R. Flood, B. Enright, M. Allen, S. Barry, A. Dalton, H. Doyle, D. Tynan and D. Fitzmaurice (1995), *Solar Energy Materials and Solar Cells* 39, 83.

M. Froment, M. C. Bernard, R. Cortes, B. Mokili and D. Lincot (1995), *J. Electrochem. Soc.* 142, 2642.

S. A. Galloway, A. W. Brinkman, K. Durose, P. R. Wilshaw and A. J. Holland (1996), *Appl. Phys. Letters* 68, 3725.

P. J. George, A. Sanchez, P. K. Nair and L. Huang (1996(a)), *J. Crystal Growth* 158, 53.

P. J. George, A. Sanchez-Juarez and P. K. Nair (1996(b)), *Semicond. Sci. Technol.* 11, 1090.

S. Hayashi, H. Sanda, M. Agata and K. Yamamoto (1989), *Physical Review B* 40, 5544.

H. Higuchi, T Arita, T. Aramoto, T Nishio, K Hiramatsu, A. Hanafusa, N. Ueno, K. Omura, N. Nakayama, H. Takakura and M. Murozono (1993), *Conference Record of the 23rd IEEE Photovoltaic Specialists Conference*, 409.

M. Ichimura, F. Goto, Y. Ono and E. Arai (1999), *J. Crystal Growth* 198/199, 308.

J. Ihanus, M. Ritala, M. Leskelä, T. Prohaska, R. Resch, G. Friedbacher and M. Grasserbauer (1997), *Appl. Surf. Sci.* 120, 43.

O. A. Ileperuma, C. Vithana, K. Premaratne, S. N. Akuranthilaka, S. M. McGregor and I. M. Dharmadasa (1998), *J. Mat. Sci.: Materials in Electronics* 9, 367.

M. Ilieva, D. Dimova-Malinovska, B. Ranguelov and I. Markov (1999), *J. Phys. Condens. Matter* 11, 10025.

K. Jackowska and M. Skompska (1986), *Polish J. Chem.* 60, 551.

R. Jayakrishnan, S. R. Kumar and R. K. Pandey (1994), *Semicond. Sci. Technol.* 9, 97.

R. Jayakrishnan, J. P. Nair, B. A. Kuruvilla, S. K. Kulkarni and R. K. Pandey (1996), *Semicond. Sci. Technol.* 11, 116.

D. R. Johnson (2000), *Thin Solid Films* 361-362, 321.

W. M. Kane, J. P. Spratt and L. W. Hershinger (1966), *J. Appl. Phys.* 37, 2085.

G. Kanellis, J. F. Morhange and M. Balkanski (1980), *Physical Review B* 21, 1543.

S. J. Kirtchmar (1965), *Electrochimiya* 1, 609.

S. Kolhe, S. K. Kulkarni, A. S. Nigavekar and S. K. Sharma (1984), *Solar Energy Materials* 10, 47.

S. Kolhe, S. K. Kulkarni, A. S. Nigavekar and V. G. Bide (1987), *J. Mat. Sci.* 22, 1067.

F. A. Kröger (1978), *J. Electrochem. Soc.: Solid-State Science and Technology* 125, (12), 2028.

A. Kylner, J. Lindgren and L. Stolt (1996), *J. Electrochem. Soc.* 143, 2062.

J. S. Lee, H. B. Im, A. L. Fahrenbruch and R. H. Bube (1987), *J. Electrochem. Soc.: Solid State Science and Technology* 134, 1790.

E. L. Lind and R. H. Bube (1962), *J. Chem. Phys.* 37, 2499.

C. D. Lokhande and S. H. Pawar (1989), *phys. stat. sol. (a)* 111, 17.

R. Lozada-Morales and O. Zelaya-Angel (1996), *Thin Solid Films* 281-282, 386.

A. B. Lundin and G. A. Kitaev (1965), *Inorg. Mater.* 1, 2107.

P. Maivald, H. J. Butt, S. A. C. Gould, C. B. Prater, B. Drake, J. A. Gurley, V. B. Elings and P. K. Hansma (1991), *Nanotechnology* 2, 103.

H. Matsumoto, K. Kuribayashi, H. Uda, Y. Komatsu, A. Nakano and S. Ikegami (1984), *Solar Cells* 11, 409

S. Matthew, P. S. Mukerjee and K. P. Vijayakumar (1995), *Thin Solid Films* 254, 278.

D. Mattox (1996), in: Handbook of Thin Film Process Technology, Eds. David A. Glocker and S. Ismat (Institute of Physics Publishing, Bristol, 1996) pE1.0:1.

J. F. McCann and M. S. Kazacos (1981), *J. Electroanal. Chem.* 119, 409.

A. Mendoza-Galván, G. Martínez and R. Lozada-Morales (1996), *J. Appl. Phys.* 80, 3333.

B. Miller and A. Heller (1976), *Nature* 262, 680.

K. Mitchell, A. L. Fahrenbruch and R. H. Bube (1975), *J. Vacuum Sci. Technol.* 12, 909.

G. C. Morris and R. Vanderveen (1992), *Solar Energy Materials and Solar Cells* 27, 305.

G. C. Morris and S. K. Das (1993), *Conference Record of the 23rd IEEE Photovoltaic Specialists Conference*, 469.

K. K. Nanda and S. N. Sahu (1997), *Appl. Surf. Sci.* 119, 50.

H. Nguyen Cong, M. Dieng, C. Sene and P. Chartier (2000), *Solar Energy Materials and Solar Cells* 63, 23.

D. W. Niles, D. Rioux and H. Höchst (1993), *J. Appl. Phys.* 73, 4586.

J. Nishino, S. Chatani, Y. Uotani and Y. Nosaka (1999), *J. Electroanal. Chem.* 473, 217.

P. O'Brien and T. Saeed (1996(a)), *J. Crystal Growth* 158, 497.

P. O'Brien, J. R. Walsh, I. M. Watson, L. Hart and S. R. P. Silva (1996(b)), *J. Crystal Growth* 167, 133.

M. E. Özsan, D. R. Johnson, M. Sadeghi, D. Sivapathasundaram, L. M. Peter, M. J. Furlong, G. Goodlet, A. Shingleton, D. Lincot, B. Mokili and J. Vedel (1994), *Proceedings of the First World Conference of Photovoltaic Energy and Conversion (Conference Record of the 24th IEEE Photovoltaic Specialists Conference)*, 327

R. K. Pandey, S. A. Sahu and S. Chandra (1996), in Handbook of Semiconductor Electodeposition, (Marcel Dekker Inc., New York).

R. K. Pandey, S. Mishra, S. Tiwari, P. Sahu and B. P. Chandra (2000), *Solar Energy Materials and Solar Cells* 60, 59.

L. M. Peter (1978(a)), *Electrochim. Acta* 23, 165.

L. M. Peter (1978(b)), *Electrochim. Acta* 23, 1073.

G. P. Power, D. R. Peggs and A. J. Parker (1981), *Electrochemica Acta* 26, 681.

R. P. Raeffaelle, H. Forsell, T. Potdevin, R. Friedfeld, J. G. Montovani, S. G. Bailey, S. M. Hubbard, E. M. Gordon and A. F. Hepp (1999), *Solar Energy Materials and Solar Cells* 57, 167.

K. Ramanathan, R. G. Dhere and T. J. Coutts (1993), *Conference Record of the 23rd IEEE Photovoltaic Specialists Conference*, 466.

M. Rami, E. Benamar, M. Fahoume and A. Ennaoui (1999), *phys. stat. sol. (a)* 172, 137.

A. Rohatgi, R. Sudarsanan, S. A. Ringel and M. H. MacDougal (1991), *Solar Cells* 30, 109.

R. Rossetti, S. Nakahara and L. E. Brus (1983), *J. Chem. Phys.* 79, 1086.

G. Sasikala, R. Dhanasekaran and C. Subramanian (1997), *Thin Solid Films* 302, 71.

G. Sasikala, P. Thilakan and C. Subramanian (2000), *Solar Energy Materials and Solar Cells* 62, 275.

M. Stoev and A. Katerski (1996), *J. Mater. Chem.* 6, 377.

K. Shirai, Y. Moriguchi, M. Ichimura, A. Usami and M. Saji (1996), *Jpn. J. Appl. Phys.* 35, 2057.

S. A. Tomás, O. Vigil, J. J. Alvarado-Gil, R. Lozada-Morales, O. Zelaya-Angel, H. Vargas and A. Ferreira da Silva (1995), *J. Appl. Phys.* 78, 2204.

J. Toušková, D. Kindl, L Dobiášová and J. Toušek (1998), *Solar Energy Materials and Solar Cells* 53, 177.

O. Trujilo, R. Moss, K. D. Vuong, D. H. Lee, R. Noble, D. Finnigan, S. Orloff, E. Tenpas, C. Park, J. Fagan and X. W. Wang (1996), *Thin Solid Films* 290/291, 13.

H. Uda, S. Ikegami and H. Sonomura (1990), *Jpn J. Appl. Phys.* 29, 30.

A. Vecht (1966), In: Physics of Thin Films, Advances in Research and Development, Vol 3, Edited by Georg Hass asnd Rudolf E. Thun (Academic Press, New York, 165).

S. Veprek, Z. Iqbal, H. R. Oswald, F. -A. Sarrot, J. J. Wagner and A. P. Webb (1981), *Solid State Communications* 39, 509.

D. M. Wilcox and D. B. Holt (1969), *J. Mater. Sci.* 4, 672.

T. Yoshida and N. Matsui (1993), *J. Appl. Phys.* 73, 5222.

T. Yoshida, K. Yamaguchi, T. Kazitani, T. Sugiura and H. Minoura (1999), *J. Electroanal. Chem.* 473, 209.

J. Yoshino, J. Morimoto and H. Wada (1997), *J. Mat. Sci. Letters* 16, 1977.

D. R. T. Zahn, C. H. Maierhof, A. Winter, M. Reckzugel, R. Srama, A. Thomas, K. Horn and W. Richter (1991), *J. Vac. Sci. Technol. B* 9, 2206.

M. Zhu, X. Guo, G. Chen, H. Han, M. He. and K. Sun (2000), *Thin Solid Films* 360, 205.